NESO
National Energy System Operator

Delivered in Partnership with
Imperial College London

Final Report

Data-Driven Online Monitoring and Early Warning for GB System Stability (DOME)

Independent expert analysis/opinion provided by:
Dr Yue Zhu, Dr Yunjie Gu, Prof. Tim Green
Department of Electrical and Electronic Engineering,
Imperial College London

NESO
National Energy System Operator

Disclaimer

This Final Report and the Supplementary Report 1&2 are the independent expert opinion of the author(s). It does not represent the views of Imperial College London or Imperial Consultants.

1 Contents

FIGURES

2 Executive Summary

2.1 Project Overview

The Data-Driven Online Monitoring and Early Warning for GB System Stability (DOME) project was proposed to examine whether on-line impedance measurement of the GB system with limited number of injections and with system ambient data is feasible, and how it can give early warnings of emerging oscillations. Beyond these, DOME was designed to explore the possibilities of using the identified impedance to trace the root-cause of oscillations and further provide guidance on equipment re-tunning to damp those oscillatory modes.

2.2 Work Package Descriptions and Modifications

The DOME project contains 5 work packages (WPs). Due to the restrictions and difficulties on acquiring the critical PMU data within the project period, and some newly occurred oscillation events in the UK, this project shifted part of its focus from analysing the noise feature in PMU data to data-driven oscillation tracing and impedance identification methods studies. As a result, 2 work packages: WP1 and WP2 have been modified to align with the actual work completed within the project scope.

The **original** work packages were designed as below.

- WP1 (3 months) : Assessment of Measurement Noise
  To develop a statistical model of the background noise in the measured voltages and currents in transmission systems.
  Deliverable from WP1 is a short technical report on noise characteristics of PMU data.
- WP2 (3 months): Optimal Injection Level
  To determine the optimal level for effective monitoring of the stability of the entire system upon the background noise.
  Deliverable from WP2 is a short technical report on the rating required of a dedicated injection device and the viability of injection via existing third-party inverter-based resources.
- WP3 (5 months): Location Choices for Injection
  To determine how many injection points and remote measurement points are needed for sufficient characterisation of a system.

Deliverable from WP3 is a short technical report on how many injection points and measurement points are needed to identify adequately the modes of a region of the GB transmission system or indeed the whole system.

- WP4 (5 months): Verification
  To determine the optimal level and point of injection for effective monitoring of the stability of the entire system upon the background noise.
  Deliverable from WP4 is a set of results verifying the work of WP1 to WP3.
- WP5 (2 months): Global Engagement
  To engage with international associations and ESOs to disseminate the methodology and identify potential systems for field tests.
  Deliverable from WP5 is a set of dissemination activities and report that outlines how a field trial of the method could be conducted.

The **modified** version of WP1 and WP2 are:

- WP1 (3 months): Assessment of Relationship Between Oscillation Tracing Methods and Participation Factors
  It is important for the viability of the overall method to establish the theoretical basis and limits of model-free methods of oscillation tracing (such as Dissipative Energy Flow, DEF) and how they compare with identification of participation factors from state-space and whole-system impedance models. DEF has been used by some system operators for several years to identify the sources and sinks of oscillations in traditional synchronous machine systems. Two questions now need answering. First, can DEF, or modifications of it, be relied upon for systems containing or dominated by IBR? Second, how close is the DEF method to identifying mode shapes and participation factors for free and forced oscillations. This will be a theoretical study supplemented by examination of case-study networks in the Simulink environment.

  Deliverable from WP1 is a short technical report on oscillation tracing versus participation factors.
- WP2 (3 months): Impedance Identification Methods
  Impedance models are very useful for participation analysis when the white-box state-space models are not made available. One major benefit of using an impedance model is that it can be identified through data-driven approaches without needing access to the detailed internal model. In this work package, impedance

identification methods using frequency scanning data and using step-response data will be assessed, together with a comprehensive comparison of their relative merits. A simple simulation case study will also be employed to provide results for both of the methods. Suggestions will be made on how to select the appropriate method for root-cause tracing and system early warning in different circumstances.

The deliverable from WP2 is a short technical report on impedance identification methods. The report can be integrated with the WP3 report since WP2 and WP3 are closely related.

If example PMU data from the GB system can be made available before the project end data, then analysis of quantisation, bandwidth and noise will be carried out to explore if the PMUs are sufficient for on-line model identification. A supplementary report would be delivered once the analysis is completed.

All other work packages remain the same.

2.3 Project Completion

All work packages have been successfully completed, as summarised below.

1) **WP1**: The DEF method, along with its variants such as the complex dissipating energy flow (cDEF) and electrical dissipating energy flow (eDEF) methods, have been thoroughly examined. Their interrelationships have been clarified, leading to the proposal of a unified dissipating energy flow (uDEF) method. This method encompasses all variants of DEF and serves as a comprehensive approach for data-driven oscillation root-cause tracing. A technical report summarising the work in WP1 has been submitted to NESO. Additionally, a pre-designed Excel spreadsheet for uDEF calculations using PMU data has been created and submitted to NESO for verification with real events.
2) **WP2**: Both time-domain (TDID) and frequency-domain impedance identification (FDID) methods have been fully analysed, with a justification of their relative merits. Recommendations for selecting the appropriate identification method in various scenarios have been provided.
3) **WP3**: A methodology using a limited number of perturbations (e.g., a single perturbation) to restore the whole-system impedance/admittance model has been developed. This model, which contains all dynamic information of the system, can be used to identify oscillatory modes and provide early warnings of oscillation events. This

technique is referred to as Hybrid Data/Model-Driven Impedance Identification, considering its nature of using the time-domain data collected in the system and existing knowledge to the system network model. Studies and discussions on specific problem such as multiple perturbations and partial measurement have been provided.

4) **WP4**: Three simulation case studies have been conducted to verify the uDEF method. Additionally, two simulation case studies have been performed to validate the Hybrid Data/Model-Driven Whole-System Admittance Identification method.
5) **WP5**: International collaborations have been established with ISO New England by sharing oscillation data generated in the DOME project, enabling cross-verification of the DEF variants and the uDEF method. Project researchers have also presented outcomes, including both uDEF and Hybrid Data/Model-Driven Impedance Identification, to peers, engineers, and ESOs at global conferences, such as the 2024 IEEE PES General Meeting.

2.4 Deliverables

The deliverables of the projects are:

- 1 final report accompanied by 2 self-contained supplementary technical reports.
- 1 technical reports for WP1, and 1 joint technical report for WP2&3.
- 1 pre-designed Excel spreadsheet which calculates uDEF and generate plots from the PMU data.
- 1 journal article (submitted to IEEE Transactions on Industrial Electronics) [1].
- 1 technical document (published on-line as a preprint:
  Yue Zhu, Hazem Karbouj, Xiaoyao Zhou, et al. Unified Dissipation Energy Flow. TechRxiv. August 12, 2024.)
- Oscillation data from simulation case studies developed in this project are provided to NESO for further studies. The data are transformed to the format required by NESO.

3 Introduction

3.1 Background

As Synchronous Generators, SGs, are gradually replaced by Inverter-Based Resources, IBRs, the control-defined behaviour of IBRs can introduce instabilities which appear as oscillations in the system voltage in response to small or large disturbances. Sub/super-synchronous oscillations at a variant of frequencies attributed to IBRs have been reported in UK and worldwide [1][3]. Such oscillations could be caused by poorly designed control schemes of some IBRs or interactions among controllers of several IBRs. Some of these oscillations have had significant consequences, such as nation-wide power outage [4]. Since IBR vendors usually do not disclose the analytical model of their product, the system becomes insufficiently modelled. As a result, the conventional model-based approaches for investigating oscillations are meeting significant obstacles. The lack of adequate models motivates researchers to investigate methods of using the abundance of data as a compensation, i.e., data-driven methods. There are two routes for implementing data-driven methods:

1) Directly using the time-domain data, such as PMU data from an oscillation event, to identify the root-cause of oscillations. Since no models are involved in this route, it can be known as a *model-free* method.
2) Adding a perturbation to the system and identify the system model from its time-domain response data, which is then used for potential oscillation risk detection.

The first method is very useful for a post-event analysis using PMU data, while the second is suitable for on-line system monitoring and oscillation early warning.

3.2 Scope of the Project

The aim of this project is to explore data-driven methods for system oscillation analysis and assess the feasibility of implementing these methods within the GB network. The project encompasses both routes of data-driven methodologies. A comprehensive analysis of existing methods, such as the DEF and its variants, is integral to the project. Additionally, the development of a practical solution for implementing data-driven system model identification is required.

The scope of the project is concluded in Figure 1.

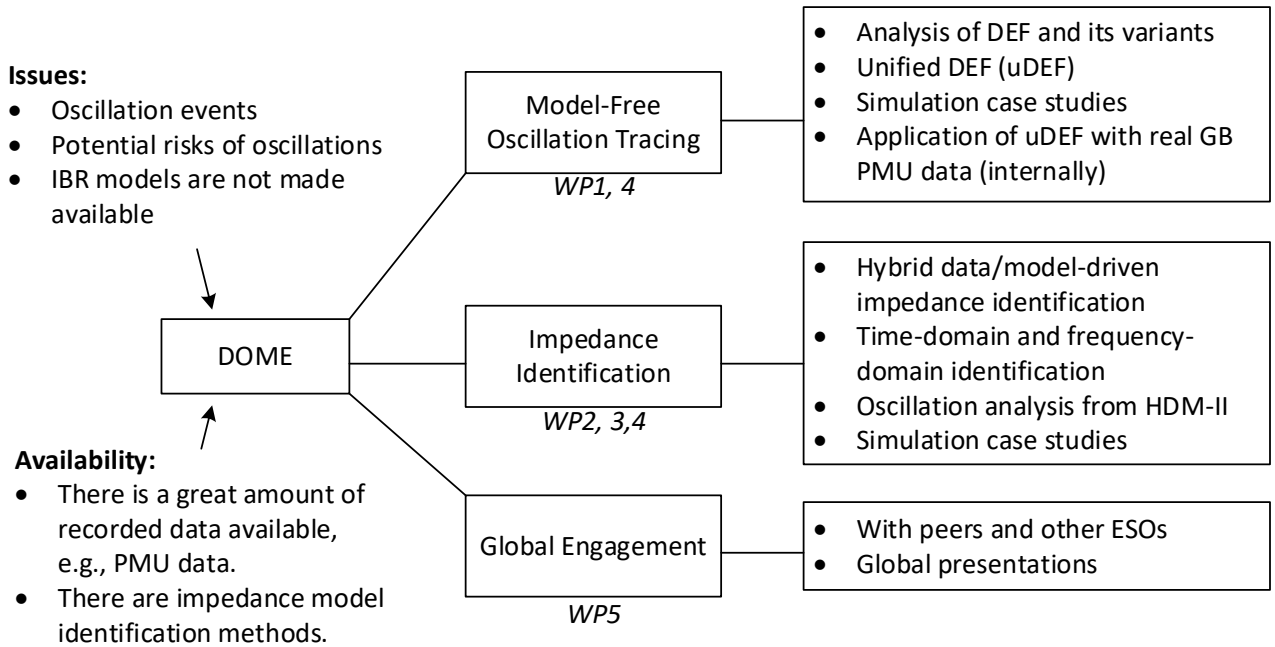

Figure 1 DOME project scope.

4 Technical Details

4.1 Model-free oscillation tracing

For model-free oscillation tracing method, a new approach named unified dissipating energy flow (uDEF) has been proposed. Analysis and discussions have been made on its link to existing DEF methods and its link to the theorical oscillation mode.

Three simulation case studies have been conducted to examine oscillations arising from different causes:

1) 8.8 Hz oscillation in a modified IEEE 14-bus system, caused by poorly tuned current control of 3 grid-following IBR.
2) 1.5 Hz oscillation in a modified IEEE 14-bus system, caused by large amounts of active power output from 3 grid-following IBR.
3) 20 Hz oscillation in a 7-bus system, caused by poorly tuned AC voltage control of two grid-following IBR.

Through these case studies, the proposed uDEF method can consistently identify oscillation sources and sinks with good accuracy, whereas the original DEF method and its variants may fail in certain cases. Furthermore, the model-free analysis results are validated against analytical findings.

Detailed descriptions of the uDEF method and simulation results are provided in **Supplementary Report 1**.

4.2 Data-driven Admittance Identification

By identifying the whole-system impedance/admittance model Z^{sys} and Y^{sys}, oscillatory modes can be detected before real events occur. Furthermore, impedance-based participation analysis enables pinpointing the root causes of these modes. However, a fully data-driven approach would require introducing perturbations at every location with a connected IBR, which is impractical.

To address this challenge, this project proposes a Hybrid Data/Model-Driven Impedance Identification technique. This method utilises prior knowledge of the network's nodal admittance matrix, which includes transmission line and load admittances. By applying a limited number of perturbations at certain locations, and collecting response data at each location, the acquired data is integrated with the nodal admittance matrix to reconstruct Z^{sys} and Y^{sys}. The process of identifying Z^{sys} and Y^{sys} is divided into two categories: time-domain identification and frequency-domain identification, which are analysed in this project, with their relative merits discussed.

This novel approach enables large-scale system impedance identification, making it feasible for complex networks such as the GB system.

Three case studies have been conducted to verify the proposed method:

1) A 4-bus system with 2 grid-following IBR and 1 SG. Perturbation is introduced at 1 bus and measurements are taken at all buses with apparatus connected.
2) A 7-bus system with 5 grid-following IBR and 1 SG. Perturbation is introduced at 1 bus and measurements are taken at all buses with apparatus connected.
3) A 7-bus system with 5 grid-following IBR and 1 SG. Perturbation is introduced at 1 bus and measurements are taken at only 3 buses with apparatus connected.

Detailed descriptions of the Hybrid Data/Model-Driven Impedance Identification and simulation results are provided in **Supplementary Report 2**.

5 Global Engagement and Activities

The following activities have been taken to engage with global associations and disseminate the proposed methods:

1) Dr. Yue Zhu and Dr. Yunjie Gu have engaged with Dr. Slava Maslennikov, the Technical Manager of the Advanced Technology Solutions Department, ISO New England Inc., on application of cDEF and uDEF. Data from the 3 case studies of this project has been shared with ISO New England for verification of cDEF while it is found that for one case (1.5 Hz oscillation case) cDEF is not giving the correct indication of oscillation sources and sinks.
2) Dr. Yunjie Gu presented the outcome of uDEF in 2024 IEEE PES General Meeting in Seattle as an invited speaker. Title: *Tracing oscillations from data – is there a universal approach?*
3) Dr. Yue Zhu presented the concept and some results of Hybrid Data/Model-Driven Impedance Identification in 2024 IEEE PES General Meeting in Seattle as an invited speaker. Title: *Impedance-Based Method for SSO Root-Cause Tracing and Early Warning.*
4) Dr. Yue Zhu approached Prof. Lingling Fan (an expert in oscillation analysis and Fellow of IEEE) from University of South Florida to exchange ideas on impedance identification techniques, especially on time-domain identification methods. Some ideas have been merged with this project, and Prof. Fan is a contributing author of the ongoing journal paper developed from this project.
5) Dr. Yue Zhu was engaged by NESO as an external researcher, to support with the work on using uDEF method to analysis real oscillation events. The results have been delivered to NESO for reference. An excel spreadsheet containing all equations used by uDEF method is also provided to NESO for future applications.

6 Conclusions and Future Works

The Data-Driven Online Monitoring and Early Warning for GB System Stability (DOME) project has successfully demonstrated the feasibility and effectiveness of using data-driven methods for system oscillation analysis and early warning in the GB network. The project has achieved its objectives through the development and validation of innovative techniques such as the unified dissipating energy flow (uDEF) method and the Hybrid Data/Model-Driven Impedance Identification technique.

Key findings and accomplishments of the project include:

1. **Unified Dissipating Energy Flow (uDEF) Method**: The uDEF method has been proposed and validated through multiple simulation case studies. It has shown certain accuracy in identifying oscillation sources and sinks compared to traditional DEF methods.

2. **Impedance Identification Methods**: Both time-domain and frequency-domain impedance identification methods have been thoroughly analysed. The project has provided recommendations for selecting the appropriate method based on specific scenarios, enhancing the capability for early warning and root-cause analysis of oscillations.

3. **Hybrid Data/Model-Driven Impedance Identification**: This novel approach has been developed to address the challenges of large-scale system impedance identification. By integrating limited perturbation data with existing network models, the Hybrid Data/Model-Driven Impedance Identification enables comprehensive system analysis and early warning for complex networks like the GB system.

4. **Global Engagement and Dissemination**: The project has established international collaborations and disseminated its findings through conferences and publications. These efforts have facilitated knowledge exchange and validation of the proposed methods with global peers and industry experts.

Overall, the DOME project has made contributions to the field of power system stability and oscillation analysis. The developed methods and findings provide valuable insights and practical solutions for enhancing the stability and reliability of power systems with high penetrations of IBR. Future work could focus on refining the uDEF methods and build a stronger theorical basis for it, perfecting the Hybrid Data/Model-Driven Impedance Identification method by providing guidance on choosing the best placement of injections, and methods on merging overfitted results, and exploring the their application in real-world scenarios.

7 References

[1] Yue Zhu, Yunjie Gu, Jessica Santos Döhler, et al. Hybrid Data/Model-Driven Whole-System Admittance Identification via Single-Point Injections. TechRxiv. March 28, 2025. DOI: 10.36227/techrxiv.174319968.84007233/v1

[2] Y. Cheng, L. Fan et al., “Real-world subsynchronous oscillation events in power grids with high penetrations of inverter-based resources,” IEEE Transactions on Power Systems, vol. 38, no. 1, pp. 316–330, 2022.

[3] X. Xie, X. Zhang, H. Liu, H. Liu, Y. Li and C. Zhang, "Characteristic Analysis of Subsynchronous Resonance in Practical Wind Farms Connected to Series-Compensated Transmissions," in IEEE Transactions on Energy Conversion, vol. 32, no. 3, pp. 1117-1126, Sept. 2017, doi: 10.1109/TEC.2017.2676024

[4] J. Bialek, “What does the GB power outage on 9 august 2019 tell us about the current state of decarbonised power systems?,” Energy Policy, vol. 146, 2020, Art. no. 111821.

NESO
National Energy System Operator

Delivered in Partnership with
Imperial College London

Supplementary Report 1

Data-Driven Online Monitoring and Early Warning for GB System Stability (DOME)

Independent expert analysis/opinion provided by:
Dr Yue Zhu, Dr Yunjie Gu, Prof. Tim Green
Department of Electrical and Electronic Engineering,
Imperial College London

NESO
National Energy System Operator

1 Contents

TABLES

FIGURES

2 Introduction

As Synchronous Generators, SGs, are gradually replaced by Inverter-Based Resources, IBRs, the control-defined behaviour of IBRs can introduce instabilities which appear as oscillations in the system voltage in response to small or large disturbances. Sub/super-synchronous oscillations attributed to IBRs have been reported worldwide and occurred at a variety of frequencies [1]. Such oscillations could be caused by poorly designed control schemes of some IBRs or interactions among controllers of several IBRs. Some of these oscillations have had significant consequences [2]. The conventional model-based approaches, such as the state-space approach, for investigating oscillations are meeting an obstacle because the system is not sufficiently and precisely modelled. In the meantime, IBR vendors would not disclose any of the internal control designs due to intellectual property issues. The lack of adequate models motivates us to investigate methods of using the abundance of data as compensation, e.g. phasor measurement unit (PMU) data, dynamic system monitoring (DSM) data, and supervisory control and data acquisition (SCADA) data. Such methods can be considered as data-driven methods or, more precisely, model-free methods. A model-free method investigates the root cause of system oscillations without a model, using the PMU data recorded during the oscillation. This supplementary report discusses methods of model-free root-cause tracing.

This report serves as a supplementary report for DOME Final Report. It is developed originally from DOME WP1 Report but with updates in both theory and simulation results.

3 Dissipating Energy Flow (DEF)

3.1 Introduction of DEF

A successful model-free method is the Dissipating Energy Flow (DEF) method [3]. This method is called model-free but is not entirely model-free since it is based on the assumption that the structure of the models, the swing equations, is known, although the detailed parameters are not. The DEF method is closely associated with the energy-based (Lyapunov) method. Dissipation is defined as the *rate of reduction of energy over time*. From Lyapunov's theory, we know that the total energy (Lyapunov function) of the system converges to the minimum if the total dissipation is non-negative, and hence the system is stable.

The DEF method makes use of the fact that a system governed by swing equations has a distributed energy function, where each apparatus (generator or transmission line) has its own energy function and the total energy function of the system is the sum of the energy functions of all apparatuses. Using this distributed energy structure, we can study the flow of energy in a network, so the contribution to system stability can be clearly identified for each apparatus. The DEF method calculates the transient energy flow into an apparatus during an oscillation. The transient energy trajectory contains two parts. The first part fluctuates which reflects the charging and discharging of energy storage elements during the transient. The second part is monotonic and reflects the dissipation: if the dissipation is negative (energy flow is positive), the apparatus under consideration provides energy for oscillation so is the source of the oscillation. If the dissipation is positive the apparatus is providing damping so is a sink of oscillation.

3.2 The Ambiguity of DEF

The DEF has been proven successful in tracing the origins of oscillations for conventional power systems, as has been demonstrated by its practical application in New England [4]. This success has motivated people to apply it to inverter-based power systems. However, misleading results have been reported during the application [5]. This is not surprising because inverters have very different dynamic models compared to synchronous generators and the mathematical foundation for the original DEF method may no longer hold when inverters become dominant. Another issue is whether modifications can be made to the DEF method to adapt it to the dynamics of inverters. It is presented in [5] that such a modification seems possible, but no rigorous justifications are given.

In this section, we rethink the foundations of the DEF method and explore the possibility of a generic DEF method covering both synchronous generators and inverters.

3.3 Discussions

The key to the DEF method is a proper definition of the energy flow. The definition of energy flow is not unique and there are two principles to follow for a meaningful definition:

- Conservation: the net energy flows into a node must be zero.
- Consistency: the flows are associated with consistent energy functions.

The first principle can be satisfied by using the intrinsic conservation of current flow (Kirkhoff's law)

$$\sum I_n = 0 \tag{1}$$

where the summation includes the contributions from all branches that terminate at a given node. The current flow can be turned into energy flow (power) by multiplying the nodal voltage U in the equation:

$$\sum I_n^* \cdot U = 0 \tag{2}$$

where I_n^* refers to the conjugate of I_n, which is to align with the calculation of complex power. This equation implies a solution of using $\mathrm{Re}(I^*U)$ to indicate energy flow, which is the natural energy flow in a circuit. The real-part is taken here to represent the active power. The associated energy function is the electromagnetic energy in circuit elements (inductors and capacitors), and the associated dissipation is resistive loss.

For the purpose of stability analysis, $\mathrm{Re}(I^*U)$ cannot be used directly because it includes both the steady-state energy and the oscillation energy, and we are more interested in the oscillatory energy flow rather than the background steady-state energy flow. That said, we need to remove the steady-state energy flow. To this end, the energy flow is modified as

$$F_{ep} = \mathrm{Re}(\Delta I^* \Delta U) \tag{3}$$

where the deviation around the steady-state values is used to remove the steady-state energy flow. F_e here refers to the dissipating electromagnetic energy flow. Here we call it eDEF-P, where P refers to the active power.

If the energy function is not electromagnetic energy, the natural energy flow defined above is no longer useful in indicating stability and new definitions are needed. In [3] the definition below is used:

$$\sum I_n^* \dot{U} = 0 \tag{4}$$

where U is replaced by $\dot{U} = \frac{dU}{dt}$ and the conservation condition still holds. This equation can be transformed to

$$\sum S_n \varpi_U = 0 \tag{5}$$

where $S_n = I_n^* U$ is the complex power flowing from a branch to the given node, and

$$\varpi_U = \frac{d \ln A_U}{dt} + j \frac{d \theta_U}{dt} \tag{6}$$

is the complex frequency of U, with A_U and θ_U being the amplitude and angle of U. The real part of the complex frequency represents the variation of the amplitude of the signal, and the imaginary part is the usual frequency representing the variation of phase. The conservation equation (5) induces the energy flow below

$$F_{orig} = \mathrm{Im}(\Delta S\, \Delta\varpi_U), \tag{7}$$

which is found to be associated with the mechanical energy functions of swing equations. Here, F_{orig} refers to the originally defined DEF. The detailed deduction of (7) can be found in [3]. A more generic format of (7) is

$$F_{orig} = \mathrm{Re}\left(\Delta I^* \Delta \dot{U}\right), \tag{8}$$

which is given in [3]. For (7), it can be further expanded as

$$F_{orig} = \Delta P \Delta \frac{d\,\theta_U}{dt} + \Delta Q \frac{\Delta d \ln A_U}{dt} \tag{9}$$

which gives a similar format to the mechanical energy function in a synchronous generator.

3.4 Variants of DEF

Along with the penetration of IBR in power systems, DEF is found to fail in systems where IBR becomes the dominant. Several modifications have been made on the original DEF to accommodate systems with IBRs. One example is the complex DEF (cDEF) defined in [6]:

$$F_c = \mathrm{Im}\left(e^{j\phi} \Delta I^* \Delta \dot{V}\right), \tag{10}$$

where $e^{j\phi}$ is a rotation factor to account for the resistive component of transmission line impedances. The rotation factor is determined by the reactance-resistance ratio $K = \frac{X}{R}$ of the transmission lines

$$e^{j\phi} = \frac{K}{\sqrt{1+K^2}} + j\frac{1}{\sqrt{1+K^2}} \tag{11}$$

cDEF is proved to be accurate in tracing forced oscillations, but not discussed in tracing self-excited (free) oscillations, which are more of concerns in modern power systems.

[5] also suggests using another version of conservation equations

$$\sum U \frac{dI_n^*}{dt} = 0 \tag{12}$$

and the derived energy flow is

$$F_d = \mathrm{Re}(\Delta S \Delta \varpi_I^*) \tag{13}$$

which expands to

$$F_d = \Delta Q \Delta \frac{d\,\theta_I}{dt} + \Delta P \Delta \frac{d\ln A_I}{dt} \tag{14}$$

This set of equations is essentially the duality of the mechanical DEF method in [3] and therefore is named the dual-mechanical DEF (dDEF) method here. The dDEF is rooted in the duality of GFL to GFM [7], in which GFL apparatuses use reactive power for synchronisation, and use active power to control voltage. An alternative format of dDEF is

$$F_d = \mathrm{Im}\left(\Delta \dot{I}^* \Delta V\right). \tag{15}$$

However, it should be highlighted that the duality only holds rigorously when the network is resistive, whereas most transmission lines are inductive in practice. Also, the duality does not consider other outer loops in GFL control, such as dc-link loops and ac voltage loops. Therefore, the dDEF method for inverters does not have as rigorous a foundation as the original DEF method.

[8] explores several different types of DEF. They key idea is to calculate the active power and reactive power of oscillatory components. For active power, it is the same as F_{ep} defined in (3). For Reactive power, it is defined as

$$F_{eq} = \mathrm{Im}(\Delta I^* \Delta U)$$

To distinguish with eDEF-P, here we define F_{eq} as eDEF-Q, where Q refers to the reactive power. Based on eDEF-P and eDEF-Q, the following judgement are made:

- $F_{ep} < 0$: active source
- $F_{ep} > 0$: active sink
- $F_{eq} < 0$: reactive source
- $F_{eq} > 0$: reactive sink

Sometimes an IBR could be an active sink and meanwhile a reactive source. In such as case, it is difficult to determine the actual root cause of the oscillation. The original DEF, together with all variants, are concluded in Table 1.

Table 1 Summary of different definitions of energy flow.

DEF	Conservation	Flow
DEF	$\sum I_n^* \frac{dU}{dt} = 0$	$\mathrm{Re}(\Delta I^* \Delta \dot{U})$
eDEF-P	$\sum I_n^* U = 0$	$\mathrm{Re}(\Delta I^* \Delta U)$
eDEF-Q	$\sum I_n^* U = 0$	$\mathrm{Im}(\Delta I^* \Delta U)$
cDEF	$\sum I_n^* \frac{dU}{dt} = 0$	$\mathrm{Im}(e^{j\phi} \Delta I^* \Delta \dot{V})$
dDEF	$\sum U \frac{dI_n^*}{dt} = 0$	$\mathrm{Im}(\Delta \dot{I}^* \Delta V)$

From the discussion above, it is clear that the DEF method has some ambiguity and should be used carefully. These definitions serve different purposes and may yield conflicting results if not properly used. For example, a resistor creates positive dissipation for dDEF-P but has zero or negative dissipation for DEF. As a result, for a composite system without a consistent set of energy functions, use of DEF for stability analysis should be avoided. In cases where DEF are applied, it is important to consider which types of problems are being investigating. If it is an electromagnetic resonance, then resistive dissipation is most useful (eDEF-P). When investigating swings of generators, friction dissipation (DEF) is most useful. And if there is a problem with PLL synchronisation, dual friction dissipation can be considered. If a composite oscillation with the interaction of different types of apparatuses is being investigated, it is difficult to trust results from a single version of DEF.

4 Unified Dissipating Energy Flow (uDEF)

4.1 Definition

By comparing across all variants of DEF, and noting the fact that they are essentially different combination of $\Delta I, \Delta V \; and \; \Delta \dot{V}$, here a unified dissipating energy flow (uDEF) method is proposed, which covers all possible definitions of DEF in a bi-linear form.

Formally, uDEF is defined as

$$\mathrm{uDEF} = [\Delta I_d, \Delta I_q] \boldsymbol{W} [\Delta V_d, \Delta V_q, \Delta \dot{V}_d, \Delta \dot{V}_q]^{\mathsf{T}}, \tag{16}$$

where $\boldsymbol{W}$ is a 2×4 weight matrix, I_d and I_q are the currents in *d*-*q* frame, V_d and V_q are the voltages in *d*-*q* frame, the dot over a variable denotes derivation over time $\dot{V} = dV/dt$, and the prefix Δ denotes the small-signal oscillation around the operating point.

4.2 uDEF VS Existing DEF

Based on the flow equation in Table 1, it is easy to find that DEF and its variants can be represented by uDEF with different configurations of $\boldsymbol{W}$. The configurations are summarised in Table 2.

Table 2 Summary of equivalence of existing DEF methods with uDEF.

DEF	Flow	W Configuration
DEF	$\mathrm{Re}(\Delta I^* \Delta \dot{U})$	$\boldsymbol{W} = \begin{bmatrix} 0 & 0 & 0 & 1 \\ 0 & 0 & -1 & 0 \end{bmatrix}$
eDEF-P	$\mathrm{Re}(\Delta I^* \Delta U)$	$\boldsymbol{W} = \begin{bmatrix} 1 & 0 & 0 & 0 \\ 0 & 1 & 0 & 0 \end{bmatrix}$
eDEF-Q	$\mathrm{Im}(\Delta I^* \Delta U)$	$\boldsymbol{W} = \begin{bmatrix} 0 & 1 & 0 & 0 \\ -1 & 0 & 0 & 0 \end{bmatrix}$
cDEF	$\mathrm{Im}(e^{j\phi} \Delta I^* \Delta \dot{V})$	$\boldsymbol{W} = \begin{bmatrix} 0 & 0 & \sin\phi & \cos\phi \\ 0 & 0 & -\cos\phi & \sin\phi \end{bmatrix}$
dDEF	$\mathrm{Im}(\Delta \dot{I}^* \Delta V)$	$\boldsymbol{W} = \begin{bmatrix} 0 & 0 & 0 & -1 \\ 0 & 0 & 1 & 0 \end{bmatrix}$

The detailed proof of the relationships can be found in [9].

4.3 Discussions

While it has been established that all existing DEF methods are equivalent to uDEF under a specific configuration $\boldsymbol{W}$, it remains pertinent to explore whether uDEF encompasses all potential variants of DEF, including those that have yet to be investigated.

Two natural questions first arise: 1) the reason why uDEF focuses solely on the derivation of voltages instead of currents, and 2) the absence of higher-order derivations.

For the first question, integration by parts can be utilised on the derivation of currents as

$$\int \Delta \dot{I} \, \Delta V \, dt = \Delta I \, \Delta V - \int \Delta I \, \Delta \dot{V} \, dt \tag{17}$$

It can be easily found from (17) that $\Delta \dot{I} \Delta V$ and $\Delta I \Delta \dot{V}$ have opposite DC components (represented in the integration) and, therefore, just flip the sign in $\boldsymbol{W}$.

For the second question, a sinusoidal oscillation signal can be given as an example:

$$\Delta V = A\sin(\omega t + \phi) \tag{18}$$

its second-order derivation is

$$\Delta \ddot{V} = -A\omega^2 \sin(\omega t + \phi) = -\omega^2 \Delta V \tag{19}$$

which means $\Delta \ddot{V}$ is proportional to ΔV so higher-order derivations do not generate additional information, provided that the oscillations have a single frequency.

As a result, the uDEF defined in (16) covers all possibilities of variants of DEF.

4.4 Conservation of uDEF

The uDEF exhibits a fundamental property of conservation across the network. Specifically, the quantity of uDEF that enters a node is equal to the quantity that exits, resulting in a net uDEF of zero at any given node. This principle aligns with Kirchhoff's current law:

$$\sum_m \Delta I_{x(m,n)} = 0 \tag{20}$$

where $\Delta I_{x(m,n)}$ is the oscillating current flows from node *m* to node *n*, and *x* denotes either *d* or *q* axis. Multiplying oscillating voltage on the equation yields

$$\sum_m \Delta I_{x(m,n)} \Delta V_{y(n)} = 0 \tag{21}$$

where $\Delta V_{y(n)}$ is the oscillating voltage on node *n*, and *y* also denotes either *d* or *q* axis. Similarly, we have

$$\sum_m \Delta I_{x(m,n)} \Delta \dot{V}_{y(n)} = 0 \tag{22}$$

Combining (20) and (21), and traversing *x* and *y* across *d* and *q*, we get

$$\sum_m \mathrm{uDEF}_{(m,n)} = 0 \tag{23}$$

where $\mathrm{uDEF}_{(m,n)}$ denotes uDEF from node *m* to node *n*.

The conservation property enables users to make distinctions between sources and sinks of uDEF and attribute negative and positive contributions towards system stability accordingly.

5 Connection of uDEF with Damping

There are multiple ways to use uDEF, subject to the configuration of ***W***. It has been shown that the original DEF and cDEF are effective in tracing the conventional oscillations of synchronous generators dominated by angle swings, but not always effective in tracing inverter-induced oscillations. The eDEF, on the other hand, has been demonstrated effective for some inverter-induced oscillations, but there is no guarantee that it will work for all inverter-induced oscillations. A scientific methodology is needed to determine the effectiveness of DEF and select the right version of DEF for a specific type of oscillation.

This section aims to solve this problem by building a connection between uDEF and the damping of the whole system. The term damping has been used extensively in literature, but its actual meaning can be vague. In this paper, we quantify damping precisely by $\mathrm{Re}\lambda$, the real part of the eigenvalues of the whole-system dynamics. This quantification is rationalised by the fact that eigenvalues are directly related to the small-signal stability of the system and are universal and neutral to technologies. We aim to show uDEF is connected to $\mathrm{Re}\lambda$ and this connection determines the effectiveness of uDEF. For this task, two steps are involved: (i) the connection between uDEF and the admittance of the plant where the uDEF is measured, and (ii) the connection between the plant admittance and the whole-system eigenvalue.

5.1 Oscillation Phasor

To assist analysis, we first introduce the concept of oscillation phasor as an extension to the classic phasor method. Consider a sinusoidal oscillating voltage $\Delta V = \sqrt{2}A\sin(\omega t + \phi)$, where A is the root-mean-square (RMS) amplitude of the oscillation, and ω and θ are the angular frequency and phase of the oscillation. The corresponding oscillation phasor $\Delta\tilde{V}$ is defined as

$$\Delta\tilde{V} = A\angle\theta, \tag{24}$$

such that

$$\Delta V = \sqrt{2}\mathrm{Re}\left(\Delta\tilde{V}e^{j\omega t}\right), \tag{25}$$

where we used the standard notation $\angle\theta = e^{j\omega t}$ for brevity.

The oscillation phasor is similar in spirit to the classic phasor, except that the frequency ω here is the oscillation frequency rather than the fundamental frequency, so the properties of classic phasors are inherited by oscillation phasors. The conjugate product of the

current and voltage oscillation phasors gives the complex oscillation power $\Delta\tilde{I}^*\Delta\tilde{V}$, whose real part equals the dc component of the instantaneous oscillation power $\Delta I\Delta V$, that is

$$\mathrm{dc}(\Delta I\Delta V) = \mathrm{Re}\left(\Delta\tilde{I}^*\Delta\tilde{V}\right) \tag{26}$$

where dc(·) denotes the dc component (average value) of a signal. The time derivative of an oscillation signal corresponds to a multiplier of $j\omega$ on the oscillation phasor, that is, $\Delta\dot{V} \sim j\omega\,\Delta\tilde{V}$. Therefore, we have

$$\mathrm{dc}(\Delta I\,\Delta\dot{V}) = \mathrm{Re}(\Delta\tilde{I}^*\,j\omega\,\Delta\tilde{V}) = -\,\omega\,\mathrm{Im}(\Delta\tilde{I}^*\Delta\tilde{V}) \tag{27}$$

If the oscillating current ΔI is induced by the oscillating voltage ΔV applied on an admittance $Y(s)$, we have the following relationships

$$\Delta\tilde{I} = Y(j\omega)\Delta\tilde{V} \tag{28}$$

Combining (26), (27), and (28) yields

$$\mathrm{dc}(\Delta I\Delta V) = A^2\mathrm{Re}Y \tag{29}$$

$$\mathrm{dc}\left(\Delta I\Delta\dot{V}\right) = -A^2\mathrm{Im}Y \tag{30}$$

where we drop the $j\omega$ in $Y(j\omega)$ for brevity. It is clear that $\Delta I\Delta V$ and $\Delta I\Delta\dot{V}$ are proportional to the real and imaginary parts of the admittance *Y*.

5.2 Connection of uDEF with Admittance Matrix

For uDEF with inter-multiplication between *dq* components, the relationship with admittance is similar to (29) and (30) but more complicated due to the cross-coupling between the *d* and *q* axis. To ease notation, we define a matrix version of uDEF as

$$\mathbf{uDEF} = \begin{bmatrix}\Delta I_d \\ \Delta I_q\end{bmatrix}\begin{bmatrix}\Delta V_d & \Delta V_q & \Delta\dot{V}_d & \Delta\dot{V}_q\end{bmatrix} \tag{31}$$

Which is related to (16) by

$$\mathrm{uDEF} = \langle \boldsymbol{W}, \mathbf{uDEF}\rangle_{\mathrm{F}} \tag{32}$$

where $\langle,\rangle_{\mathrm{F}}$ denotes the Frobenius inner product. Essentially, the **uDEF** matrix gives the eight components of uDEF corresponding to the eight elements of ***W***. According to the properties of oscillation phasor

$$\mathrm{dc}(\mathbf{uDEF}) = \mathrm{Re}\left(\begin{bmatrix} \Delta\tilde{I}_d \\ \Delta\tilde{I}_q \end{bmatrix}^* \begin{bmatrix} \Delta\tilde{V}_d & \Delta\tilde{V}_q & j\omega\Delta\tilde{V}_d & j\omega\Delta\tilde{V}_q \end{bmatrix} \right). \tag{33}$$

The current oscillations are related to the voltage oscillations via the admittance matrix $\boldsymbol{Y}$ of the plant under observation

$$\begin{bmatrix} \Delta\tilde{I}_d \\ \Delta\tilde{I}_q \end{bmatrix} = \underbrace{\begin{bmatrix} Y_{dd} & Y_{dq} \\ Y_{qd} & Y_{qq} \end{bmatrix}}_{\boldsymbol{Y}} \begin{bmatrix} \Delta\tilde{V}_d \\ \Delta\tilde{V}_q \end{bmatrix} \tag{34}$$

Which yields

$$\mathrm{dc}(\mathbf{uDEF}) = \mathrm{Re}\left(\boldsymbol{Y}^* \begin{bmatrix} \Delta\tilde{V}_d \\ \Delta\tilde{V}_q \end{bmatrix}^* \begin{bmatrix} \Delta\tilde{V}_d & \Delta\tilde{V}_q & j\omega\Delta\tilde{V}_d & j\omega\Delta\tilde{V}_q \end{bmatrix} \right). \tag{35}$$

Or simply

$$\mathrm{dc}(\mathbf{uDEF}) = \mathrm{Re}\left(\boldsymbol{Y}^* \begin{bmatrix} \boldsymbol{A} & j\omega\boldsymbol{A} \end{bmatrix} \right) \tag{36}$$

where

$$\boldsymbol{A} = \begin{bmatrix} \Delta\tilde{V}_d \\ \Delta\tilde{V}_q \end{bmatrix}^* \begin{bmatrix} \Delta\tilde{V}_d & \Delta\tilde{V}_q \end{bmatrix} \tag{37}$$

represents the amplitudes of the voltage oscillations. (36) can be rewritten as

$$\mathrm{dc}(\mathbf{uDEF}_{[1:2]}) = \mathrm{Re}\left(\boldsymbol{Y}^* \boldsymbol{A} \right) \ , \ \mathrm{dc}(\mathbf{uDEF}_{[3:4]}) = -\omega\,\mathrm{Im}\left(\boldsymbol{Y}^* \boldsymbol{A} \right) \tag{38}$$

where we use the subscript [:] to denote a sub-matrix containing the corresponding columns (e.g., $\mathbf{uDEF}_{[1:2]}$ means the first and second columns of **uDEF)**. From the equation above, we see that

$$\boldsymbol{Y}^* \boldsymbol{A} = \mathrm{dc}\left(\mathbf{uDEF}_{[1:2]} - j\omega^{-1}\ \mathbf{uDEF}_{[3:4]} \right) \tag{39}$$

so we define the complex matrix

$$\mathbf{uDEF}_c = \mathbf{uDEF}_{[1:2]} + j\omega^{-1}\ \mathbf{uDEF}_{[3:4]} \tag{40}$$

which is related to the admittance matrix by

$$\boldsymbol{Y} = \mathrm{dc}(\mathbf{uDEF}_c)\ \boldsymbol{A}^{*-1} \tag{41}$$

It is clear that there is a one-to-one linear mapping between uDEF and the admittance matrix.

5.3 Connection of Admittance with Damping

The connection between the whole-system eigenvalue and the admittance of a plant has been established in previous work on admittance (impedance) Sensitivity [9][11]

$$\Delta\lambda = -\left\langle \mathrm{Res}_\lambda^* \hat{\boldsymbol{Z}}^\top, \Delta \boldsymbol{Y} \right\rangle_{\mathrm{F}} \tag{42}$$

where Res_λ is the residue of a transfer function at the pole (eigenvalue) λ associated with the oscillation ($\lambda = \sigma \pm j\omega$), $\hat{\boldsymbol{Z}}$ is the whole-system impedance at the node under investigation, and $\boldsymbol{Y}$ is the admittance of the plant connected to the same node.

$$\Delta\lambda = -\epsilon\left\langle \boldsymbol{A}^{-\top} \mathrm{Res}_\lambda^* \hat{\boldsymbol{Z}}^\top, \mathrm{dc}(\mathbf{uDEF}_c) \right\rangle_{\mathrm{F}} \tag{43}$$

$$\mathrm{Re}\Delta\lambda = -\epsilon\left\langle \left[\mathrm{Re}(\boldsymbol{A}^{-\top} \mathrm{Res}_\lambda^* \hat{\boldsymbol{Z}}^\top) \quad \omega^{-1}\mathrm{Im}(\boldsymbol{A}^{-\top} \mathrm{Res}_\lambda^* \hat{\boldsymbol{Z}}^\top)\right], \mathrm{dc}(\mathbf{uDEF}) \right\rangle_{\mathrm{F}} \tag{44}$$

Therefore, uDEF will precisely indicate the contribution towards damping from the plant under observation if

$$\boldsymbol{W} = \left[\mathrm{Re}(\boldsymbol{A}^{-\top} \mathrm{Res}_\lambda^* \hat{\boldsymbol{Z}}^\top) \quad \omega^{-1}\mathrm{Im}(\boldsymbol{A}^{-\top} \mathrm{Res}_\lambda^* \hat{\boldsymbol{Z}}^\top)\right] \tag{45}$$

5.4 Discussions on Use of uDEF

Although it is proved in Section 5.3 that uDEF is linked with the the change on damping of the oscillatory mode, it is difficult to find the exact **W** which make uDEF and $\mathrm{Re}\Delta\lambda$ identical. This is because the matrix ***A*** defined in (37) is singular, meaning it does not have an inverse in the traditional sense. Therefore, equation (41) does not have a unique solution. For practical applications, the proper configuration of ***W*** depends on the cause of the oscillations. Nonetheless, trying different configurations of W can provide insightful information. The results are provided in the next Section.

6 Case Studies

In this section, 3 case studies are provided to demonstrate the uDEF results from different configurations of ***W*** for typical oscillations.

6.1 Case-1: 8.8 Hz Oscillation Caused by IBR Current Controller

A modified IEEE 14-bus with 3 extra grid-following IBRs is employed for the oscillation study, as shown in Figure 1.

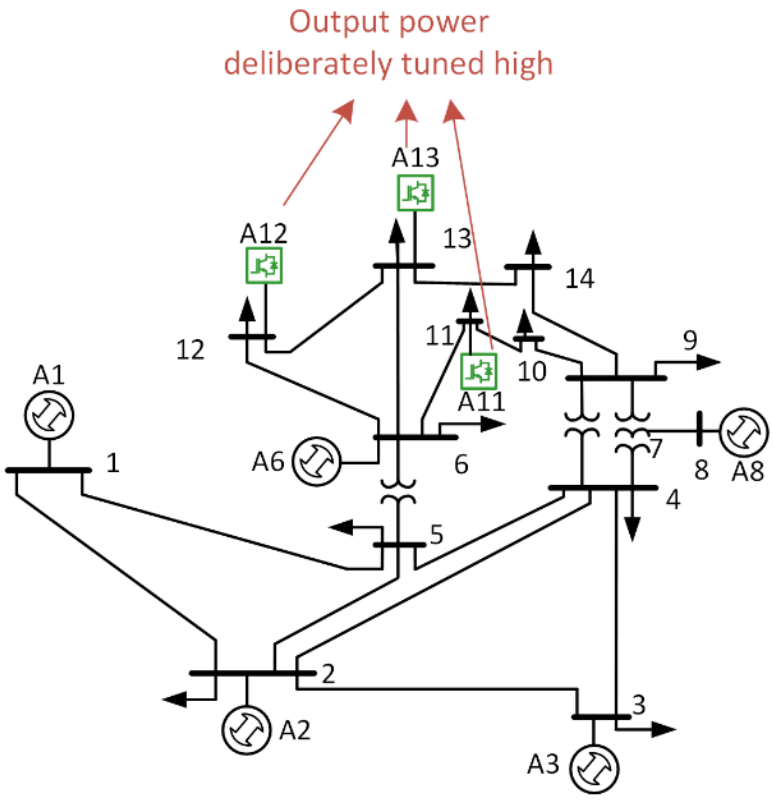

Figure 1 Modified IEEE 14-bus system with 3 extra grid-following IBRs connected to bus-11,12,13. The current control bandwidth of A11, A12, A13 is deliberately tuned low, with A12 tuned the worst: 280 Hz for A11 and A13, 180 Hz for A12.

The deliberately detuned current controller of the IBRs creates an oscillatory mode of 8.8 Hz on the right-half plane, hence creating oscillations in the system, as shown in Figure 2.

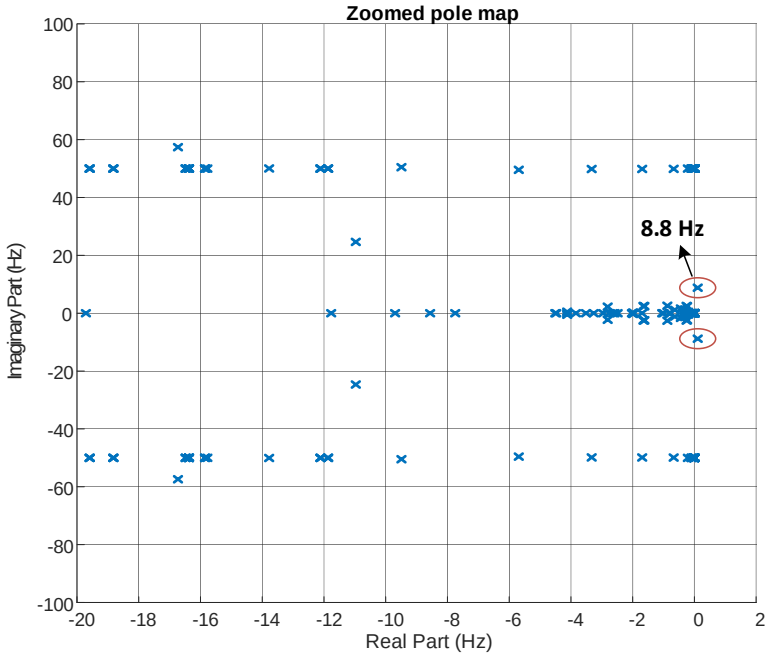

(a)

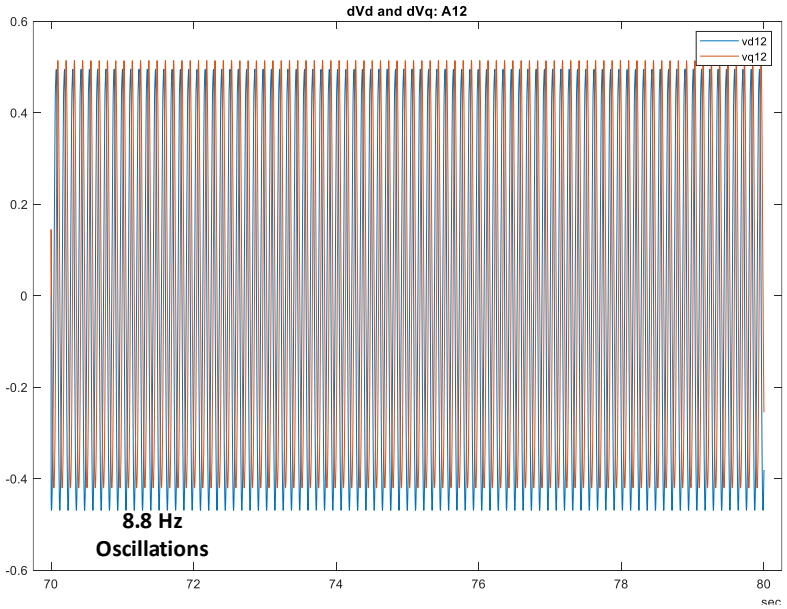

(b)

Figure 2 (a) Eigenvalue plot shows an 8.8 Hz mode on the right-half plane, meaning a free oscillation at 8.8 Hz will occur. (b) Time-domain simulation results of ΔV_d and ΔV_q of A12 confirm the free oscillation at 8.8 Hz.

The impedance-based participation analysis, namely the grey-box approach [11], is first applied to analyse the mode and set the ground truth, and the results are shown in Figure 3. It is pointed out from the grey-box approach layer-1 that the dominant of the 8.8 Hz

mode is A12, while A11, A13, and A6 are other major participants. From Layer-2, as in Figure 3 (b), it is clear that A11, A12 and A13 are providing the negative damping while A6 is providing the positive damping to the mode. Figure 3 (c) indicates the influence of each apparatus on the mode's frequency.

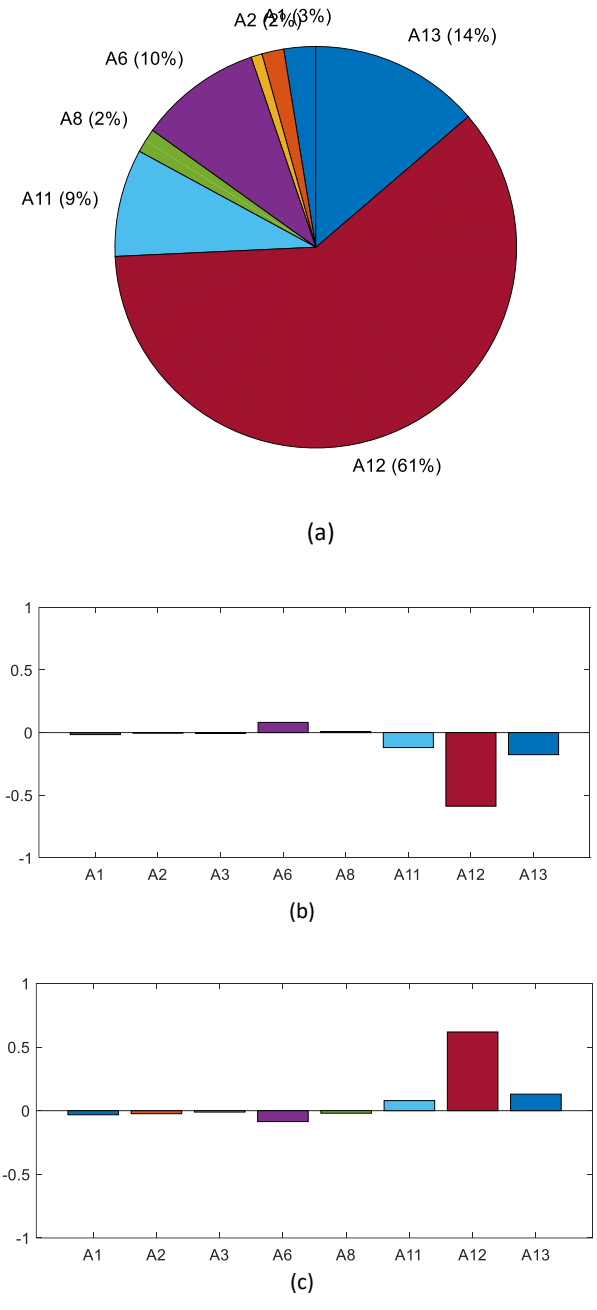

Figure 3 Grey-box approach on the 8.8 Hz mode: (a) Results from Layer-1 showing major participants, (b) Results from layer-2 showing influences on the mode's damping, and (c) Results from layer-2 showing influences on the mode's frequency.

uDEF is then calculated at each apparatus using 10~s of the measured ΔV_d, ΔV_q, ΔI_d, ΔI_q, with different configurations of ***W***. For each configuration, only one element in ***W*** is set as one, and all other elements are zero. The sampling rate is 1000 Hz. The integration of uDEF results is shown in Figure 4, in which the apparatus are separated from each other such that a comparison can be made to justify the root cause.

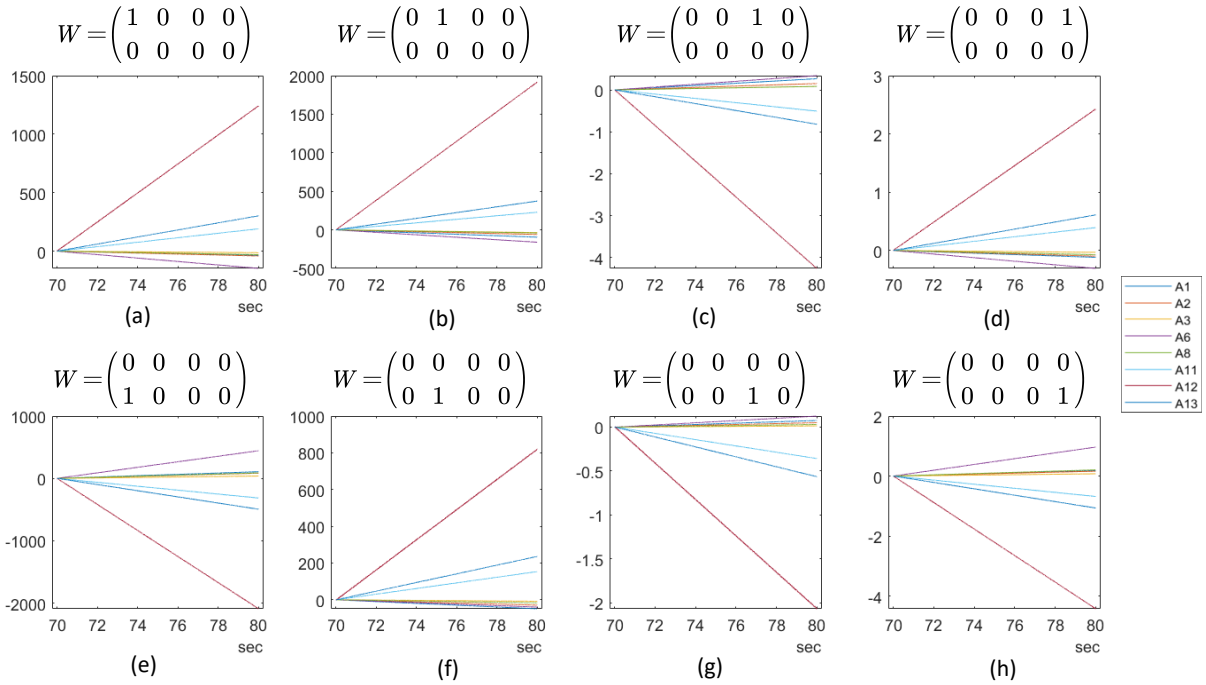

*Figure 4 uDEF integration of Case-1 with different configurations of **W**, the exact **W** is shown above each subfigures.*

To better pinpoint the oscillation sources, a set of bar charts is plotted using the normalised final value from the uDEF integration, as shown in Figure 5. It is noticed that, A12 stands out in all 8 plots, followed by A11 and A13. It means that for this 8.8 Hz mode, all 8 configurations of ***W*** can give the correct, or nearly correct indications. Although some configurations may show a reversed direction, they can be easily corrected by multiplying ***W***.

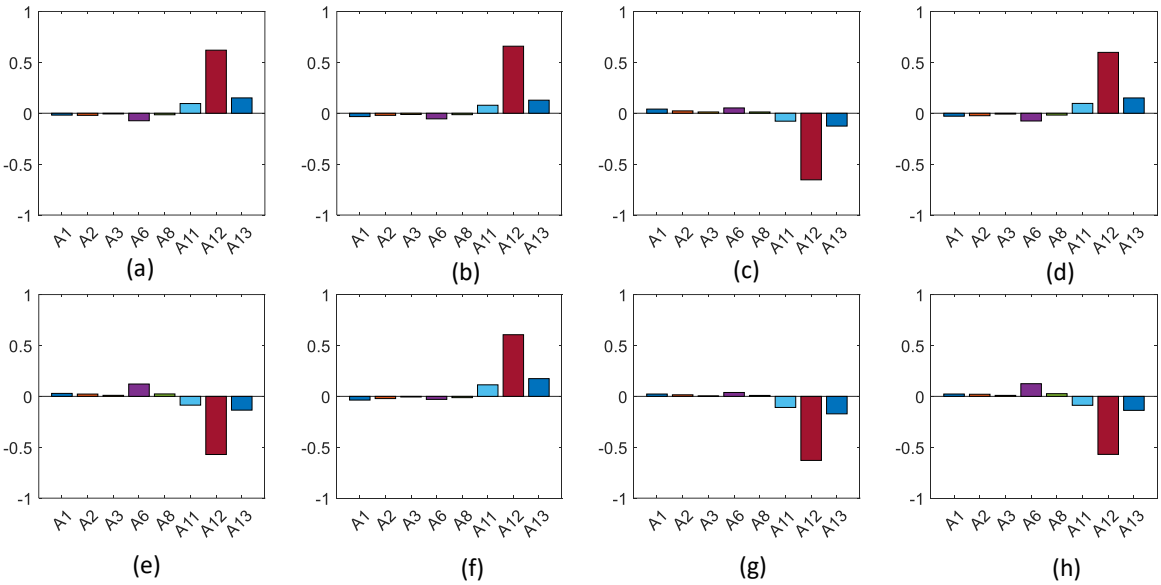

*Figure 5 Bar charts of the integration of uDEF with different configurations of **W**. The exact **W** matches with Figure 4. Values are normalised to the summation of absolute values of all bars. Positive bars refer to oscillation sources since generator convention is used.*

6.2 Case-2: 1.5 Hz Oscillation Caused by IBR Power Increment

This case uses the same modified IEEE 14-bus, while the output power of A12, A13 and A14 is increased from 0.1~pu to 1.3~pu, as shown in Figure 6.

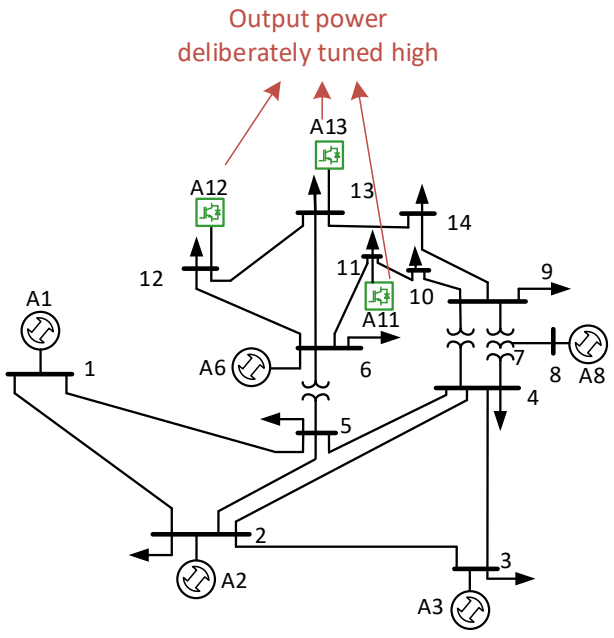

Figure 6 The modified IEEE 14-bus network. The output power of A11, A12, A13 is deliberately tuned high.

The high output power of the IBR creates a 'weak' grid environment and eventually leads to a 1.5 Hz oscillatory mode, as shown in Figure 7.

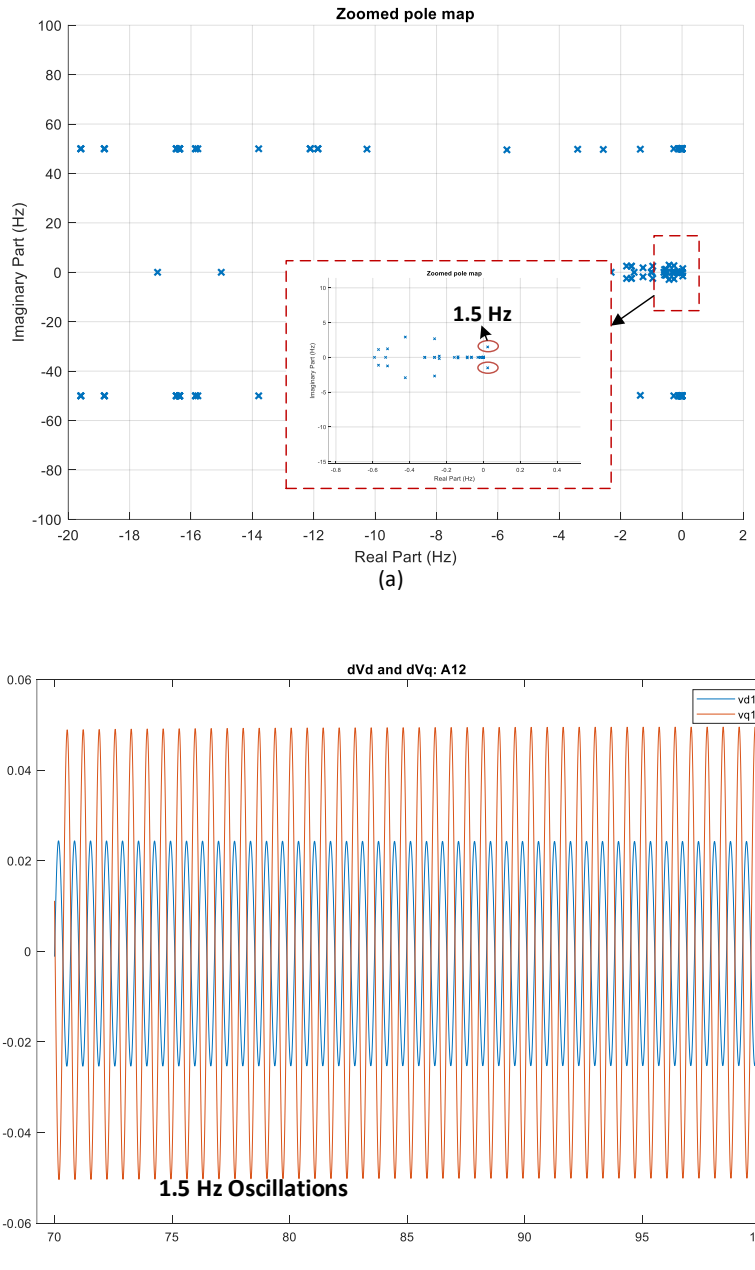

Figure 7 (a) Eigenvalue plot shows a 1.5 Hz mode on the right-half plane, meaning a free oscillation at 1.5 Hz will occur. (b) Time-domain simulation results of ΔV_d and ΔV_q of A12 confirm the free oscillation at 1.5 Hz.

Results from the Grey-box Approach, as shown in Figure 8, correctly indicate that the mode is from interactions among the three IBRs and A1 which is the slack bus generator absorbing the extra power.

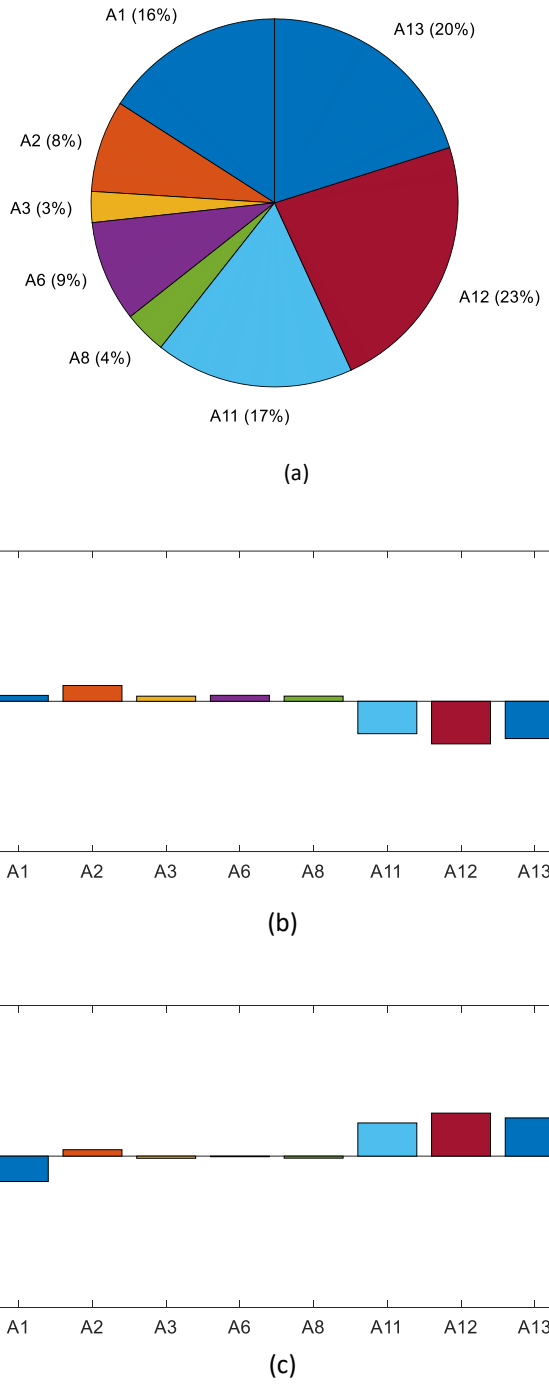

Figure 8 Grey-box approach on the 1.5 Hz mode: (a) Results from Layer-1 showing major participants, (b) Results from layer-2 showing influences on the mode's damping, and (c) Results from layer-2 showing influences on the mode's frequency.

Values of the integration of uDEF with different configurations of W are demonstrated in Figure 9. It is identified that configurations (e) and (f) can give the correct indication, while

(a) and (b) give mostly correct indications but wrongly pinpoint A6 as a major participant. Configurations (c), (d), (g) and (h) provide wrong insights on this mode.

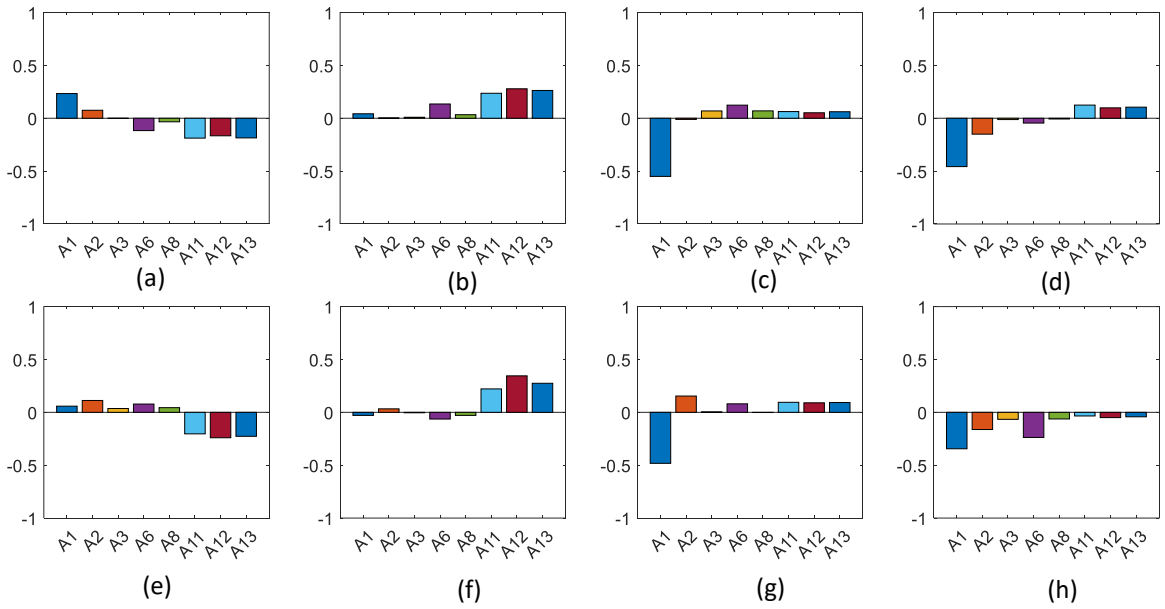

*Figure 9 Bar charts of the integration of uDEF with different configurations of **W**. Values are normalised to the summation of absolute values. Positive bars refer to oscillation sources since generator convention is used.*

6.3 Case-3: 20 Hz Oscillation Caused by IBR Voltage Controller

A 7-bus network consisting of one synchronous generator and five gird-following IBRs is established, as shown in Figure 10.

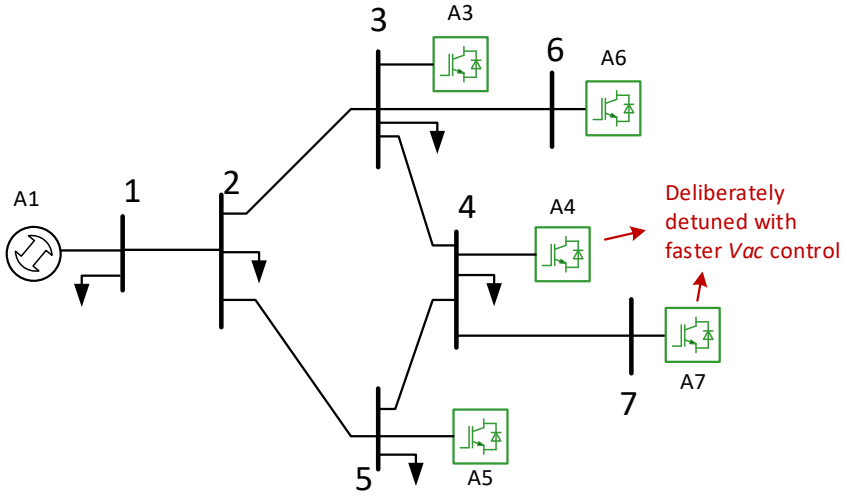

Figure 10 7-bus network. The voltage control of A4 and A7 is deliberately tuned high.

Each IBR is equipped with an AC voltage controller. The voltage control bandwidth of A4 and A7 is deliberately detuned high to create interactions among these two IBRs and further leads to a 20 Hz oscillatory mode. The system modes and the time-domain waveforms are shown in Figure 11.

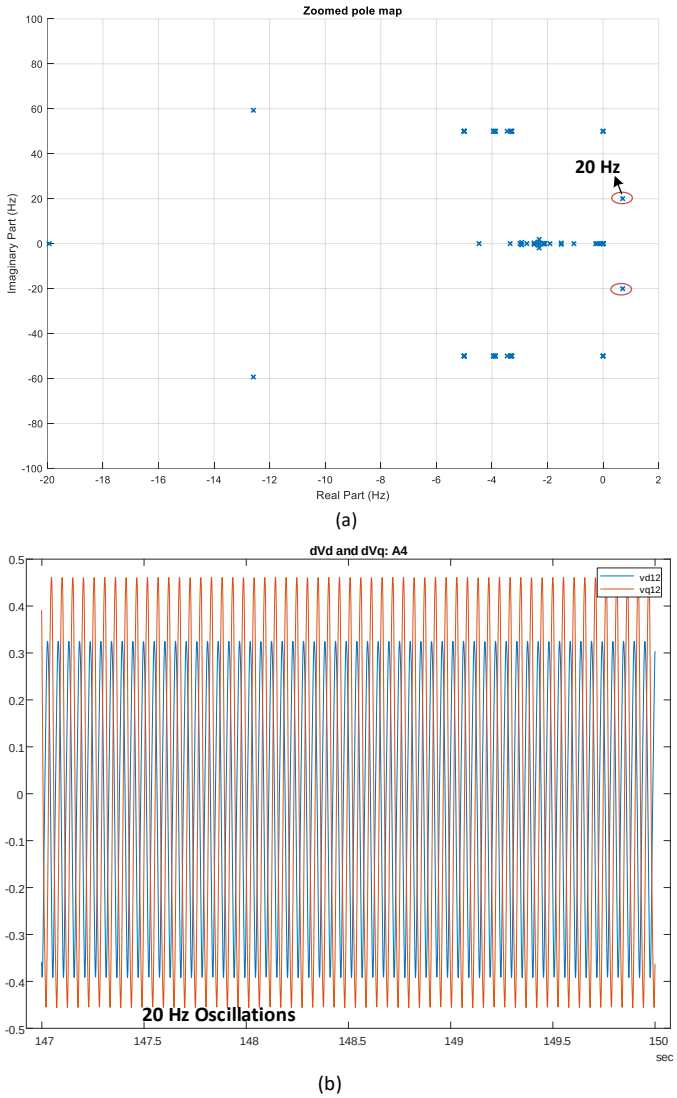

Figure 11 (a) Eigenvalue plot shows a 20 Hz mode on the right-half plane, meaning a free oscillation at 20 Hz will occur. (b) Time-domain simulation results of ΔV_d and ΔV_q of A4 confirm the free oscillation at 20 Hz.

From the results from the Grey-box approach Layer-1, as shown in Figure 12 (a), A4 and A7 are the major participants of the 20 Hz mode, which aligns with the system's configuration. In Layer-2, it is found that all apparatus are providing negative damping to the mode, while among them A4 and A7 are the main root causes, as shown in Figure 12 (b). From the impact on the oscillatory frequency shown in Figure 12 (c), it is noted that A3 and A6

are creating the major effects. Nevertheless, it is concluded that A4 and A7 are the root causes of the mode.

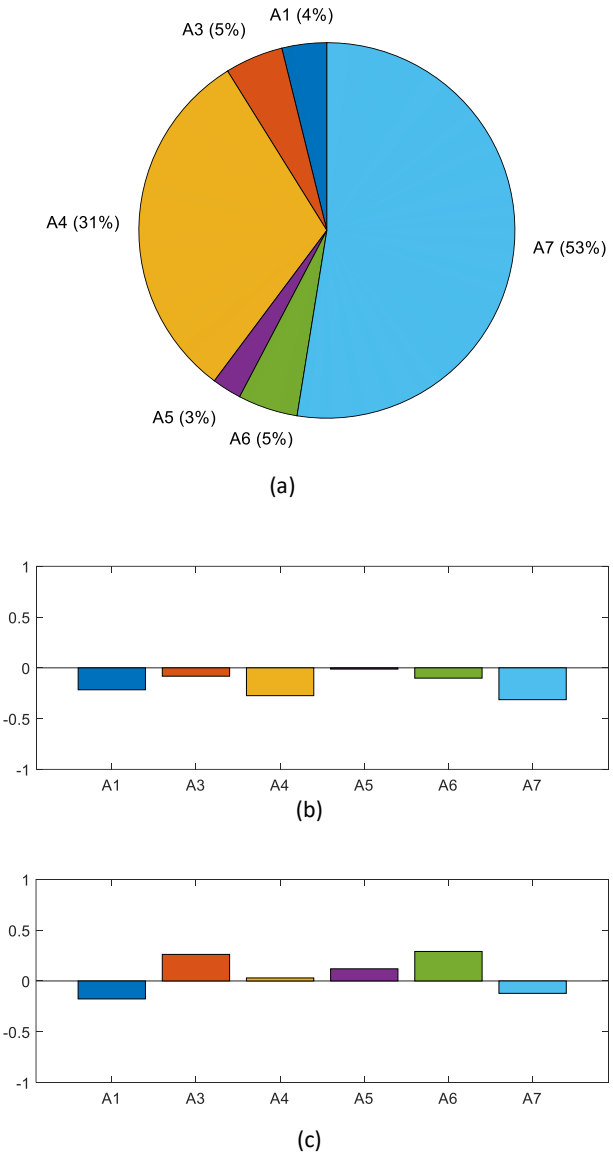

Figure 12 Grey-box approach on the 20 Hz mode: (a) Results from Layer-1 showing major participants, (b) Results from layer-2 showing influences on the mode's damping, and (c) Results from layer-2 showing influences on the mode's frequency.

uDEF calculation is then applied to the sampled current and voltage at different buses. Values of the integration of uDEF with different configurations of ***W*** are demonstrated in Figure 13. It is identified that only configurations (f) and (g) can successfully identify A4 and A7 as the root causes of the 22 Hz mode, while others are given wrong indications.

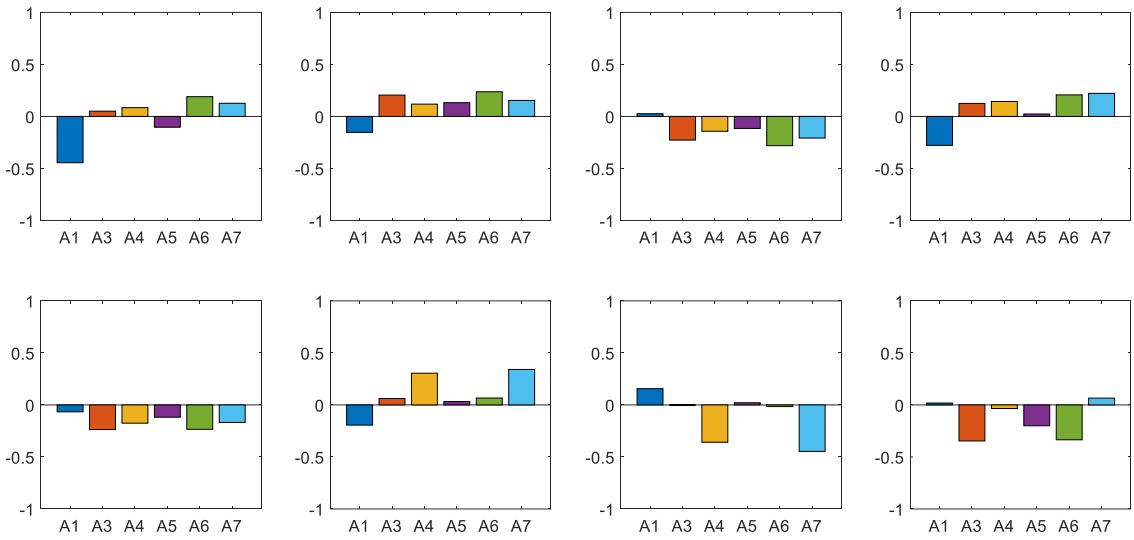

*Figure 13 Bar charts of the integration of uDEF with different configurations of **W**. Values are normalised to the summation of absolute values. Positive bars refer to oscillation sources since generator convention is used.*

6.4 Discussions

Across the three different oscillation case studies, the correct indications of the oscillation root causes come from different configurations of $\boldsymbol{W}$, depending on how the mode is introduced. Nevertheless, it is noted that the configuration (f), for which

$$\boldsymbol{W}_f = \begin{pmatrix} 0 & 0 & 0 & 0 \\ 0 & 1 & 0 & 0 \end{pmatrix} \tag{46}$$

gives the correct indication for all three typical oscillations. According to the definition of uDEF, such configuration referees to

$$\mathrm{uDEF}_f = \Delta I_q \Delta V_q. \tag{47}$$

It means that the oscillation source has a negative resistance in the q axis at the oscillatory frequency. Typically, the phase-lock loop (PLL) of grid-following IBR shapes the impedance of IBR into a negative resistance in the q axis [11], meaning that for modes in which PLL is participating, $\boldsymbol{W}_f$ is a promising configuration of $\boldsymbol{W}$. For the above three cases, further indicated by the Grey-box Layer-3 (the parameter participation), PLL indeed was participating. Nevertheless, further investigations on configurations of $\boldsymbol{W}$ for different scenarios are still needed

*Table 3 Comparison of uDEF results with different configurations of **W**: T for true, F for false indication of souses and sinks of oscillations.*

Group	***W***	Case 1 – 8.8 Hz	Case 2 – 1.5 Hz	Case 3 – 20 Hz
a	$\begin{pmatrix} 1 & & \\ & & \\ & & \end{pmatrix}$	T	F	F
b	$\begin{pmatrix} & 1 & \\ & & \\ & & \end{pmatrix}$	T	F	F
c	$\begin{pmatrix} & & 1 \\ & & \\ & & \end{pmatrix}$	T	F	F
d	$\begin{pmatrix} & & \\ & & \\ & & 1 \end{pmatrix}$	T	F	F
e	$\begin{pmatrix} & & \\ 1 & & \\ & & \end{pmatrix}$	T	T	F
f	$\begin{pmatrix} & & \\ & 1 & \\ & & \end{pmatrix}$	T	T	T
g	$\begin{pmatrix} & & \\ & & \\ & 1 & \end{pmatrix}$	T	F	T
h	$\begin{pmatrix} & & \\ & & \\ & & 1 \end{pmatrix}$	T	F	F

7 Conclusions

This supplementary introduces the principles of DEF and its variants, and proposed a unified DEF (uDEF) which covers existing DEF and its variants, as well as any possible variants. It holds the conservation property such that it can identify the sources and sinks of oscillations. It is also theoretically proved that uDEF is linked with the oscillation damping, i.e., the real part of the system eigenvalue. Three case studies and discussions are provided on the configuration of ***W*** for uDEF for typical oscillations.

8 References

[1] Cheng, Y., et al. (2023). "Real-World Subsynchronous Oscillation Events in Power Grids With High Penetrations of Inverter-Based Resources." IEEE Transactions on Power Systems 38(1): 316-330.

[2] J. Bialek, “What does the GB power outage on 9 august 2019 tell us about the current state of decarbonised power systems?,” Energy Policy, vol. 146, 2020, Art. no. 111821.

[3] L. Chen, Y. Min and W. Hu, "An energy-based method for location of power system oscillation source," in IEEE Transactions on Power Systems, vol. 28, no. 2, pp. 828-836, May 2013, doi: 10.1109/TPWRS.2012.2211627.

[4] S. Maslennikov and E. Litvinov, "ISO New England Experience in Locating the Source of Oscillations Online," in IEEE Transactions on Power Systems, vol. 36, no. 1, pp. 495-503, Jan. 2021, doi: 10.1109/TPWRS.2020.3006625.

[5] Fan, Lingling; Wang, Zhengyu; Miao, Zhixin; Maslennikov, Slava (2023). Oscillation Source Detection for Inverter-Based Resources via Dissipative Energy Flow. TechRxiv. Preprint. https://doi.org/10.36227/techrxiv.22178966.v1

[6] P. G. Estevez, P. Marchi, C. Galarza and M. Elizondo, "Complex Dissipating Energy Flow Method for Forced Oscillation Source Location," in IEEE Transactions on Power Systems, vol. 37, no. 5, pp. 4141-4144, Sept. 2022, doi: 10.1109/TPWRS.2022.3184119.

[7] Y. Li, Y. Gu and T. C. Green, "Revisiting Grid-Forming and Grid-Following Inverters: A Duality Theory," in IEEE Transactions on Power Systems, vol. 37, no. 6, pp. 4541-4554, Nov. 2022, doi: 10.1109/TPWRS.2022.3151851.

[8] X. Xie, Y. Zhan, J. Shair, Z. Ka and X. Chang, "Identifying the Source of Subsynchronous Control Interaction via Wide-Area Monitoring of Sub/Super-Synchronous Power Flows," in *IEEE Transactions on Power Delivery*, vol. 35, no. 5, pp. 2177-2185, Oct. 2020, doi: 10.1109/TPWRD.2019.2963336.

[9] Y. Zhu, H. Karbouj, X. Zhou, Y. Gu, “Unified Dissipation Energy Flow,” TechRxiv. August 12, 2024. DOI: 10.36227/techrxiv.172348945.56366598/v1.

[10] Y. Zhu, Y. Gu, Y. Li and T. C. Green, "Impedance-Based Root-Cause Analysis: Comparative Study of Impedance Models and Calculation of Eigenvalue Sensitivity," in IEEE Transactions on Power Systems, vol. 38, no. 2, pp. 1642-1654, March 2023, doi: 10.1109/TPWRS.2022.3179143.

[11] Y. Zhu, Y. Gu, Y. Li and T. C. Green, "Participation Analysis in Impedance Models: The Grey-Box Approach for Power System Stability," in IEEE Transactions on Power Systems, vol. 37, no. 1, pp. 343-353, Jan. 2022, doi: 10.1109/TPWRS.2021.3088345.

[12] J. Fang, X. Li, H. Li and Y. Tang, "Stability Improvement for Three-Phase Grid-Connected Converters Through Impedance Reshaping in Quadrature-Axis," in IEEE Transactions on Power Electronics, vol. 33, no. 10, pp. 8365-8375, Oct. 2018, doi: 10.1109/TPEL.2017.2777972.

NESO
National Energy System Operator

Delivered in Partnership with
Imperial College London

Supplementary Report 2

Data-Driven Online Monitoring and Early Warning for GB System Stability (DOME)

Independent expert analysis/opinion provided by:
Dr Yue Zhu, Dr Yunjie Gu, Prof. Tim Green
Department of Electrical and Electronic Engineering,
Imperial College London

NESO
National Energy System Operator

1 Contents

TABLES

FIGURES

2 Introduction

This report covers the topics of whole-system impedance/admittance models, methods of injecting different types of signals into the system, and identifying the whole-system impedance/admittance. Different methods for impedance identification, including time-domain identification (TDID) and frequency-domain identification (FDID), are discussed in this report with their relative merits analysed. A Hybrid Data/Model-Driven Impedance Identification method is proposed, which offers a way of restoring the whole-system impedance model from a combination of existing knowledge of the system network model and the time-domain voltage/current data. EMT simulation results will also be provided to demonstrate the process of impedance/admittance model identification, and its application in root-cause tracing. If not specifically stated otherwise, the impedance/admittance models mentioned in this report refer to frequency-domain models, rather than single (complex) values of impedance/admittance at the system base frequency. They could be state-space models, transfer functions, or frequency spectra in discrete format (frequency response data). Some results from this report have been concluded into a journal paper and submitted to IEEE Transactions on Industrial Electronics, with a preprint available online [1] .

This report serves as a supplementary report for DOME Final Report. It is developed originally from DOME WP2&3 Report but with updates in both theory and simulation results.

3 Whole-system Impedance Model

3.1 Introduction

The whole-system impedance model, or equivalently, whole-system admittance model is formalised based on a separation between the shunt-connected apparatus appearing at nodes and the lines and cables of the branches of the network that connect nodes. Thus, the system is separated into a nodal admittance matrix Y_N and an apparatus matrix Y_A. The whole-system impedance model Z^{sys} and the whole-system admittance model Y^{sys} are formed as illustrated in Figure 1.

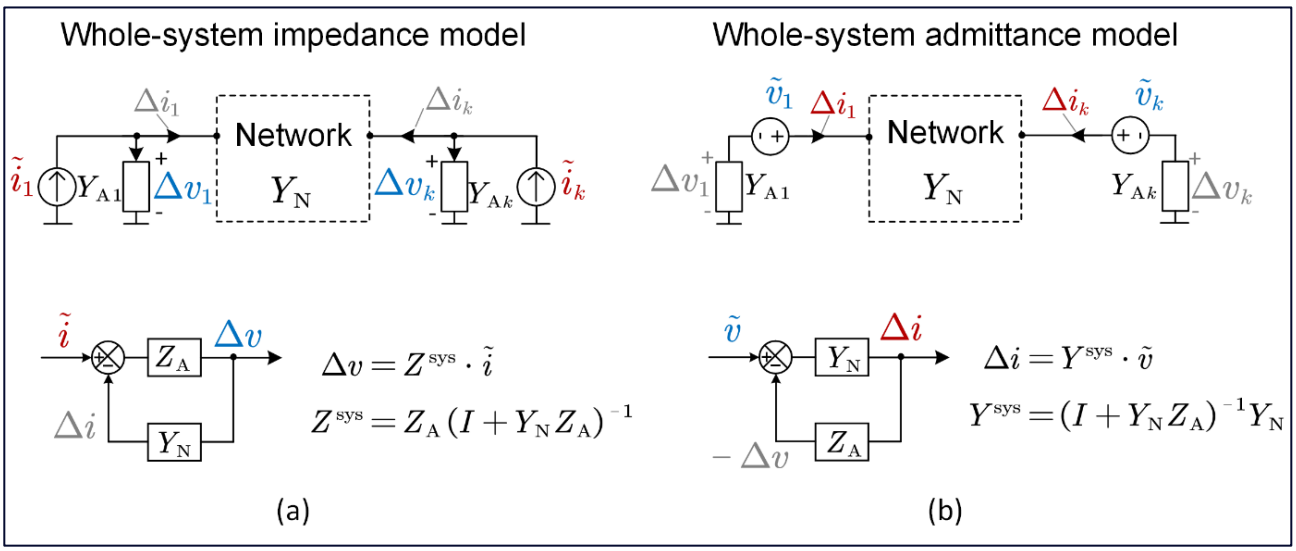

Figure 1 Formation of whole-system admittance model: by introducing small voltage perturbations at each port and taking out the current response forms the transfer function of whole-system admittance model.

Taking Z^{sys} as an example, the model is formed with a virtual nodal injection of current $\tilde{\imath}$ whereas for the nodal admittance model the injection is a nodal voltage. The current injection $\tilde{\imath}$ causes a change in current through the apparatus and therefore a change in the apparatus voltage Δv, which in turn creates a change of current flowing into the network Δi, which changes the current flow in the apparatus in a feedback fashion. This feedback arrangement is illustrated in Figure 1 (a). The response Δv to perturbation $\tilde{\imath}$ is

$$\Delta v = Z_A\,(I + Y_N Z_A)^{-1}\tilde{\imath} \tag{1}$$

where I is identity matrix and Z_A is the apparatus impedance matrix defined in the same fashion of Y_A but with apparatus impedance as its diagonal elements, i.e.,

$$Z_A = \begin{bmatrix} Z_{A1} & & \\ & \ddots & \\ & & Z_{AN} \end{bmatrix} \tag{2}$$

and $Z_{Ak} = (Y_{Ak})^{-1}$.

The whole-system impedance model is defined from equation (1) as

$$Z^{sys} = Z_A\,(I + Y_N Z_A)^{-1} \tag{3}$$

Similarly, the formulation of the whole-system admittance model is shown in Figure 1(b), using a series injection of voltage and a response in terms of current. The model is defined as

$$Y^{sys} = (I + Y_N Z_A)^{-1} Y_N \tag{4}$$

It is worth noting that Z^{sys} and Y^{sys} relate to the case where the system is complete: all devices are connected and form a closed-loop relationship.

The formulations Z^{sys} and Y^{sys} view the entire system as a multi-input multi-output (MIMO) system, as shown in Figure 2.

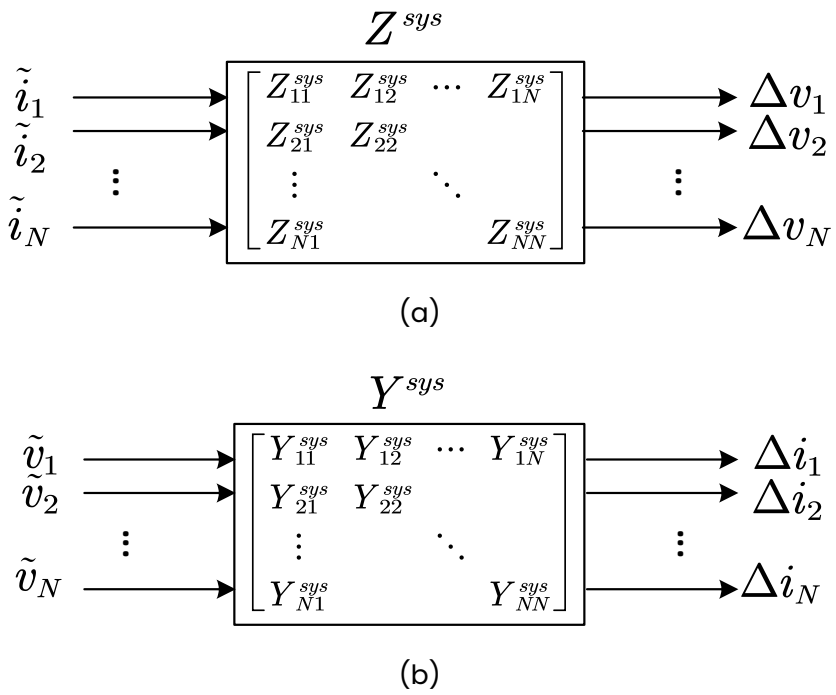

Figure 2 Illustration of MIMO systems: (a) whole-system impedance model Z^{sys}, (b) whole-system admittance model Y^{sys}.

Taking Z^{sys} as an example, its input $\{\tilde{\imath}_1, \tilde{\imath}_2, \cdots, \tilde{\imath}_N\}$ are the current perturbations introduced at each point of common coupling (PCC), and its output $\{\Delta v_1, \Delta v_2, \cdots, \Delta v_N\}$ are the corresponding voltage responses at each PCC. Since it is the closed-loop model of the system, the criteria for the system being stable is that all poles of Z^{sys} must be in the left-half plane. It is further proved in [1] that all elements in the matrix of Z^{sys} share the same poles, which equal to the eigenvalues of the system state-space model and represent the system oscillatory modes.

3.2 Whole-system impedance model for root-cause tracing

Oscillation analysis and root-cause tracing based on whole-system impedance model have been fully discussed in [3] and [4], and they are briefly introduced here.

Essentially, the system oscillatory behaviour is dependent on the eigenvalues of the state-space matrix A. For a physical system, an eigenvalue λ is either a real number or a pair of conjugate complex values. When λ is conjugate complex, i.e.,

$$\lambda = \sigma \pm j\omega, \lambda \in eig(A) \tag{5}$$

λ refers to an oscillatory mode in the system, where σ refers to the damping of the mode (the rate at which an oscillation is dampened) and ω is the oscillation frequency. When there is a mode with a small damping factor in the system, one expects to see long-lasting oscillations in the system variables following a small disturbance such as a small step change in the load or in the voltage, or an impulse like a lightning strike.

Now consider a small change added to the impedance of an IBR connected at bus-*k*, ΔZ_{Ak}, while the rest of the system unchanged. This change can be caused by a small perturbation of a control parameter of the IBR, a variation of its operating point, or scaling up or down by connecting or disconnecting a portion of apparatus from a farm of apparatuses (e.g. a wind farm). The change ΔZ_{Ak} will lead to a variation on the system eigenvalue λ, i.e., $\Delta\lambda$. If in a single-phase system where Z_{Ak} is a scalar transfer function, and within a small range around $s = \lambda$, $\Delta\lambda$ can be calculated as

$$\Delta\lambda = \frac{\partial\lambda}{\partial Z_{Ak}(\lambda)} \cdot \Delta Z_{Ak}(\lambda) \tag{6}$$

where $\frac{\partial\lambda}{\partial Z_{Ak}(\lambda)}$ represents the sensitivity of λ to the impedance of the IBR at bus-*k* at $s = \lambda$. According to the discussion in [3], such sensitivity equals the negative of the residue of Y_{kk}^{sys} at its pole $s = \lambda$, i.e.,

$$\frac{\partial\lambda}{\partial Z_{Ak}(\lambda)} = -\mathrm{Res}_{\lambda} Y_{kk}^{sys} \tag{7}$$

where $\mathrm{Res}_{\lambda} Y_{kk}^{sys}$ represents the residue of Y_{kk}^{sys} at $s = \lambda$. Substituting (7) into (6) yields

$$\Delta\lambda = -\mathrm{Res}_{\lambda} Y_{kk}^{sys} \cdot \Delta Z_{Ak}(\lambda) \tag{8}$$

In a more common scenario where the *dq*-synchronous frame is employed and $\Delta Z_{Ak}(\lambda)$ and Y_{kk}^{sys} are 2×2 square matrices, (8) can be modified to become

$$\Delta\lambda = \langle -\mathrm{Res}_{\lambda}^{*} Y_{kk}^{sys}, \Delta Z_{Ak}(\lambda) \rangle \tag{9}$$

where $\mathrm{Res}_{\lambda}^{*} Y_{kk}^{sys}$ is the conjugate transpose of the matrix of residues of Y_{kk}^{sys} at $s = \lambda$, and $\langle \cdot, \cdot \rangle$ denotes the Frobenius inner product of the two matrices. It follows from (9) that $\mathrm{Res}_{\lambda}^{*} Y_{kk}^{sys}$ quantifies how the perturbation of impedances yields the perturbation of eigenvalues and therefore is called impedance participation factor. For an observed oscillatory mode, the

larger the value of $\mathrm{Res}_{\lambda}^{*}Y_{kk}^{sys}$ that is found at bus-*k*, the larger is the participation of the apparatus at bus-*k* in the mode, and hence apparatus at buses with large residuals can be considered as the root-causes of the oscillation. For a more precise tracing, the impedance-based grey-box approach is available, as shown in Figure 2. Since this project is focused mainly on root-cause tracing, only Layer-1 (for participant analysis) and Layer-2 (for positive and negative damping provision) are of interest. This use of residuals of modes seen in impedance spectra to identify root-causes of oscillations is the fundamental method applied in this NIA project.

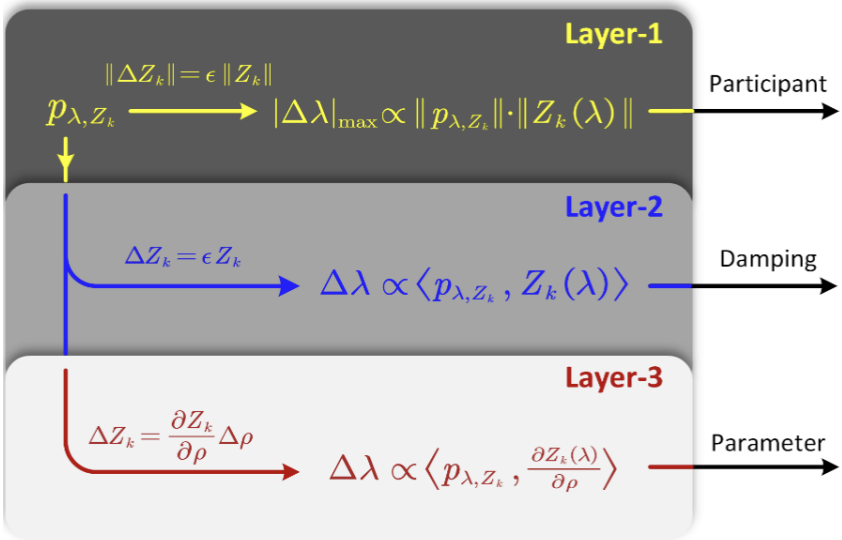

Figure 3 The Grey-box approach [3].

4 Whole-system Impedance Identification

4.1 Introduction

The process of system identification is performed by applying a known input to the system and observing the system output. The model is then estimated from the relationship between the input and output. For whole-system models based on Figure 2, it is clear that we will need to introduce small-signal current perturbations and measure the voltage responses at each PCC to estimate Z^{sys}. Alternatively, it is possible to introduce small-signal voltage perturbations and measure the current flow through the PCC to estimate Y^{sys}. The injection topologies at a PCC are illustrated in Figure 4.

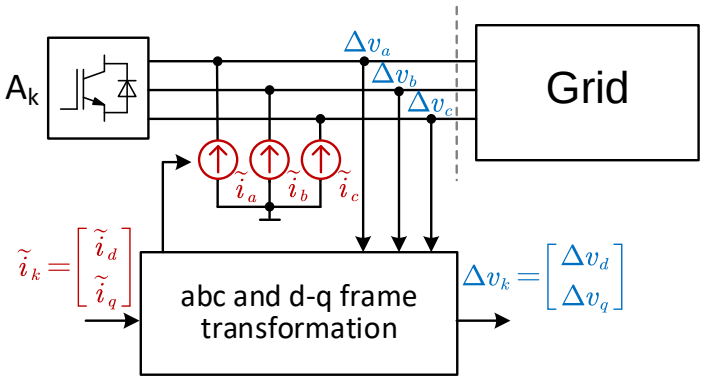

(a)

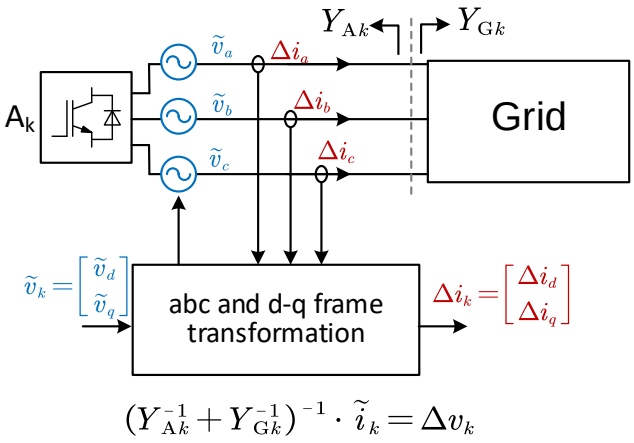

(b)

Figure 4 small-signal injections for (a) whole-system impedance identification and (b) whole-system admittance identification.

4.2 *dq*-Frame identification

It is worth noting that since the system is a three-phase system, the impedance/admittance models are all represented in a *dq* synchronous frame, so that each input is a 2×1 vector and each output is a 2×1 vector. Taking Z^{sys} as an example, Figure 2(a) should be modified to be as shown in Figure 5.

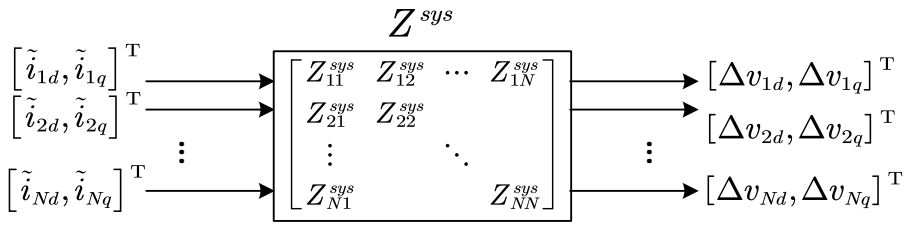

Figure 5 MIMO system in dq-frame.

Each element in Z^{sys} is then a 2×2 matrix block as

$$Z_{kk}^{sys} = \begin{bmatrix} Z_{kk,dd}^{sys} & Z_{kk,dq}^{sys} \\ Z_{kk,qd}^{sys} & Z_{kk,qq}^{sys} \end{bmatrix} \tag{10}$$

To identify all elements of Z_{ij}^{sys}, at least two linearly independent inputs are needed: $\left[\tilde{\imath}_{k,d}^{(1)}, \tilde{\imath}_{k,q}^{(1)}\right]^T$, and $\left[\tilde{\imath}_{k,d}^{(2)}, \tilde{\imath}_{k,q}^{(2)}\right]^T$, where the superscripted number represents the round of the input. Under such inputs, the relationship between input and output could be represented as

$$\begin{bmatrix} Z_{kk,dd}^{sys} & Z_{kk,dq}^{sys} \\ Z_{kk,qd}^{sys} & Z_{kk,qq}^{sys} \end{bmatrix} \cdot \begin{bmatrix} \tilde{\imath}_{k,d}^{(1)} & \tilde{\imath}_{k,d}^{(2)} \\ \tilde{\imath}_{k,q}^{(1)} & \tilde{\imath}_{k,q}^{(2)} \end{bmatrix} = \begin{bmatrix} \Delta v_d^{(1)} & \Delta v_d^{(2)} \\ \Delta v_q^{(1)} & \Delta v_q^{(2)} \end{bmatrix} \tag{11}$$

Such that Z_{kk}^{sys} can be solved from

$$\begin{bmatrix} Z_{kk,dd}^{sys} & Z_{kk,dq}^{sys} \\ Z_{kk,qd}^{sys} & Z_{kk,qq}^{sys} \end{bmatrix} = \begin{bmatrix} \Delta v_d^{(1)} & \Delta v_d^{(2)} \\ \Delta v_q^{(1)} & \Delta v_q^{(2)} \end{bmatrix} \cdot \begin{bmatrix} \tilde{\imath}_{k,d}^{(1)} & \tilde{\imath}_{k,d}^{(2)} \\ \tilde{\imath}_{k,q}^{(1)} & \tilde{\imath}_{k,q}^{(2)} \end{bmatrix}^{-1} \tag{12}$$

A typical example for linearly independent inputs is to inject only on d-axis first (e.g., active power), then inject only on q-axis (e.g., reactive power), as below:

$$\begin{bmatrix} Z_{kk,dd}^{sys} & Z_{kk,dq}^{sys} \\ Z_{kk,qd}^{sys} & Z_{kk,qq}^{sys} \end{bmatrix} \cdot \begin{bmatrix} \tilde{\imath}_{k,d} & 0 \\ 0 & \tilde{\imath}_{k,q} \end{bmatrix} = \begin{bmatrix} \Delta v_d^{(1)} & \Delta v_d^{(2)} \\ \Delta v_q^{(1)} & \Delta v_q^{(2)} \end{bmatrix} \tag{13}$$

In this special case, if only one injection is applied, e.g., $\tilde{\imath}_k = \left[0, \tilde{\imath}_{k,q}\right]^T$, a single element $Z_{kk,qq}^{sys}$ can be acquired from an element-wise calculation. This would provide useful information but is limited and it is recommended to use two linearly independent inputs in order to identify a complete *dq*-frame model.

Another factor to consider is that the impedance in *dq*-frame is usually aligned with the local synchronous frame. To link them together and form a whole-system model, the local-frames should be aligned to a global synchronous frame. This is discussed in [5]

and [6]. If the dynamics of phase-lock-loop (PLL) are omitted, the alignment can be fulfilled via the following equation:

$$Z_{k,dq'} = \begin{bmatrix} \cos(\theta_k) & -\sin(\theta_k) \\ \sin(\theta_k) & \cos(\theta_k) \end{bmatrix} Z_{k,dq} \tag{14}$$

where $Z_{k,dq'}$ is the impedance aligned to the global synchronous frame, θ_k is the voltage angle at the bus from power flow calculation. In the following discussion of this report, all impedance models are aligned to the slack bus ($\theta = 0$).

4.3 Impedance/admittance identification

There are two essential approaches to impedance identification: the time-domain identification (TDID) approach and the frequency-domain identification (FDID) approach. These methods are introduced in [7]. It is worth noting that the system discussed in this report is considered a linear time-invariant (LTI) system. The system is linear in that it is a linearisation of a non-linear system around an operating point. The real system (the grid and its resources) will be time-varying because an ever-changing operating point and repeated re-linearisation will be required. That process is ignored here on the basis that changes in operating point are gradual enough or infrequent enough for a given linearisation to be applicable for a period of time, such as a half-hour settlement period. Approaches to dealing with time-variance, such as banks of linearised models and tracking via digital twins are being investigated elsewhere.

4.3.1 Time-domain identification (TDID)

TDID makes use of the data collected in discrete time, i.e., the input $u(t)$ and output $y(t)$. A system order M (and therefore the order of the model) is usually selected using assumptions about the system or through repeated refinement. A set of algorithms are then applied to estimate the parameters in the state-space model based on the time-domain data. Example algorithms include the eigensystem realization algorithm (ERA) method and the dynamic mode decomposition (DMD) method. These methods have been successfully used for impedance identification in [8]. Commercial tools exist such as the Matlab System Identification Toolbox. This toolbox is sophisticated in that it first chooses the most appropriate algorithm based on the characteristics of the input data.

Time-domain techniques are often used when the system's behaviour can be adequately captured within a short timeframe and when the data is sampled at high frequencies. For example, it will be suited to cases where the system is excited by an impulse or a step change. However, if the system behaviour cannot be excited within a short timeframe due

to inappropriate choice of input signal, such as a ramped change on the load, it becomes inaccurate to use TDID.

4.3.2 Frequency-domain identification (FDID)

FDID establishes the relationship between input and output in frequency-domain, such as using a Bode plot. This method is usually fulfilled via discrete Fourier Transformation (DFT) or Fast Fourier Transformation (FFT). Based on the input signal, it can be further classified into wide-band (or broad-band) injection and narrowband injection. The wideband injection use signals like an impulse, a step-change, or pseudorandom binary sequence (PBS) which contains rich frequency components to excite the system. By applying an FFT on the input and output, the frequency response is then acquired. Such methods can provide identified results with a very short period of signal injection [9]. However, the wide-band injection appears not to be robust to noise. One reason is that the energy of the noise in the measurement will increase along with the increase of sample-rate, but the energy of the signal stays constant. In such a way, signal-to-noise ratio (SNR) becomes lower for high sample rate. However, if a low sample rate is chosen, the dynamics of interest in the system may not be observable. In the real system, it is not always allowed to increase the amplitude of the injected input signal. Another reason why wideband injection is problematic is the spectral leakage when doing Fourier transform, which occurs when the periodic extension of a signal is discontinued at the ends of the sample window. This is very common for a wideband injection since the harmonics of the injected signal are not necessarily multiples of the sampling frequency (frequency resolution). To this end, wideband injection for FDID is not recommended in this report. If wideband signals are available, it is recommended to use time-domain identification directly.

Narrowband injection, which is mainly about a frequency-sweep, is injecting a series of sinewaves with different frequencies and obtain a set of frequency response data through DFT at each frequency. Compared with wideband injection, it is more noise-robust and can mitigate the spectral leakage problem by choosing proper frequency points. The downside of narrowband injection is the duration needed for the sweep. Through a set of simulations and experiments, we found that, if properly designed, the frequency sweep process can take less than 30 s to sweep from 1 Hz to 100 Hz, which is considered to be acceptable.

As discussed in Section 3.2, the value of the residue is needed for getting the impedance participation factor. This means the identification of the whole-system impedance / admittance model should be a parametric identification. As a result, either wideband or

narrowband injection is applied, a parametric system needs to be estimated from the frequency response data. This is usually fulfilled via rational approximation [10]. A readily available tool is the vector fitting toolbox [11].

4.3.3 Discussions on the proper identification methods

First, as pointed out in [7], the two methods should not be in competition, but be complementary. If an ideal input for time-domain identification is readily available, such as a scheduled step change in the voltage, a time-domain identification will be suitable. This is particularly suitable for post-event analysis. An example is the power outage happened in August 2019 in GB, where oscillations were recorded from the reactive power output from Hornsea One ten minutes prior to the event in response to a 2% step change in voltage.

Alternatively, if sinewaves of different frequencies can be injected through an inverter designed for that purpose, the frequency-domain identification will be straightforward. This can be used for early warning for potential oscillation. Similar experiments have been performed by National Renewable Energy Laboratory (NREL) in a MW-level test system [13].

In this report, both methods will be tested. It will be seen that in a small-scale system, or a system with only local oscillatory modes, time-domain identification can provide a quick and easy solution for root-cause tracing whereas in a large-scale system, frequency-domain identification through frequency sweep perturbation provides more accurate results. Thus both methods are useful.

A comparison of the two methods is given in Table 1.

Table 1 Classifications of two new strength metrics

	Time-domain Identification	**Frequency-domain identification**
Injected signal	• Any format. • Ideally: impulse, step change.	• Sequence of sinusoidal waves with different frequencies.
Advantage	• Quick and easy to implement. • Could use existing (ambient) signals in the system.	• Robust to noise • Injection could be designed and configured flexibly (test range, injection amplitude, number of cycles, etc.).
Disadvantage	• Sensitive to noise.	• Time consuming. • Extra cost on the hardware

	• Dynamics are not guaranteed to be excited by the injected signals.	• Potential disturbance to system operation.
Suitable applications	• Post-event analysis with observed oscillations during known changes. • Early warning through scheduled changes in the system. • Small-scale network, or local-area oscillatory modes.	• System monitoring with specifically designed injections to identify potential risks. • Large-scale system, and inter-area modes.

4.4 Hybrid Data/Model-Driven Impedance Identification

Given the MIMO nature of the **black-box** system illustrated in Figure 5, injections and measurements at each PCC are needed to identify the entire system. However, such a high-density of injections is not practicable in view of the equipment needed or the time taken. In reality, the system operator would have a certain degree of knowledge of the grid, among which the knowledge of the network nodal admittance matrix Y_N and parameters of the synchronous generators (SGs) would be very useful for "seeding" whole-system impedance identification. This is known as the grey-box model identification.

If Y_N, which includes information about lines and load and is usually used for power flow calculation, is known beforehand, a single input with multiple outputs would be able to restore the whole system Z^{sys} or Y^{sys}. Here we take Y^{sys} as an example because we are going to introduce voltage perturbation in case studies.

The identification of Y^{sys} can be concluded in three scenarios: i) the current perturbation is added at one location and voltage response is measured at all other locations. In such a case, a single column of Y^{sys} will be measured, so is called a single-column measurement, as shown in Figure 6 (a). ii) The scenario where measurements cannot be taken everywhere so that only part of the column can be measured is called a partial-column measurement, as shown in Figure 6 (b). 3) The scenario where injections are taken at multiple locations is called multiple-column measurements, as shown in Figure 6 (c). Restoration of Y^{sys} in these 3 scenarios are introduced here.

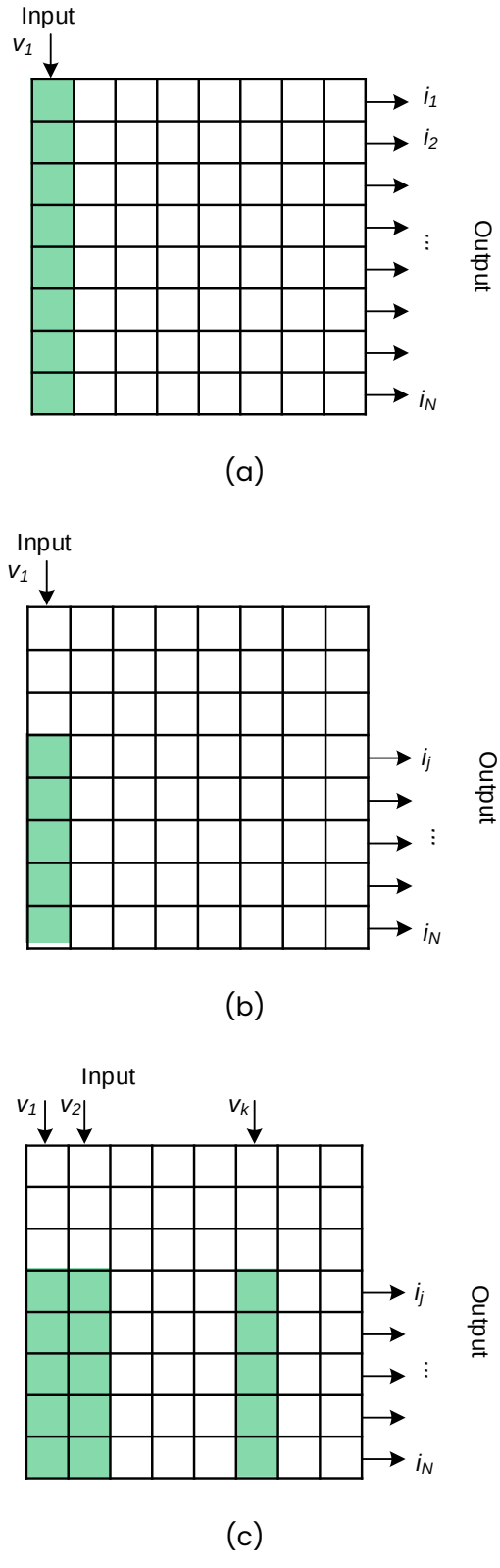

Figure 6 Three scenarios of grey-box identification of $\mathbf{Y}^{sys}$, from (a) a single-column measurement, (b) a partial-column measurement, and (c) multiple-column measurements. The elements highlighted in green are those measured from input and output.

4.4.1 Restoration of Y^{sys} from a single-column measurement.

From (4) we have

$$\left(Y^{sys}\right)^{-1} = Z_N + Z_A \tag{15}$$

where $Z_N = Y_N^{-1}$. In theory Y_N is a sparse matrix and may not be invertible. In such a case infinitesimally small shunt admittances can be added at the empty buses to make the matrix invertible. Such admittances are a reality anyway because of line parasitic capacitors. Right multiplying Y^{sys} on both sides of (15) yields

$$(Z_N + Z_A)Y^{sys} = I \tag{16}$$

(16) can be further re-written in a column format that

$$(Z_N + Z_A) \cdot \left[Y_{c1}^{sys} \middle| Y_{c2}^{sys} \middle| \cdots \middle| Y_{cN}^{sys}\right] = I, \tag{17}$$

where Y_{ck}^{sys} is the k-th column of Y^{sys}, i.e., $Y_{ck}^{sys} = \left[Y_{1k}^{sys}, Y_{2k}^{sys}, \cdots, Y_{Nk}^{sys}\right]^T$. If from a single input and multiple outputs we identify Y_{ck}^{sys}, the following equation can be easily derived from (17):

$$(Z_N + Z_A) \cdot Y_{ck}^{sys} = I_k \tag{18}$$

Where I_k is the k-th column of the identity matrix. Such that

$$Z_A Y_{ck}^{sys} = I_k - Z_N Y_{ck}^{sys} \tag{19}$$

Let $c = I_k - Z_N Y_{ck}^{sys}$, which is a column vector. Since Z_A is a diagonal matrix, from (19) Z_A can be calculated in elementwise, such that

$$Z_{Ai} = c_i \cdot \left(Y_{cki}^{sys}\right)^{-1} \tag{20}$$

By having Z_A and Z_N, the entire matrix Y^{sys} can be acquired from (15), which can further be used for root-cause tracing, as introduced in Section 33.2. Although the full matrix of Y^{sys} is restored, it is worth noting that only the diagonal elements are useful for root-cause tracing.

Because the above process utilises both the data collected in the system and the model known to the system operator, this approach is named as the hybrid data/model-driven impedance identification, as concluded in Figure 7.

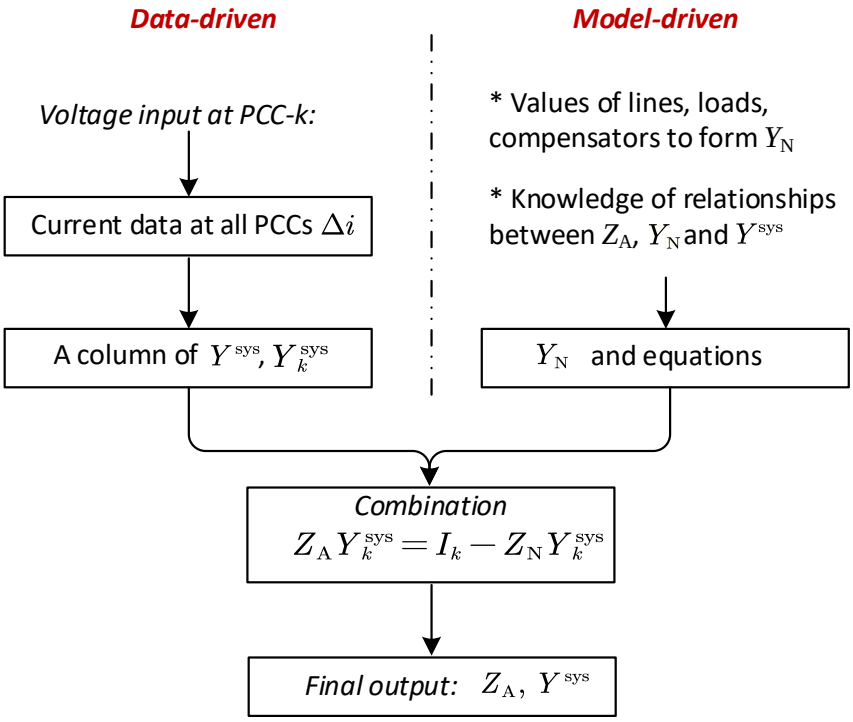

Figure 7 Illustration of the hybrid data/model-driven impedance identification.

4.4.2 Restoration of Y^{sys} from a partial-column measurement.

In many cases, measurement cannot be taken at all buses. In such cases, available information on buses without measurement unit, or reasonable assumptions on these buses can be used for Y^{sys} restoration.

For buses with SG connected, we consider its impedance Z_{Ak} known. This is because the SG's parameters are usually disclosed to the system operator. From the known parameters we could establish a realisation of SG's state-space equations, which further derives the transfer function from its port current to port voltage, i.e., Z_{Ak}.

For buses with IBR connected, especially when its model is not disclosed, it is recommended to implement a measurement unit. If not, some compromises are needed. One solution is to use a generic IBR model to represent the unmeasured IBR. Alternatively, a simple current source with very large impedance can be used, which implies the assumption that the unmeasured IBR does not participating in any of the oscillations.

For simplicity, we assume that bus-1,2,..., j -1 are those with known impedances or assumptions made, and bus-j, j+1,..., N are those with measurement units. The input

perturbation is added in bus-k. Under this assumption, (19) can be rewritten in block-matrix format as

$$\begin{bmatrix} \boldsymbol{Z_{A,11}} & \\ & \boldsymbol{Z_{A,22}} \end{bmatrix} \begin{bmatrix} \boldsymbol{Y_{ck,1}^{sys}} \\ \boldsymbol{Y_{ck,2}^{sys}} \end{bmatrix} = \begin{bmatrix} \boldsymbol{I_{k,1}} \\ \boldsymbol{I_{k,2}} \end{bmatrix} - \begin{bmatrix} \boldsymbol{Z_{N,11}} & \boldsymbol{Z_{N,12}} \\ \boldsymbol{Z_{N,21}} & \boldsymbol{Z_{N,22}} \end{bmatrix} \begin{bmatrix} \boldsymbol{Y_{ck,1}^{sys}} \\ \boldsymbol{Y_{ck,2}^{sys}} \end{bmatrix} \tag{21}$$

where $Y_{ck,1}^{sys}$ is unknown, $Y_{ck,2}^{sys}$ is measured, $Z_{A,11}$ is known and $Z_{A,22}$ is unknown. By solving (21) we have

$$\begin{aligned} Z_{A,11}\, Y_{ck,1}^{sys} &= I_{k,1} - Z_{N,11} Y_{ck,1}^{sys} - Z_{N,12} Y_{ck,2}^{sys} \\ Z_{A,22} Y_{ck,2}^{sys} &= I_{k,2} - Z_{N,21} Y_{ck,1}^{sys} - Z_{N,22} Y_{ck,2}^{sys} \end{aligned} \tag{22}$$

from which the two unknowns $Y_{ck,1}^{sys}$ and $Z_{A,22}$ can be found. The rest of the process stays the same as single-column measurement.

4.4.3 Restoration of Y^{sys} from multiple-column measurements.

If perturbations are introduced at more than one location, we will acquire data relevant to multiple columns of Y^{sys}. From each column we will be able to restore a whole-system admittance model Y_{est}^{sys}. In such a case, the system is overdetermined in that we will have multiple estimates of the same matrix and they will be somewhat different from each other.

4.4.3.1 Averaging:

A straightforward way to deal with overdetermined estimates is to average the estimated models. For example, if perturbations are introduced at two locations and measurements are taken at every bus, we will have Y_{ci}^{sys} and Y_{cj}^{sys}, which would restore two admittances: $Y_{est,i}^{sys}$ and $Y_{est,j}^{sys}$. And the average would be

$$Y_{est\_avg}^{sys} = \frac{1}{2}\left(Y_{est,i}^{sys} + Y_{est,j}^{sys}\right) \tag{23}$$

where the plus symbol refers to the parallel connection of the two systems, as illustrated in Figure 8.

When parallel connecting the two systems, the 'states' will be appended, such that the order of the averaged result $Y_{est\_avg}^{sys}$ will be the summation of the orders of the two estimated system $Y_{est,i}^{sys}$ and $Y_{est,j}^{sys}$. To avoid a high-order system, a model reduction is usually needed, such as using the minimal realisation.

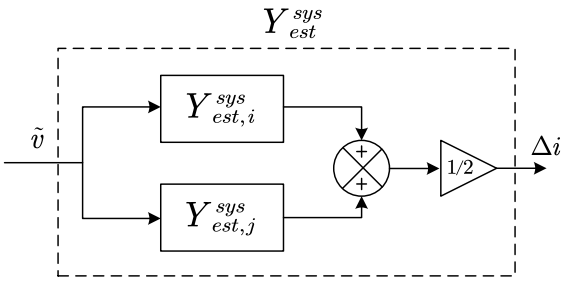

Figure 8 Average of the two estimations on Y^{sys}.

Although this method provides a simple way to merge the over-determined results and make use of all the measured data, it does not really improve the accuracy of the estimate of the system and instead may lower the accuracy. One principle of system estimation is that when the electrical distance between the injection and measurement points is small, the signal becomes more obvious and the estimation becomes accurate. Conversely, if the electrical distance is large, then the signals would be attenuated and the noise becomes the dominant such that the estimation is inaccurate. By averaging the results, the elements which are accurate from the first estimation may be negatively affected by the poor accuracy of the second estimation, and vice versa.

4.4.3.2 Weighted Averaging:

Another option is to weight the terms in the average, i.e., the buses which are close to the input have a higher weight while those far from the injection has a lower weight. With appropriate weights, the two (or more) estimates can be combined so that the results are complementary. The idea is illustrated in Figure 9. It must be noted that a method to choose appropriate weight of whole-system impedance/admittance models has not yet been addressed and further work is needed. An initial idea is that the weights could be the reciprocal of the electric distance from each bus to the injection location.

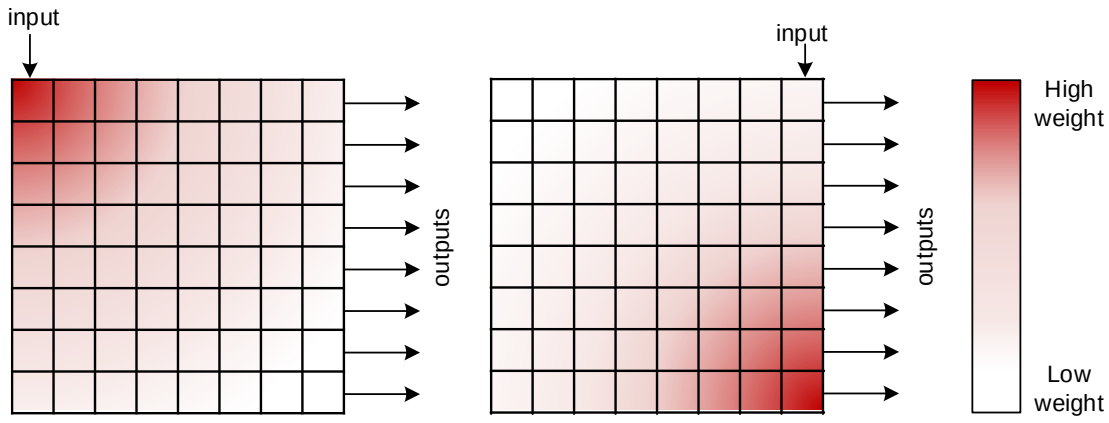

Figure 9 Demonstration of the weighted average of the estimations on Y^{sys}.

Other methods such as using Bayesian optimisation or machine learning may be possible but are considered as topics for future work.

In general, with the available knowledge to the system, the identification is essentially a grey-box model identification, as illustrated in Figure 10.

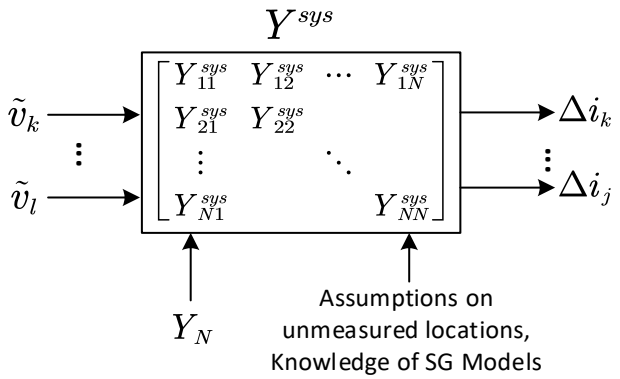

Figure 10 Grey-box model identification.

4.5 Choice of injection/measurement numbers and locations

As mentioned in Section 4.4, injections and measurements do not have to be implemented at every node, instead, input at a few nodes and partial measurements will be able to provide useful information for tracing of root-causes of oscillations. This partial-injection partial-measurement identification is illustrated in Figure 11. Since the unmeasured nodes are based on some assumptions such as ideal current sources, they should NOT be considered further for root-cause tracing. The tracing is only carried among nodes which are measured. This is a compromise of such a method.

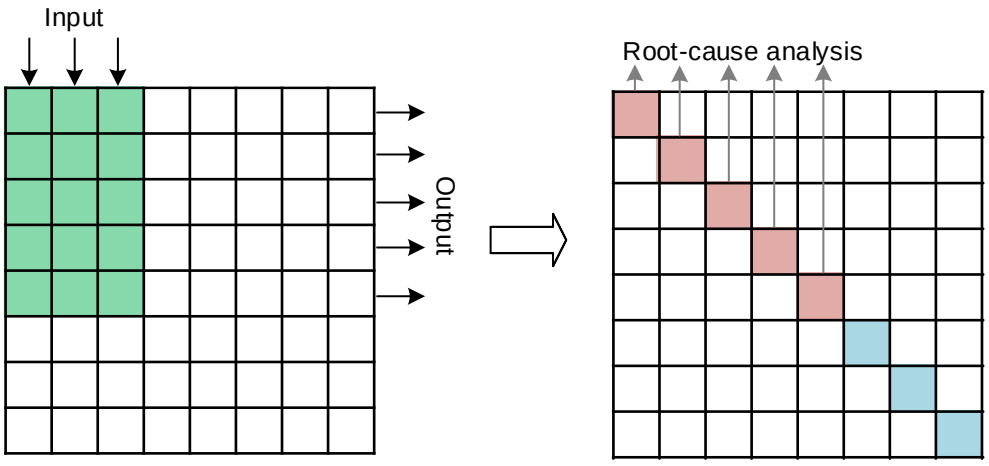

Figure 11 Partial-injection partial-measurement for whole-system impedance /admittance identification and root-cause tracing.

Theoretically, only one injection source in the system would be enough to restore the whole system impedance or admittance model. But this is not practical since signals will be attenuated due to long transmission lines, and obscured by noise. To better identify the model, multiple injections will be needed to cover the areas of interest.

The injection numbers and locations would be dependent on the system size and noise conditions. If the system is large and can be divided into several subregions which are connected via long transmission lines, a straightforward solution is to add at least one injection source in each subregion of interest. If noise is not considered at this stage, the exact location of the injection may be decided by the average electrical distance between the injection source and the IBR nodes which are measured. However, noise levels at each node may be different. As a result, it is desirable to place the injection source close to nodes with higher noise levels or add multiple injections as necessary to overcome the adverse effects of noise.

Ideally, measurement would be taken at every node, or at least at all nodes with IBR connected. But again, this may not be practicable. If only limited measurement units are to be implemented in the system, the ideal locations would be those where oscillations might be expected and areas with high density of IBRs.

4.6 Model verification

Once the system is identified, it is important to verify the estimated results. If the theoretical model is available, a comparison can be made between the estimated results and the theoretical model. Such a comparison could be a frequency-domain comparison, e.g., to compare the Bode plots. If theoretical model is not available, a time-domain comparison can be used, i.e., by applying a new input to both the estimated system, and the theoretical model and compare the match between the time-domain.

5 Case Studies

EMT simulations were performed to validate the proposed hybrid data/model-driven approach for whole-system admittance identification. The results demonstrate that this approach effectively identifies oscillatory modes and determines their root causes by applying perturbations at a single location, without requiring any knowledge of the internal design of IBRs.

5.1 4-Bus Test System – Demonstration of Identification Methods

5.1.1 System Introduction

A 4-bus, 2-IBR system is used here to demonstrate the process of model identification and root-cause tracing. The structure of the system is given in Figure 12. The current control bandwidth of IBR3 was deliberately tuned low to create an oscillatory mode.

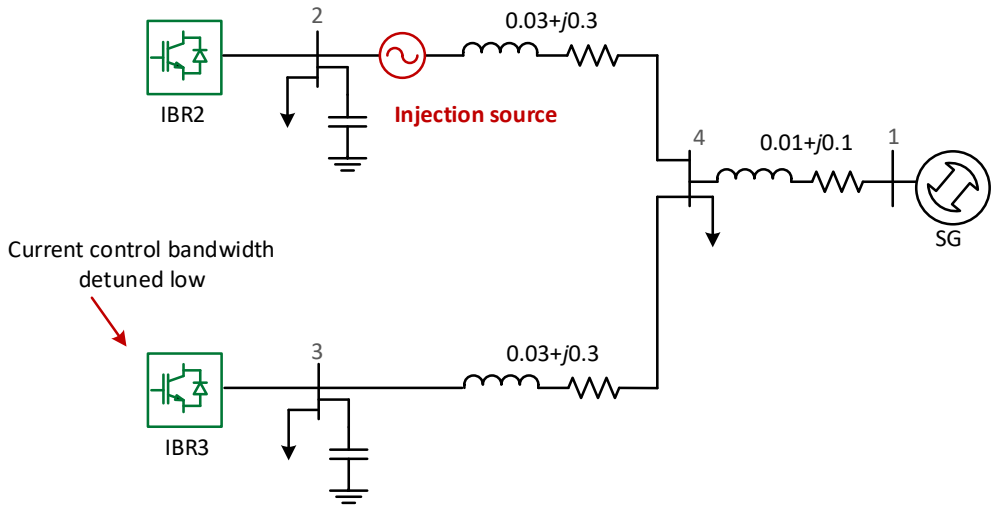

Figure 12 4-bus test system.

A voltage perturbation is introduced at bus-2 and current flowing through buses 1, 2 and 3 are measured. Both inputs and outputs are recorded in a common *d*-*q* frame. The *d*-*q* inputs on bus-2 means that we can estimate for the 3rd and 4th columns of Y^{sys}, and the 3 measurement points allow the first 6 elements to be estimated, as illustrated in Figure 13. In the following of this case study, the *d*-*q* frame is aligned to bus-1.

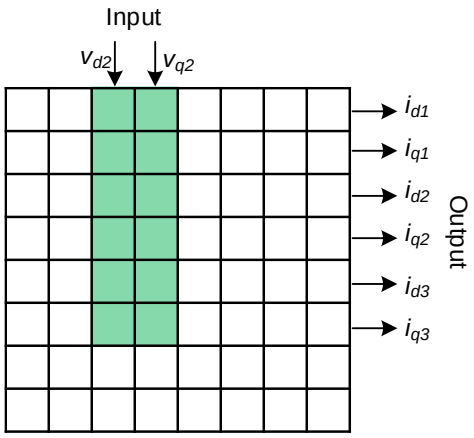

Figure 13 Illustration of the injection and measurement.

5.1.2 TDID Application

Time-domain identification is first carried out in the system, where two step-increases to the voltage are applied separately to the *d*- and *q*-axes so that they are linearly independent, such that

$$\tilde{v} = \begin{bmatrix} \tilde{v}_d^{(1)} & 0 \\ 0 & \tilde{v}_q^{(2)} \end{bmatrix}. \tag{24}$$

The magnitude of the perturbation is 0.01 pu. Current response is measured and a 2 s window is selected for time-domain identification. Figure 14 shows the current response at bus-2, $\Delta i_2 = \begin{bmatrix} \Delta i_{d2}^{(1)} & \Delta i_{d2}^{(2)} \\ \Delta i_{q2}^{(1)} & \Delta i_{q2}^{(2)} \end{bmatrix}$, where the steady state has been removed for further identification algorithms.

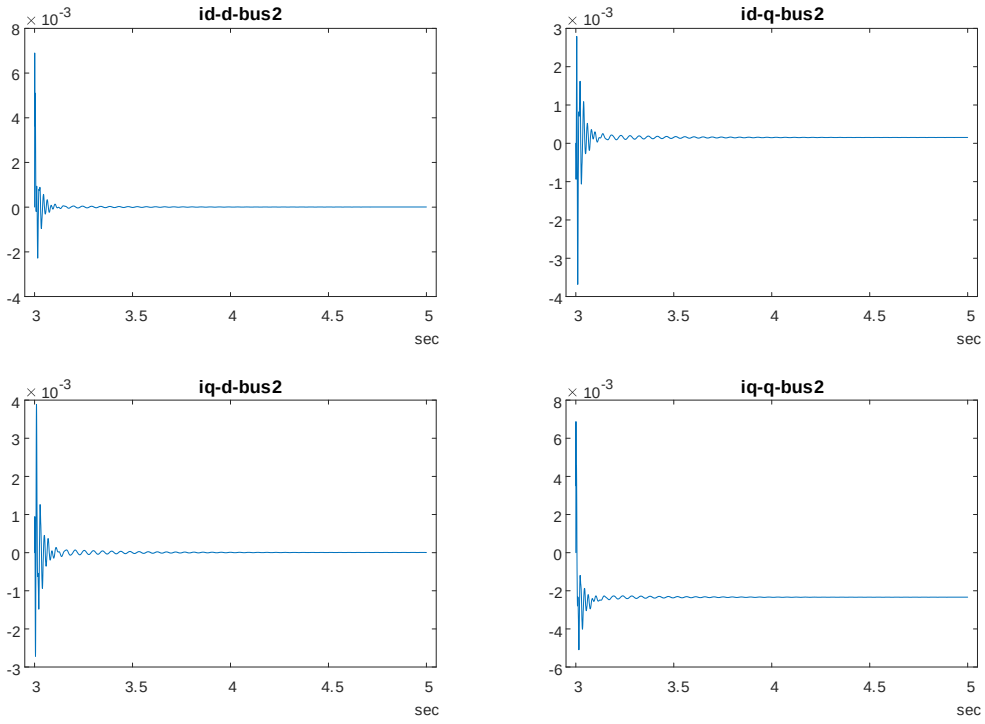

Figure 14 Current response in d-q frame at bus-2 corresponding to the voltage step change. Steady state value is removed.

The ERA method is applied to identify the data. The ERA method constructs two shifted Hankel matrix H_1 and H_2 from the measured response, after which a singular value decomposition (SVD) is performed on the Hankel matrices and eventually finds a state-space matrix A. The detailed process is introduced in [8]. It should be noted that ERA assumes the input u is an impulse input, i.e.,

$$u(k) = \begin{cases} 1, k = 0 \\ 0, k > 0' \end{cases}$$

Where *k* refers to the number of samplings. Therefore, this method does not direct leads to an input/output model, but only the s-domain system of the output data. To get the input/output model, the input signal should be transferred to s-domain, either through ERA as well, or through Laplace transform. For example, applying ERA method on $[\Delta i_1(t),\ \Delta i_2(t), \Delta i_3(t)]^T$ leads to a state-space representation of $\Delta i(s) = [\Delta i_1(s),\ \Delta i_2(s), \Delta i_3(s)]^T$. Since the input is the step change with size of 0.01, it is easy to obtain its s-domain function:

$$\tilde{v}(s) = \frac{0.01}{s}\begin{bmatrix} 1 & & \\ & 1 & \end{bmatrix} \tag{25}$$

As a result, the identified from input to the output can be derived as

$$Y^{sys}(s) = \Delta i(s) \cdot \tilde{v}(s)^{-1} \tag{26}$$

Figure 15 compares the bode diagrams from the estimated results of time-domain identification and theoretical results in d-q frame. It can be seen that the estimations have high accuracy, especially near the 'peaks' of the bode plots, which display the oscillatory modes.

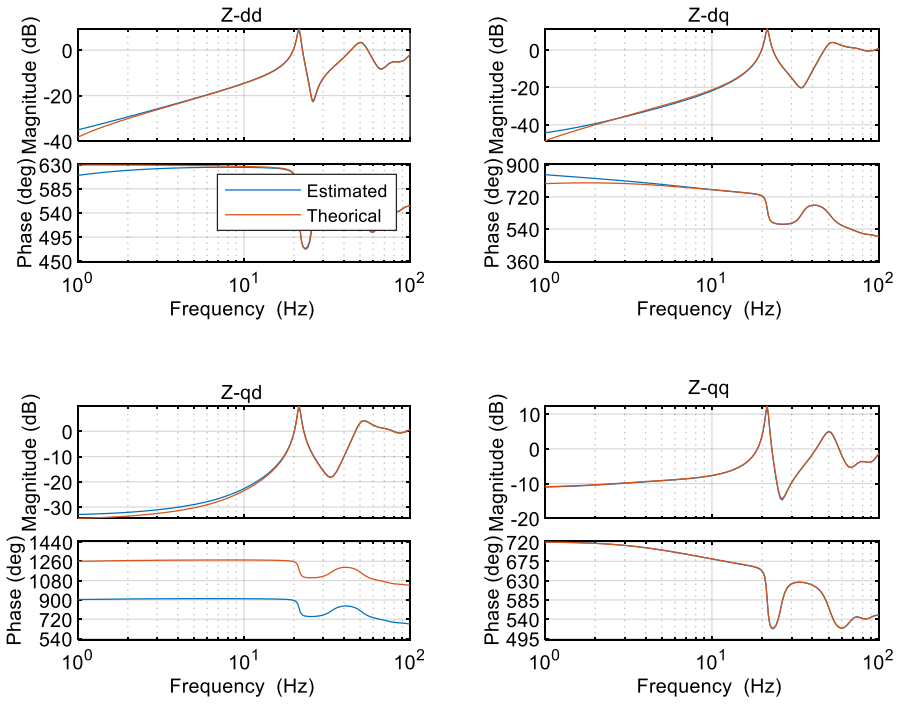

(a)

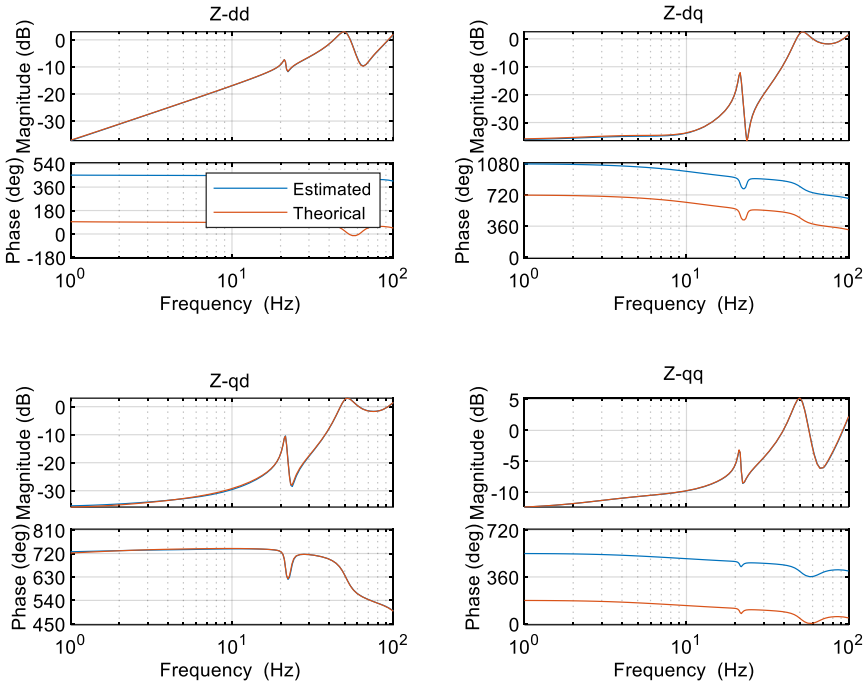

(b)

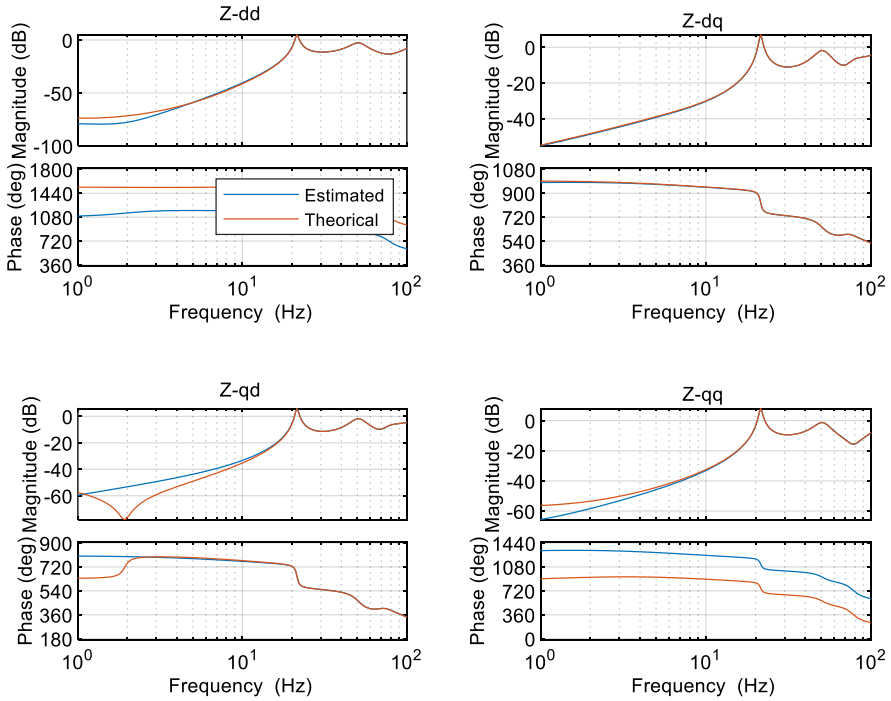

(c)

Figure 15 Estimated result in d-q frame from ERA method versus theoretical results from analytical method: (a) Y_{12}^{sys}, (b) Y_{22}^{sys} and (c) Y_{32}^{sys}.

Figure 16 compares the estimated modes and the theoretical modes between 0 and 100 Hz, from which it is clear that the modes are identified accurately, and a significant oscillatory mode, $\lambda = -0.48 \pm 28.46$ Hz is identified. It shows that modes can be successfully identified from the time-domain identification.

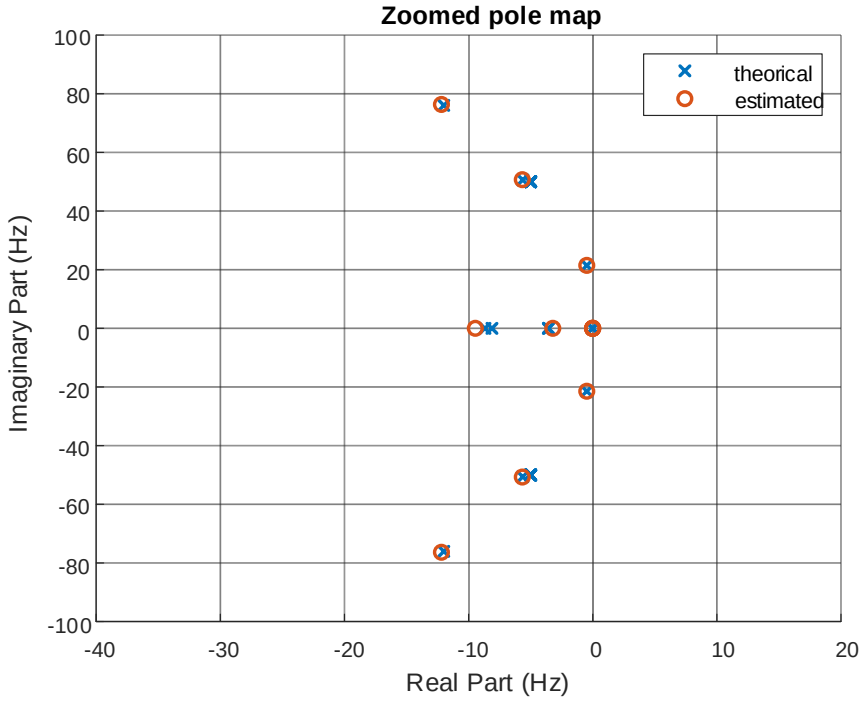

Figure 16 Estimated modes from ERA method versus theoretical results

Since bus-4 is an empty bus with no equipment connected, Y_{42}^{sys} has a value of zero. As a result, we could give Y_{42}^{sys} a very small value, e.g., $\begin{bmatrix} 10^{-6} & \\ & 10^{-6} \end{bmatrix}$. In such a way, a full column of Y^{sys} is restored. From (15)-(20), the impedances of IBR-2 and IBR-3, i.e., Z_{A2} and Z_{A3} can be recovered, as shown in Figure 17. The estimated results generally match with theoretical values but errors are present. These errors are mainly caused by the inverse calculation in (20) which enlarges the error in Y_{22}^{sys} and Y_{32}^{sys}. Nevertheless, the estimated values are in an acceptable range, and can be used for the next step which is the restoration of the matrix of Y^{sys}. For Z_{A1}, which is the impedance of the SG, the theoretical value is applied.

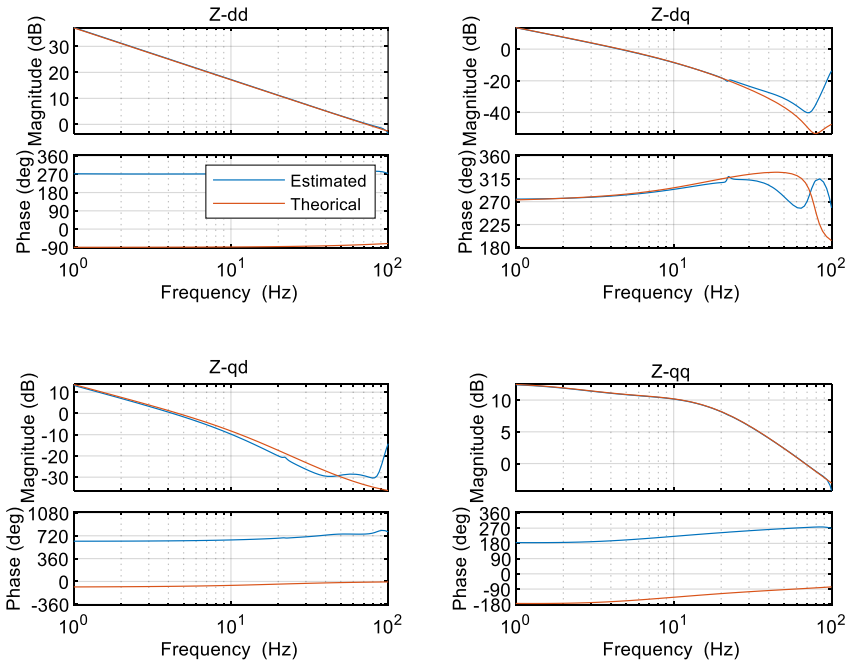

(a)

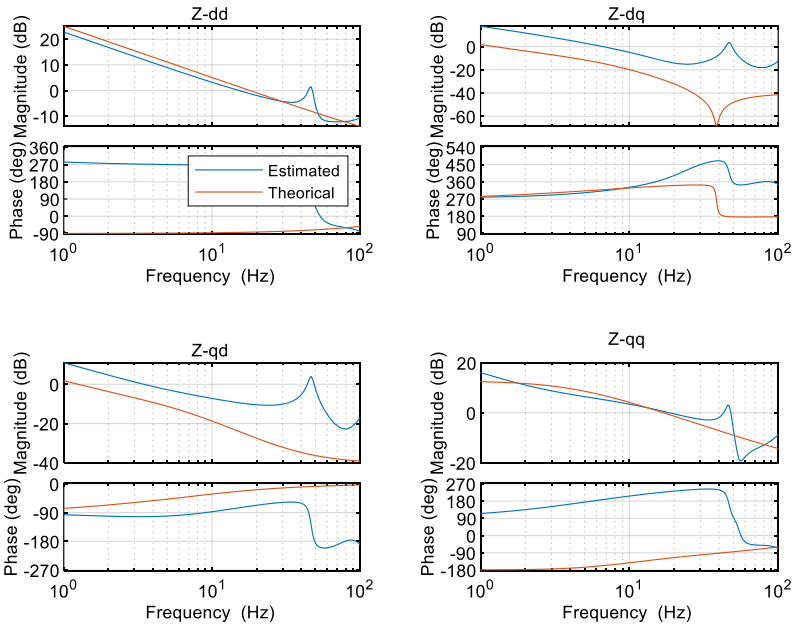

(b)

Figure 17 Estimated IBR impedance in d-q frame from ERA method VS theoretical results: (a) Z_{A2}, (b) Z_{A3}.

Eventually, the whole matrix of Y^{sys} can be restored from (15). Since only the diagonal elements will be used for root-cause tracing, the restored Y_{11}^{sys}, Y_{22}^{sys} and Y_{33}^{sys} are shown in Figure 18. In general, the estimated results match reasonably closely with the theoretical results. Although some mismatches are observed in the bode plots, the estimation is accurate near the oscillation frequency. This means that the results can be used for tracing the root-causes of the oscillations.

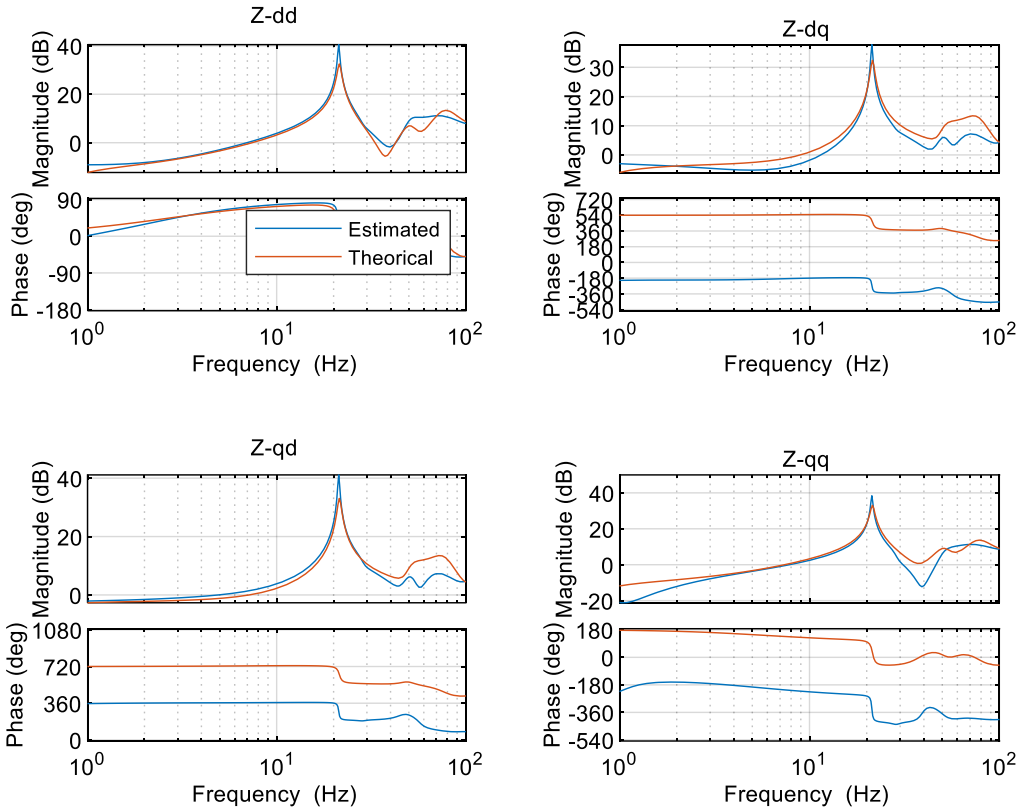

(a)

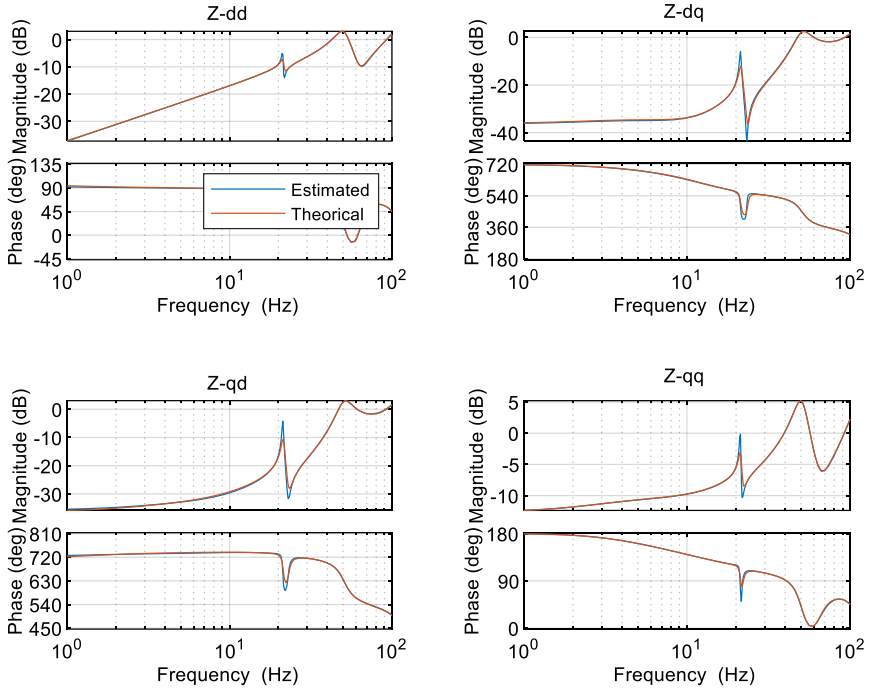

(b)

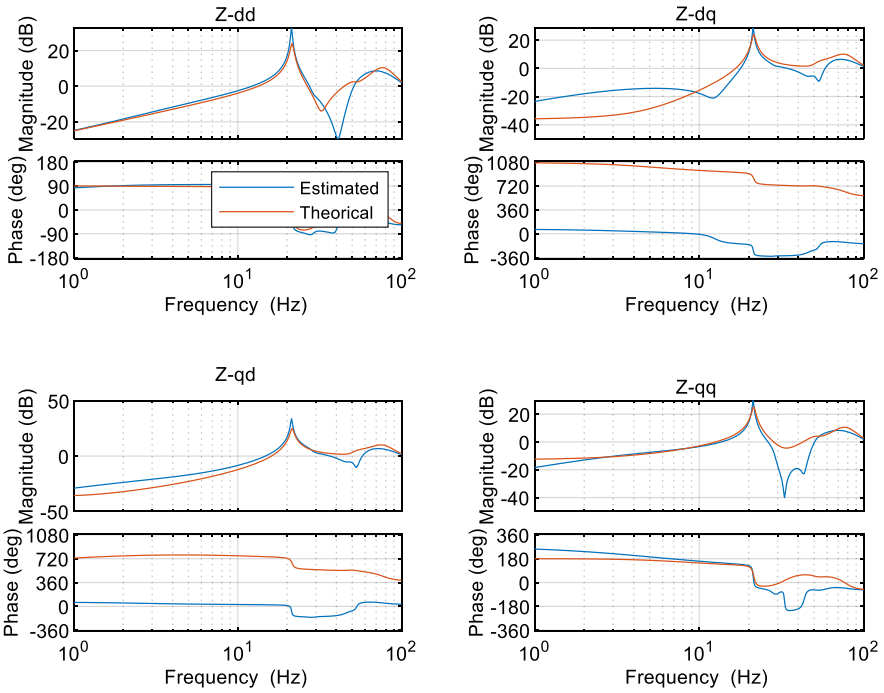

(c)

Figure 18 Estimated IBR impedance in d-q frame from ERA method VS theoretical results: (a) Y_{11}^{sys},(b) Y_{22}^{sys} and (c) Y_{33}^{sys}.

5.1.3 FDID Application

Frequency-domain sweep is also applied showing the process of frequency identification. Instead of injecting step changes at PCCs, the frequency sweep injects sinusoidal waveforms at different frequencies, in d-axis and q-axis, successively. For each frequency, the injected amplitude and cycle can be different. In this case study, the sweep selected 47 frequency points from 1~100 Hz. For frequency below 20 Hz, 2 cycles are injected to reduce time. For frequency above 20 Hz, 5 cycles are injected to improve accuracy. The amplitude are chosen as 0.01 pu for all frequencies. The injected waveforms are shown in Figure 19. The entire process takes about 35 seconds.

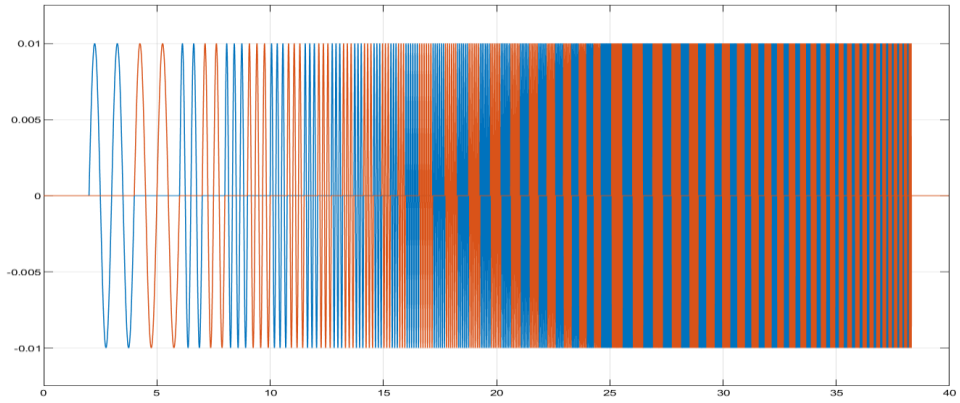

Figure 19 Frequency sweep waveforms. Blue is on d-axis and red is on q-axis.

If the input signal is

$$\tilde{v} = A_c \cos 2\pi f_c t$$

From the measured output, the system gain and phase can be calculated from DFT:

$$Y^{sys}(j2\pi f_c) = \frac{2}{A_c k_c T_c} \int_0^{k_c T_c} \Delta i(t) \cdot e^{-j2\pi f_c t}\, dt, \tag{27}$$

where $\Delta i(t)$ is the current output, A_c is the injected amplitude, $k_c$is the cycle number, T_c is the period of the injected frequency, and f_c is the frequency. By having the response at all frequencies and in both d-axis and q-axis, the spectra of Y_{12}^{sys}, Y_{22}^{sys} and Y_{32}^{sys} can be acquired, as shown in Figure 20. Results are also compared with theoretical bodes and the ERA estimations. It can be seen that a good accuracy is achieved in frequency sweep.

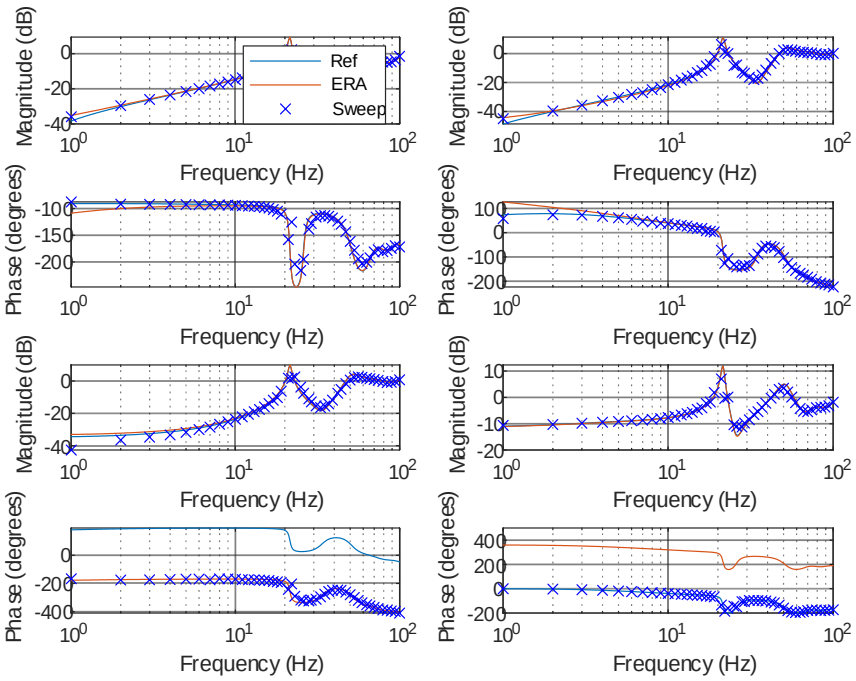
Ref
ERA
Sweep
Magnitude (dB)
Phase (degrees)
Frequency (Hz)

(a)

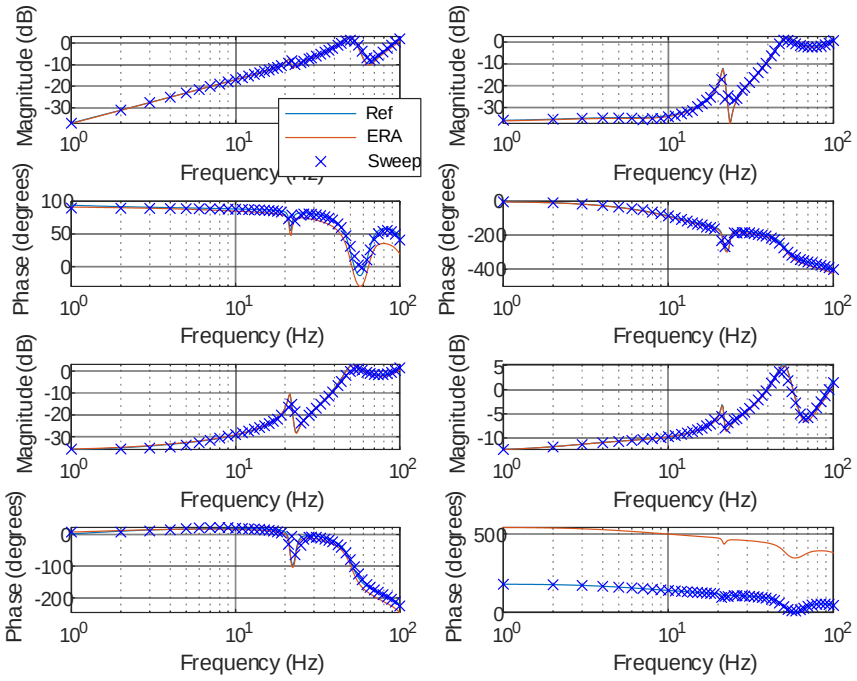
Ref
ERA
Sweep
Magnitude (dB)
Phase (degrees)
Frequency (Hz)

(b)

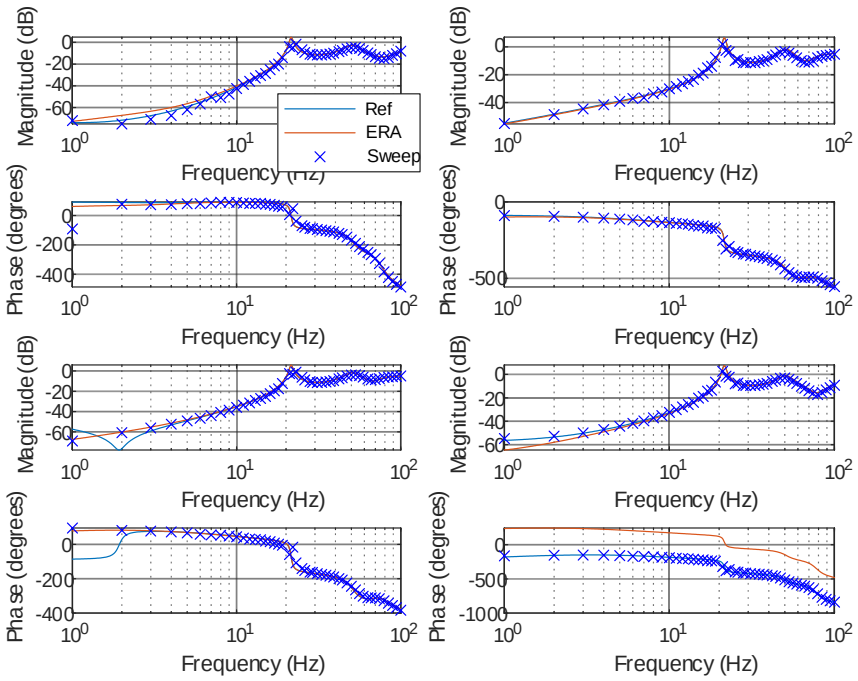

(c)

Figure 20 Frequency sweep results (blue crosses) of (a) Y_{12}^{sys}, (b) Y_{22}^{sys} and (c) Y_{32}^{sys}. Results are compared with both the theoretical and ERA results.

Diagonal elements Y_{11}^{sys}, Y_{22}^{sys} and Y_{33}^{sys} are then restored using 4.4.1, as shown Figure 21, from which it can be seen that good accuracy are achieved.

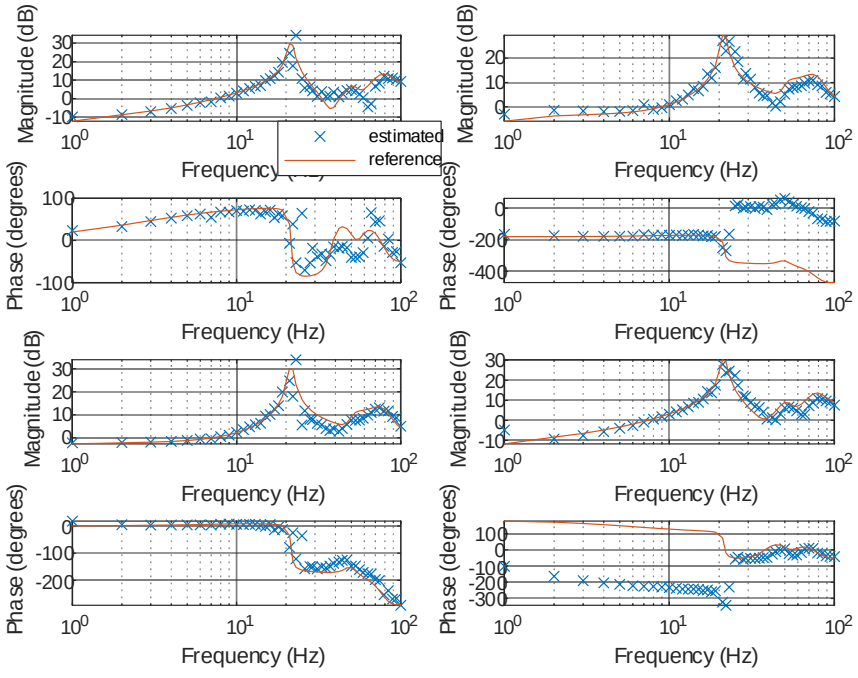

(a)

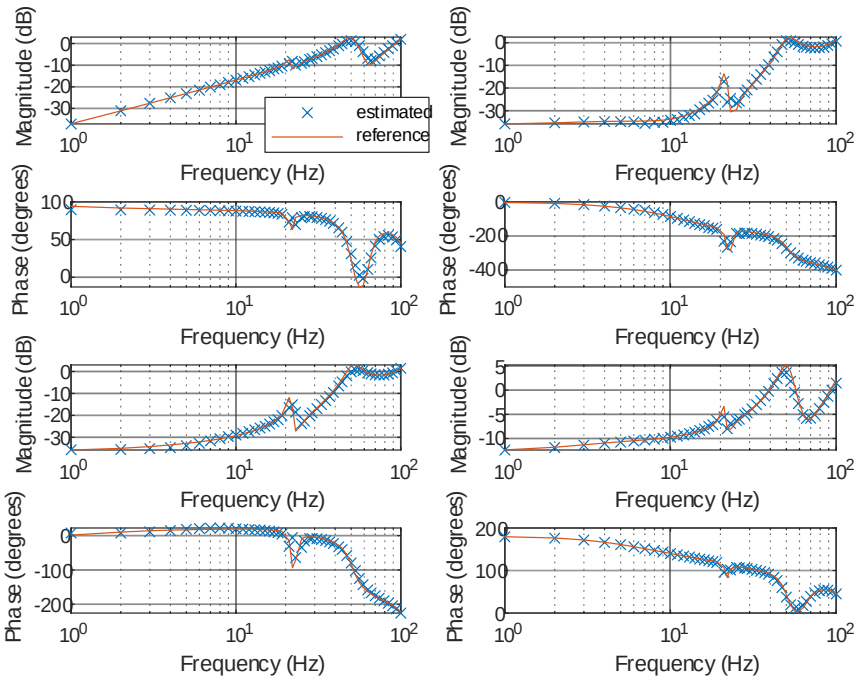

(b)

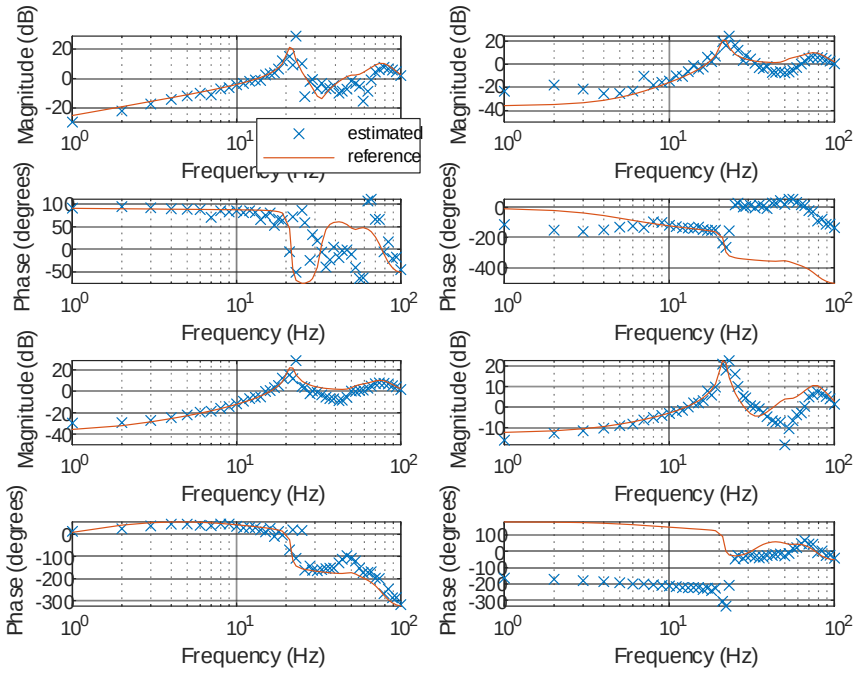

(c)

Figure 21 Restored diagonal elements (a) Y_{11}^{sys}, (b) Y_{22}^{sys} and (c) Y_{33}^{sys} from frequency sweep, compared with theoretical results.

From the frequency sweep results, also known as frequency response, the state-space model, as well as the poles and residues of the system can be acquired through vector fitting techniques [14]. This is not further discussed in this report.

5.1.4 Root-Cause Tracing

With the estimations on diagonal elements of Y^{sys}, root-cause tracing can be carried out among these buses, with the help of the grey-box approach, as introduced in 3.2. In this section, the estimation from the ERA method is used to trace the root-cause of the 28.46 Hz mode identified from Figure 16.

The Grey-box approach is first applied using the theoretical results. A screenshot of the developed Matlab APP is shown in Figure 22. It can be seen from Layer 1 that A3, which is the detuned IBR is the dominant. Further from Layer 2, A3 is found to be the major reason of the low damping of this mode. Layer 3 tells that by increasing the current control bandwidth of A3, the mode can be better damped. The results align with the system configuration as the current control bandwidth of A3 was deliberately detuned low.

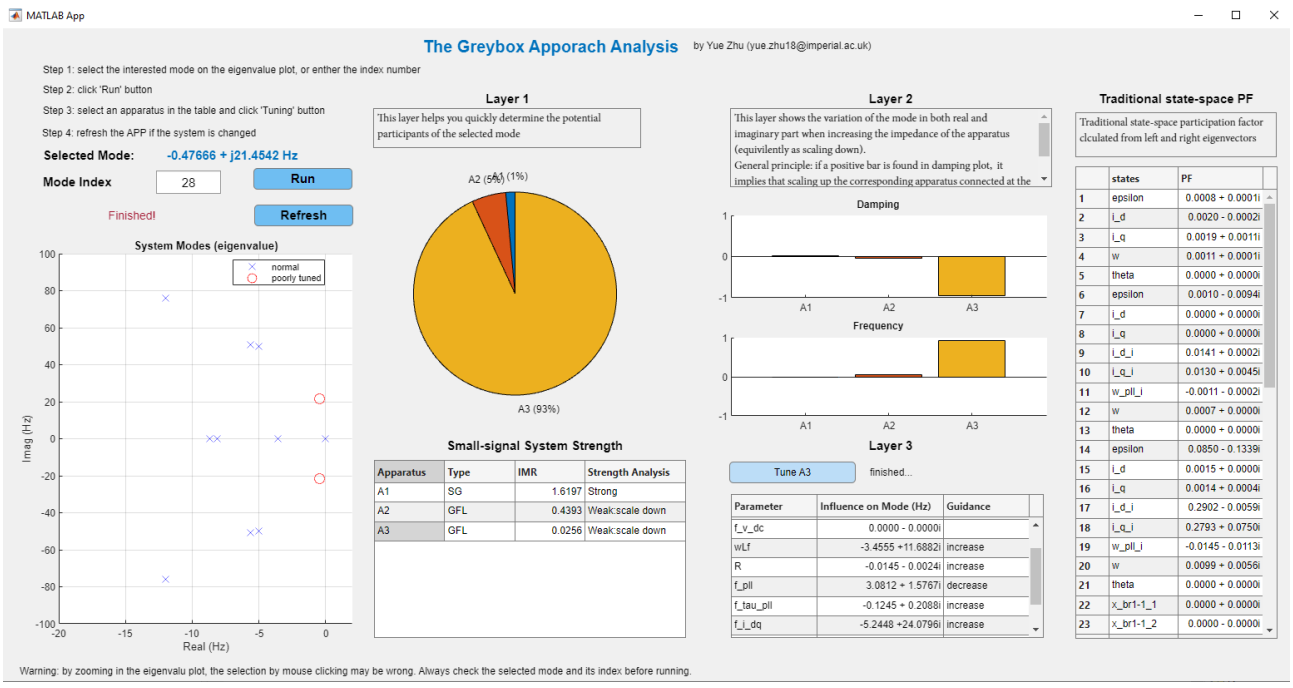

Figure 22 Screenshot of the grey-box approach in Matlab APP.

The estimation results from 4.3.1 is then employed for the Grey-box approach, and the results are shown in Figure 23. It can be clearly seen that the results from time-domain identification successfully match with theoretical results and indicate that the root-cause of the mode is A3. This demonstrates that by introducing two linearly independent step

changes at one location and measuring response at other locations, the oscillatory modes and their root-cause can be successfully identified.

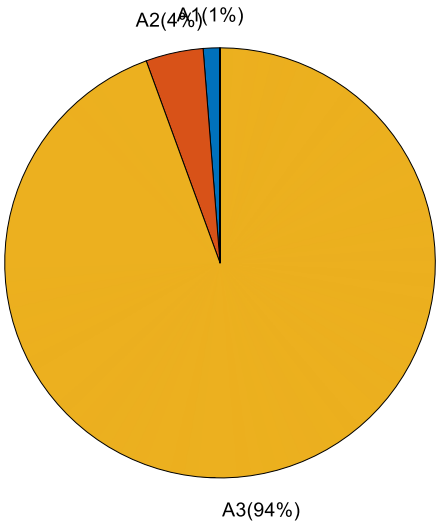

(a)

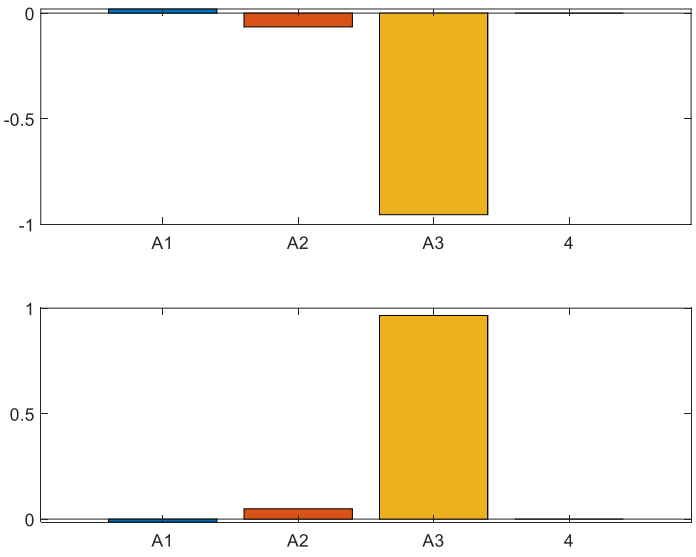

(b)

Figure 23 Results from the Grey-box approach using estimation results: (a) layer-1, (b) layer-2.

5.2 7-Bus Test Systems – Full Column Measurement

In order to verify the proposed method in a larger scale system with more IBRs present, a 7-bus system with 1 SG and 5 grid-following (GFL) IBRs was established in Matlab Simulink for EMT simulation, as shown in Figure 24. The voltage control bandwidth of IBR at bus-4 and 7 are deliberately detuned high to create an oscillatory mode of around 18.3 Hz, which is caused by the voltage control interaction of these two buses. A voltage perturbation $\tilde{V}_3$ was introduced at bus-3.

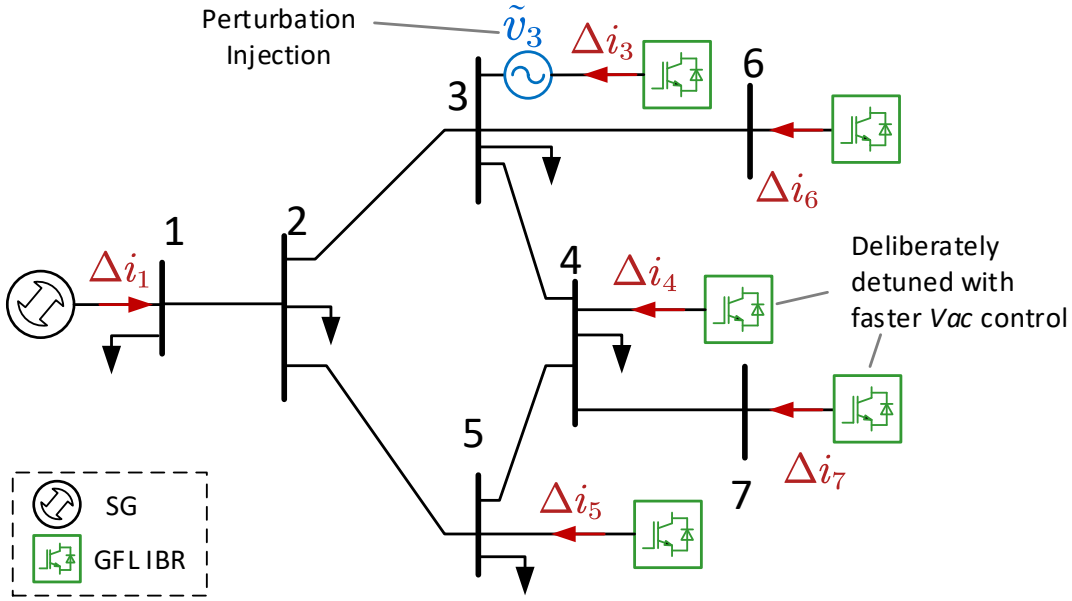

Figure 24 A 7 bus system with one SG and 5 GFL IBRs. The voltage perturbation is added at bus-3 and current responses are taken at bus-1,3,4,5,6,7.

The perturbation was selected as a step change with 0.02 pu size, adding at t = 1 s. Two rounds of perturbations were performed, in which the perturbation was added on d-axis and q-axis respectively. Therefore, the expressions of perturbations in time-domain and s-domain are

$$\tilde{v}_{3dq}(t)=\begin{bmatrix}\tilde{v}_{3d}^{(1)}(t) & 0\\ 0 & \tilde{v}_{3q}^{(2)}(t)\end{bmatrix},\tilde{v}_{3dq}(s)=\frac{0.02}{s}\begin{bmatrix}1 & 0\\ 0 & 1\end{bmatrix} \tag{28}$$

where the superscript represents the round of perturbation. Current responses were measured at all buses with apparatus connected, i.e., $\Delta i=[\Delta i_1,\Delta i_3,\Delta i_4,\Delta i_5,\Delta i_6,\Delta i_7]^T$, where

$$\Delta i_{kdq}(t)=\begin{bmatrix}\Delta i_{kd}^{(1)}(t) & \Delta i_{kq}^{(2)}(t)\\ \Delta i_{kq}^{(1)}(t) & \Delta i_{kq}^{(2)}(t)\end{bmatrix}, k\in\{1,3,\cdots,7\} \quad (29)$$

To establish the whole-system model in *dq* frame, the voltage and current data shall be aligned to a global steady *dq* frame which contains very few dynamics during perturbations. This paper selected the rotating frame at bus-1 as the global reference. A phase-locked loop (PLL) on bus-1's voltage was employed to create a rotating angle θ_1. It is worth noting that the bandwidth of this PLL is configured low (1~Hz in this case) to minimise frame dynamics. θ_1 was then employed for *dq* to *abc* frame transformation of $\tilde{v}_3$, as well as for *abc* to *dq* transformations of current measurement Δi at all buses. The employment of PLL for frame alignment, as well as the frame transformation of $\tilde{v}_3$ and Δi_k are illustrated in Figure 25.

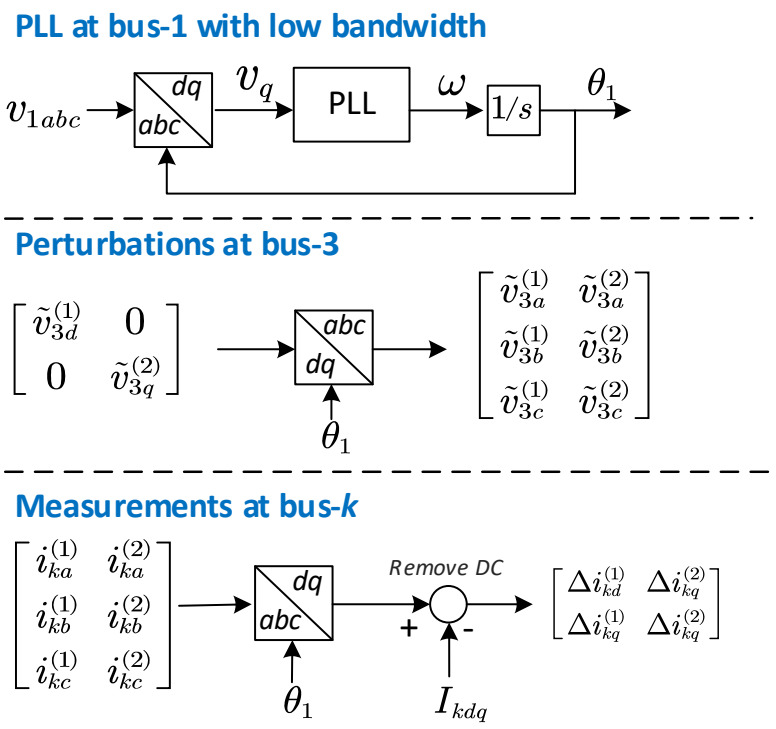

Figure 25 Perturbation and measurement in dq frame aligned to bus-1.

The time-domain data of $\Delta i(t)$ during the transient response period was used for TDID, sampled at 1200~Hz with a 2 s window length. Notably, the total simulation time required for identification can be kept very short—in this case, 3 s. ERA method was then applied to fit $\Delta i(t)$ with $\Delta i(s)$. It is worth noting that the ERA was performed to the whole column of Δi collectively, rather than on an element-by-element basis. To select a proper system order, a small initial value can be used first, in this case, $M_{\text{init}} = 10$. By applying ERA, a fitted state-

space system $\Delta i(s)$ with order of *M* is acquired. To verify the accuracy, the impulse response of $\Delta i(s)$ can be compared with the original responses in time domain. The normalised root mean squared error (nRMSE), which quantifies the difference between predicted response and actual response, is applied to assess the model accuracy. nRMSE is defined in (30).

$$\mathrm{nRMSE} = \frac{1}{\mathrm{range}(\Delta i_0)} \sqrt{\frac{1}{n} \sum_{k=1}^{n} \left(\Delta i_{fit}(k) - \Delta i_0(k)\right)^2} \tag{30}$$

Figure 1 shows the original responses and the predicted responses with different selections of *M* for element Δi_{7dq}. It is found that with *M*=20, nRMSE are all below 1%, which is considered a very accurate fit. With a set of trial and error tests, *M* was selected as 20 for ERA in this case study.

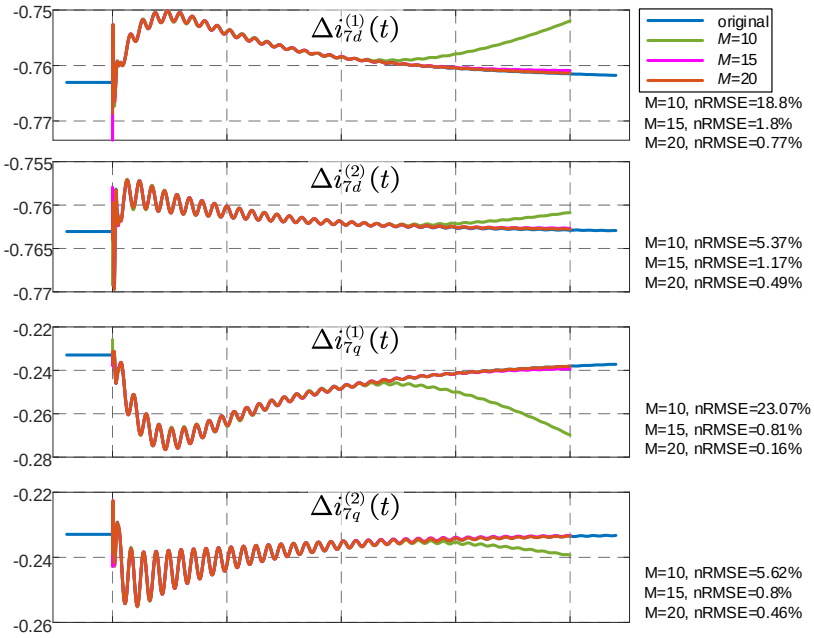

Figure 26 step response at bus-7.

Combining the fitted $\Delta i(s)$ with the system input $\tilde{v}_3(s)$, the third column of Y^{sys} can be estimated as

$$\mathrm{Y}_3^{\mathrm{sys}} = \frac{s}{0.02} \Delta i(s) \tag{31}$$

Note that Y_3^{sys} in (31) excludes the term Y_{23}^{sys}, which is corresponding to bus-2. Since no apparatus is connected at this bus, it is clear to set Y_{23}^{sys} a very small number, e.g., 10^{-1}, based on the definition of Y^{sys}.

As a closed-loop model, the poles of Y_3^{sys} are identical to the eigenvalue of the system state-space model, which represents the oscillatory modes. Figure 27 shows the system eigenvalue from the theoretical state-space model and the estimated model from ERA, and the two are matched accurately. It is identified from the estimated results that an 18.3 Hz mode is very close to the imaginary axis. This demonstrates the ability of the proposed hybrid data/model-driven method to identify the system's potential oscillation risks.

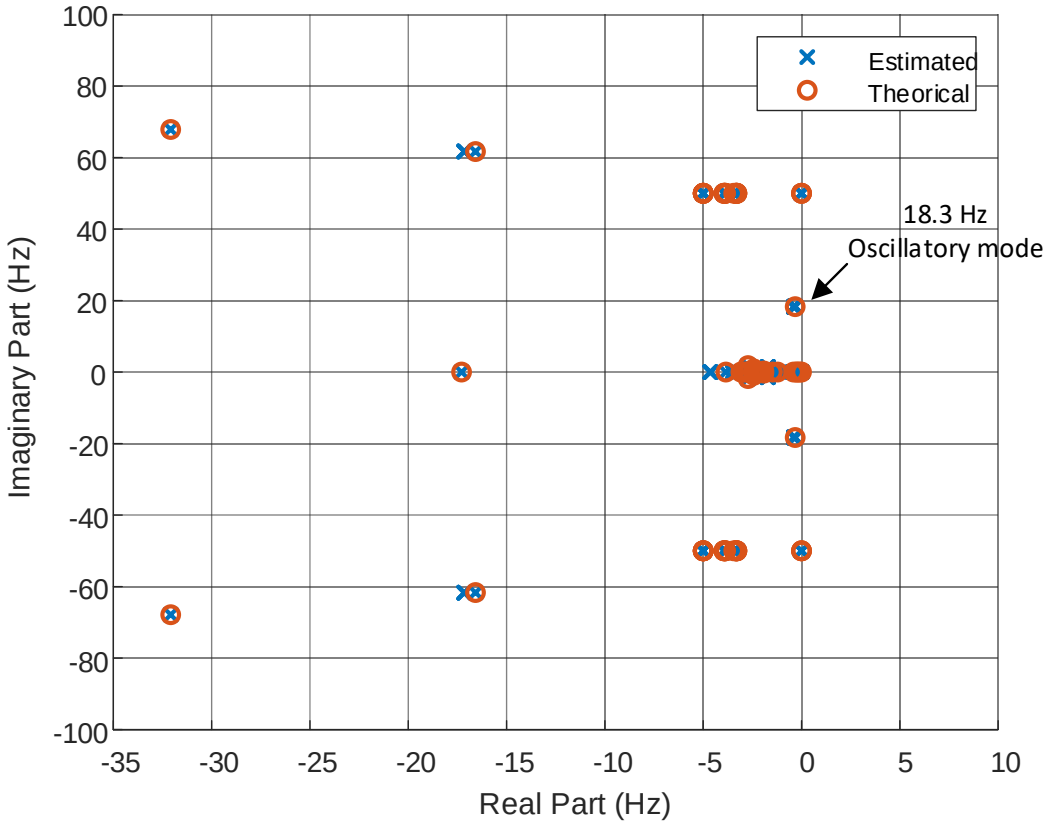

Figure 27 Pole map of Y_3^{sys}: theoretical and estimated results.

Bode plots of some randomly selected elements in Y_3^{sys}, compared with the theoretical model, are provided in Figure 28. It demonstrates that the estimation of the column Y_3^{sys} from a step response using ERA is accurate.

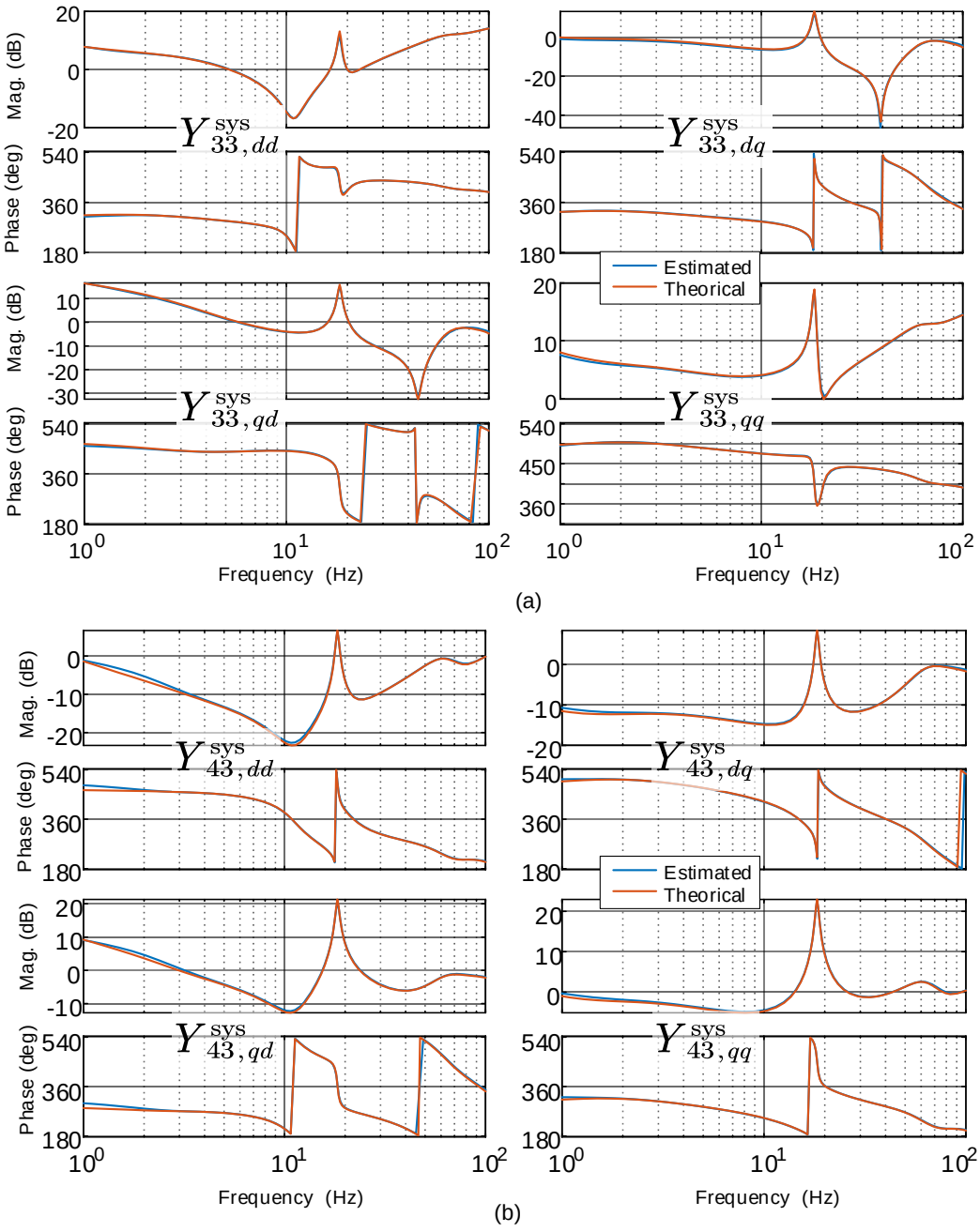

Figure 28 Bode plots of estimated Y_{33}^{sys} and Y_{43}^{sys} and their theoretical models, showing accurate estimation of column elements of Y_3^{sys} from the ERA method.

In order to reduce the computational complexity, frequency response data (FRD) sampling is performed on the estimated $Y_3^{sys}(s)$ and transform this analytical model into a numerical model $Y_3^{sys}(j\omega)$. Through this operation, the computational complexity can be reduced to $\mathcal{O}(m \cdot N^3)$, where m is the total number of frequencies for FRD. Eventually, $Y_3^{sys}(j\omega)$ can be acquired. This information is then combined with the pre-known information of network nodal admittance Y_N and yields the estimation of the apparatus

impedance $Z_A(j\omega)$ from (10). Substituting $Z_A(j\omega)$ into (4) yields the full matrix of $Y^{sys}(j\omega)$. And eventually, by applying the vector fitting on $Y^{sys}(j\omega)$, the analytical model of $Y^{sys}(s)$ can be acquired, including its diagonal elements which contain useful information for root-cause analysis. Two randomly chosen diagonal elements of Y^{sys} are demonstrated in, proving the efficacy of the proposed method in identifying the diagonal elements of the whole-system admittance model via single-point injection.

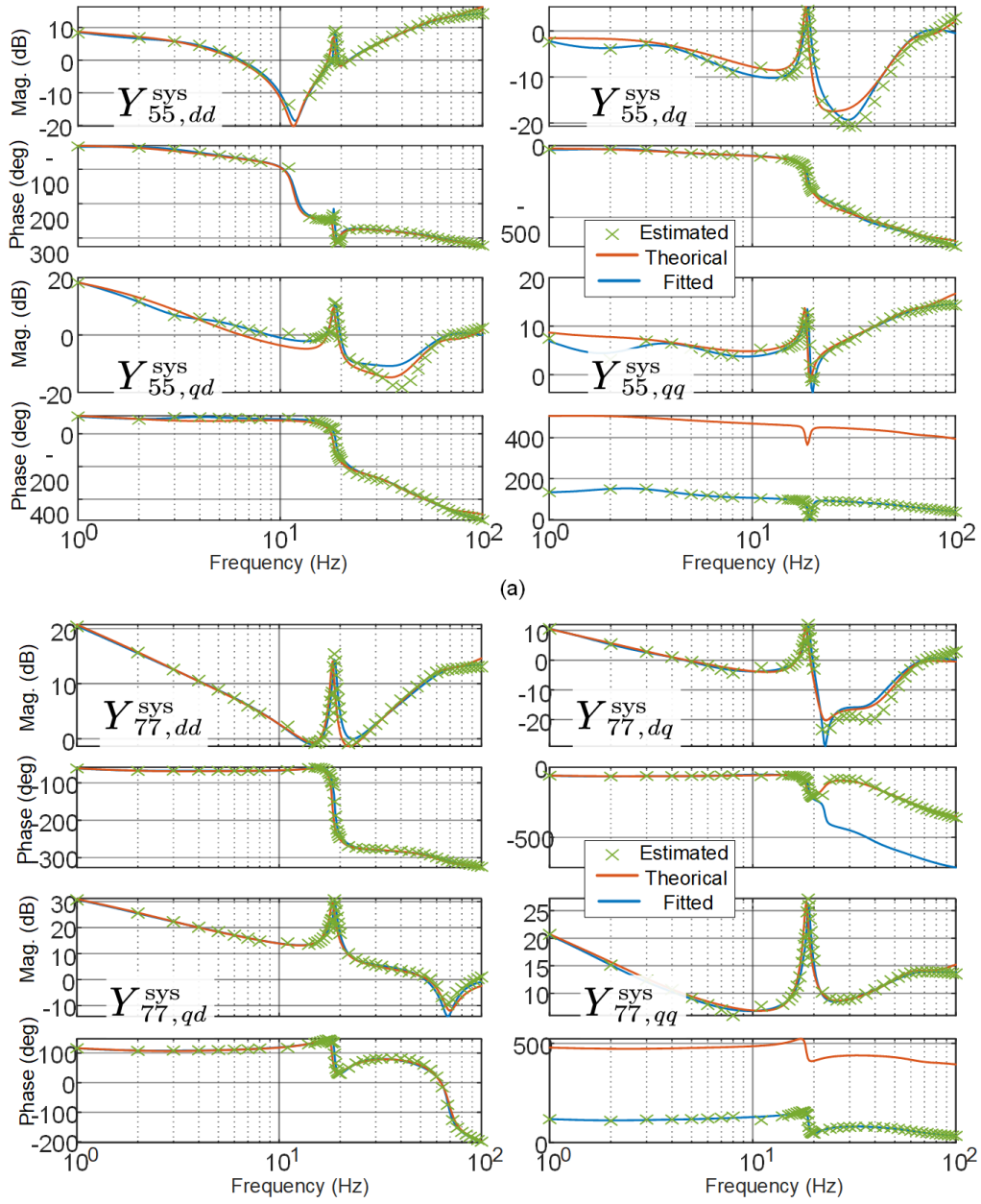

Figure 29 Bode plots of the restored diagonal elements $Y^{sys}_{55}(s)$ and $Y^{sys}_{77}(s)$, their theoretical models, and vector fitting results from the estimation, showing accurate estimations of diagonal elements of Y^{sys} from the proposed hybrid data/model-driven whole-system admittance identification.

The estimation of the diagonal elements Y^{sys}, together with Z_A can be used for root-cause analysis based on the grey-box approach proposed in [3], a powerful tool developed based on the relationship in (9). The results from the grey-box layer 1 and layer 2 are shown in Figure 30. It can be easily identified that IBRs at bus-4 and bus-7 are the root causes of this 18.3~Hz mode, which stand out in layer 1 and, in the meantime, provide negative damping in layer 2. It aligns with the fact that these two IBRs were deliberately detuned with higher AC voltage control bandwidth. Figure 30 also shows that the root-cause analysis based on the hybrid data/model-driven method matches with theoretical results from the grey-box approach.

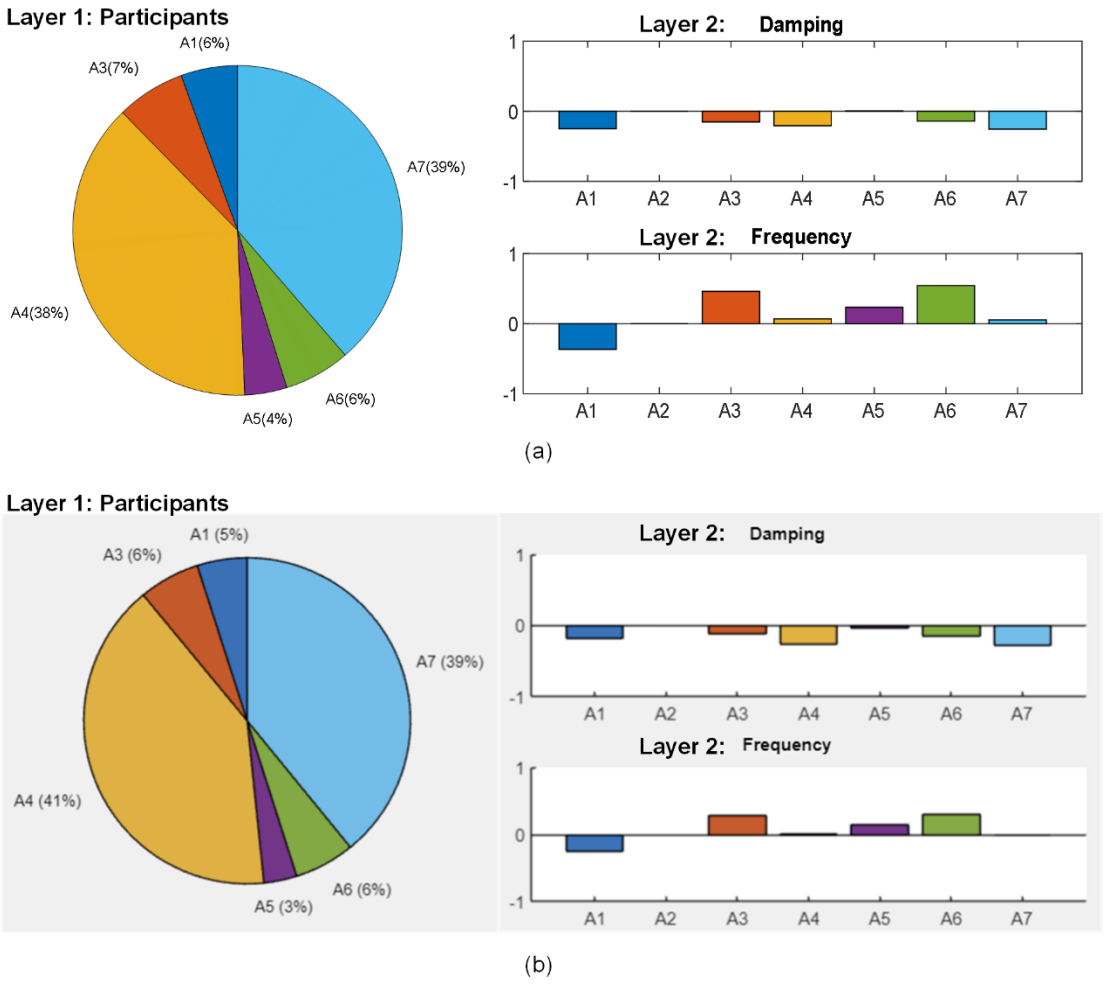

Figure 30 Root cause analysis based on the grey-box approach: (a) estimated from the proposed hybrid data/model-driven method, (b) theoretical results

This case study demonstrates that the proposed method can identify the oscillatory modes together with their root causes via a single-point injection in EMT simulations

where only black-box IBR models are available. The entire simulation time can be maintained very short, and for this case, 3 s for each round with 2 rounds in total.

5.3 7-Bus Test Systems – Partial Column Measurement

This case demonstrates the partial measurement scenario, where the same 7-bus system is employed and only current at bus-3,5,7 are measured. The analytical model of SG1, i.e., Z_{A1}, is considered known. For places where current is unmeasured, the impedance of the corresponding IBR is considered as infinite, i.e., they are treated as ideal current source.

By Applying (21) and (22), an estimation of the column Y_3^{sys} is acquired. The estimation of Y_{33}^{sys} will be as accurate as shown in Figure 28 (a), while Y_{53}^{sys} and Y_{73}^{sys} encounter errors, as shown in Figure 31, since some assumptions (e.g., treating some IBR as ideal current source) were applied. However, it can be found from Figure 31 that the estimation around 18.3 Hz, which is of major concern for the oscillation, is still accurate. Meaning that such estimations from the partial measurements are still useful for oscillation analysis.

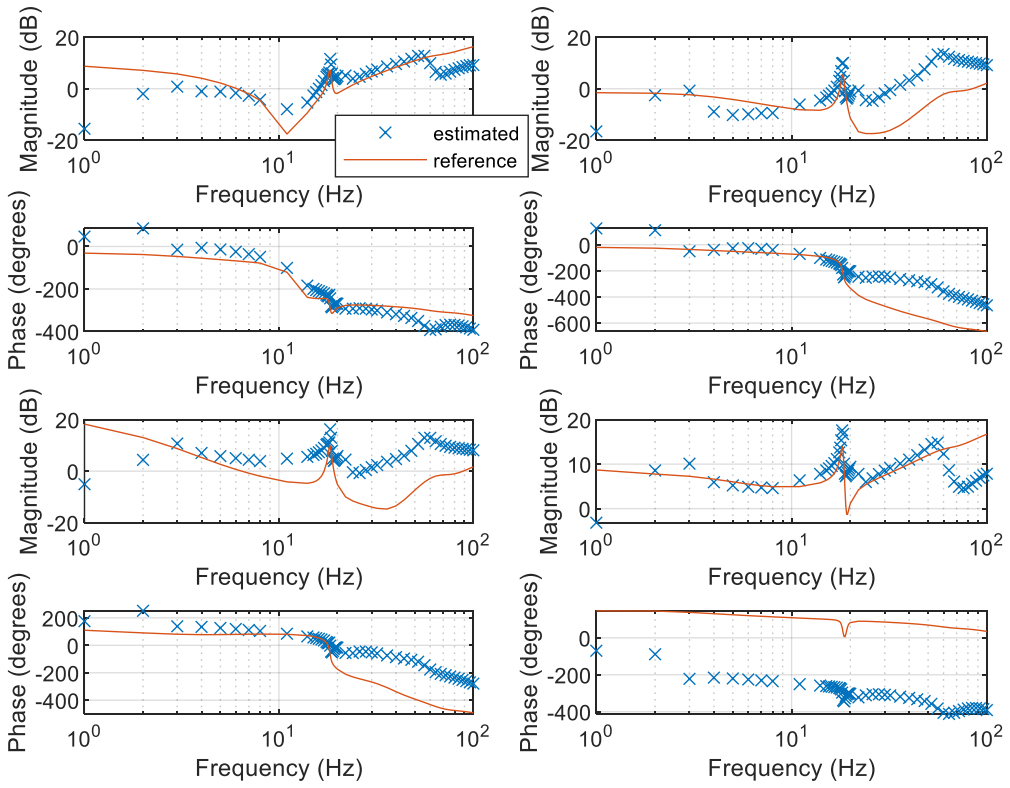

(a)

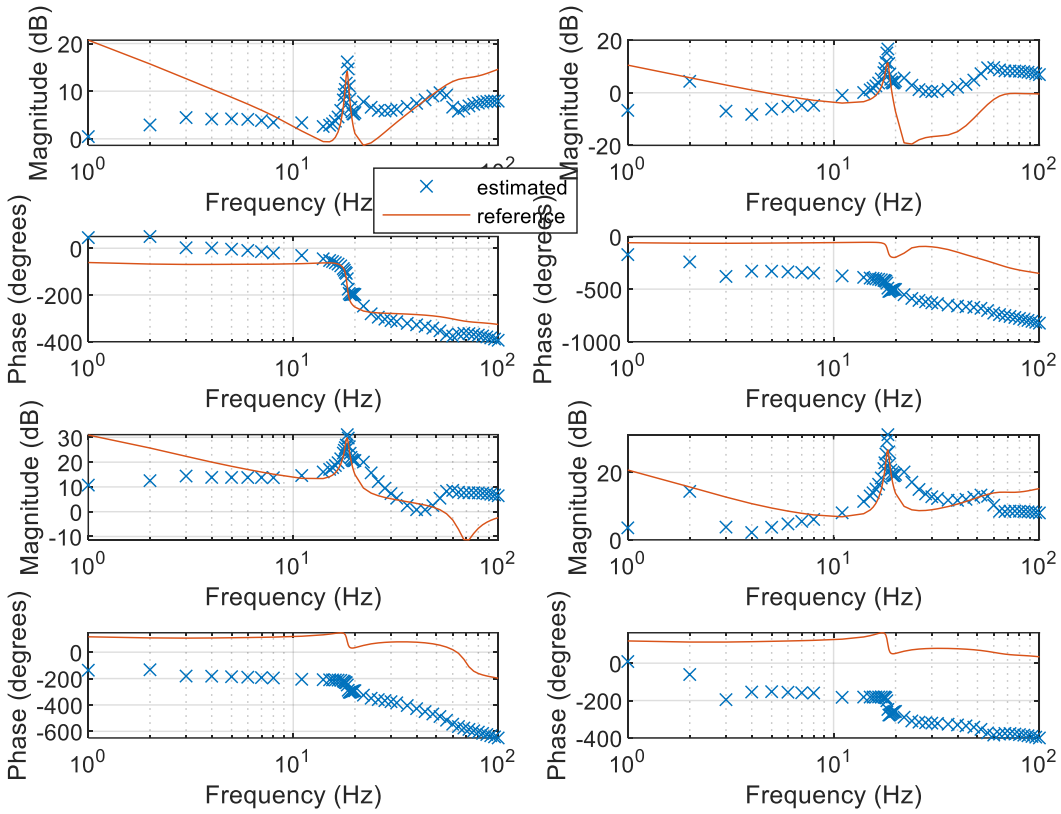

(b)

Figure 31 Estimations of (a) Y_{53}^{sys} and (b) Y_{73}^{sys}, errors occur due to assumptions used in the system, while the estimation around the oscillating frequency 18.3 Hz, which are shown as 'peak' in the spectra, is still accurate.

And finally, the diagonal elements Y_{55}^{sys} and Y_{77}^{sys} can be restored. The restored frequency response, together with the fitting results are shown in Figure 32. It is found that the estimation around 18.3 Hz remains accurate. Impedance participation factor, which is layer 1 of the grey-box approach, is then applied to identify the root cause among the three IBRs, as shown in Figure 33. It is clearly seen that A7 is the dominant of the mode, which aligns with the fact the mode is caused by the voltage interaction within A4 and A7. It is proved from this case that even if the measurement is not taken at each of the bus, root-cause analysis can still be applied on those which are measured.

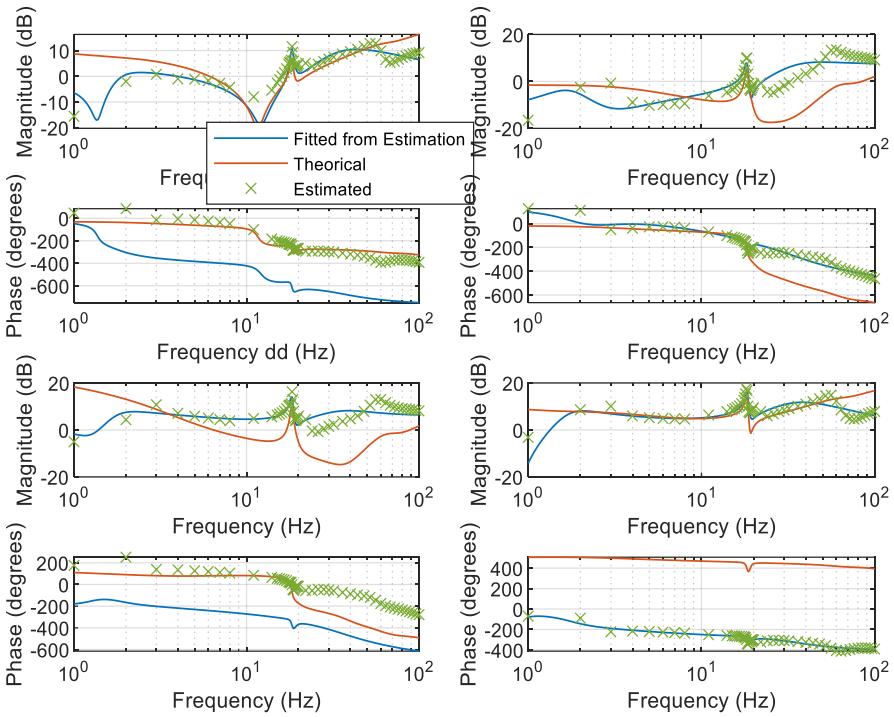

(a)

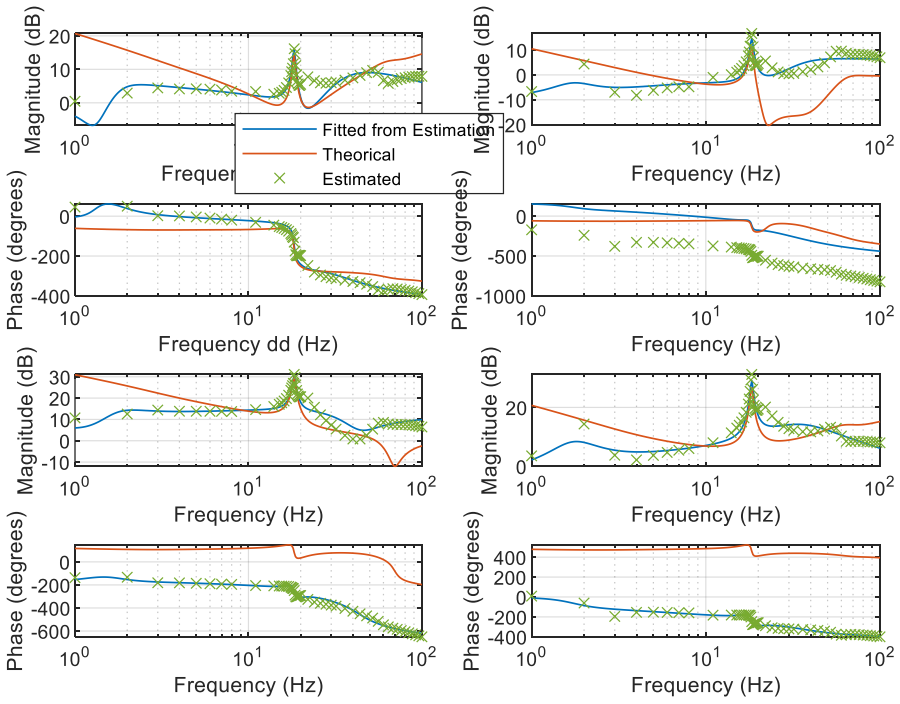

(b)

Figure 32 Estimations of (a) Y_{55}^{sys} and (b) Y_{77}^{sys} and the vector fitting results. The estimation around the oscillating frequency 18.3 Hz, which is shown as a 'peak' in the spectra, are still accurate.

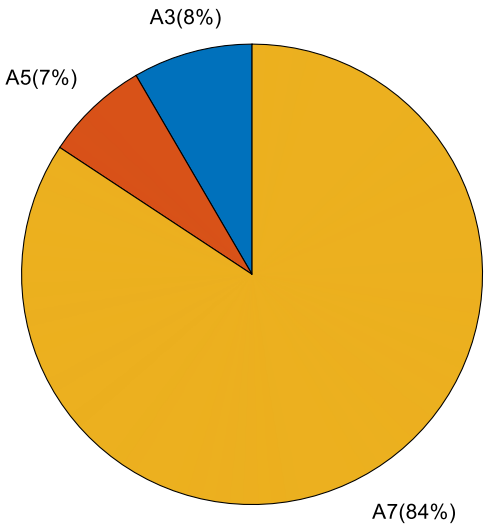

Figure 33 Impedance participation analysis (grey-box layer 1) on A3, A5, A7, correctly showing that A7 is the root cause of the18.3 Hz oscillatory mode.

6 Conclusions

In this supplementary report, both time-domain identification and frequency-domain identification approaches for whole-system impedance/admittance identification is discussed. Furthermore, a hybrid data/model-driven approach whole-system impedance identification method is proposed and verified from simulation case studies. The conclusions drawn are:

- Impedance/admittance model identification is useful for analysing potential oscillations and for post-event analysis to identify the root-cause. Both the time-domain identification and frequency-domain identification methods can be used. Whereas the proper equipment for system frequency scan is still under study and is absent for now, the time-domain identification making use of responses during events like step changes in the voltage or in the load would be an appropriate solution. Various algorithms can be chosen for time-domain identification, such as least-square method and eigensystem realization algorithms.
- For time-domain impedance (or admittance) identification, it is important to know the details of the system input, including: the location where the event happened, the size of the change, and, preferably, a record of the waveform of the input. It also requires knowledge of system power flow, especially the information of loads and lines. It is preferable to know the parameters of synchronous generators (SG) so that analytical models of SGs can be applied as a priori information. A difficult case is buses which are

not monitored by PMUs but with IBR connected where some assumptions have to make, such as using a generic model to represent the IBR, or, in a very simplified case, using an ideal current source. Most of the above knowledge will be accessible by the system operator so the issues raised can be dealt with.

- When the input location is far from the locations measured, the estimation of the relevant off-diagonal elements of the whole-system impedance matrix will be inaccurate. Multiple inputs at a variety of locations during a certain period would be useful to improve the accuracy but a proper method to merge the over-determined systems is needed. This needs further study.
- For a long-term system monitoring purposes, special equipment designed for frequency sweep, used in conjunction with frequency-domain identification, will be needed.

7 References

[1] Yue Zhu, Yunjie Gu, Jessica Santos Döhler, et al. Hybrid Data/Model-Driven Whole-System Admittance Identification via Single-Point Injections. TechRxiv. March 28, 2025. DOI: 10.36227/techrxiv.174319968.84007233/v1

[2] Y. Zhu, “Impedance model analysis and measurement for power system stability,” Ph.D. dissertation, Imperial College London, 2022.

[3] Y. Zhu, Y. Gu, Y. Li, T. C. Green, “Participation Analysis in Impedance Models: The Grey-Box Approach for Power System Stability” in IEEE Transactions on Power Systems, vol. 37, no. 1, pp. 343-353, Jan. 2022, doi: 10.1109/TPWRS.2021.3088345.

[4] Y. Zhu, Y. Gu, Y. Li and T. C. Green, "Impedance-Based Root-Cause Analysis: Comparative Study of Impedance Models and Calculation of Eigenvalue Sensitivity," in IEEE Transactions on Power Systems, vol. 38, no. 2, pp. 1642-1654, March 2023, doi: 10.1109/TPWRS.2022.3179143

[5] C. Zhang, M. Molinas, A. Rygg and X. Cai, "Impedance-Based Analysis of Interconnected Power Electronics Systems: Impedance Network Modeling and Comparative Studies of Stability Criteria," in IEEE Journal of Emerging and Selected Topics in Power Electronics, vol. 8, no. 3, pp. 2520-2533, Sept. 2020, doi: 10.1109/JESTPE.2019.2914560.

[6] Y. Gu, Y. Li, Y. Zhu and T. C. Green, "Impedance-Based Whole-System Modeling for a Composite Grid via Embedding of Frame Dynamics," in IEEE Transactions on Power Systems, vol. 36, no. 1, pp. 336-345, Jan. 2021, doi: 10.1109/TPWRS.2020.3004377.

[7] Ljung, L., & Glover, K. (1981). Frequency domain versus time domain methods in system identification. Automatica, 17(1), 71-86.

[8] L. Fan and Z. Miao, "Time-Domain Measurement-Based DQ -Frame Admittance Model Identification for Inverter-Based Resources," in IEEE Transactions on Power Systems, vol. 36, no. 3, pp. 2211-2221, May 2021, doi: 10.1109/TPWRS.2020.3040360.

[9] B. Matthias and K. Rudion. "Identification of grid impedance by broadband signals in power systems with high harmonics." Energies 14.21 (2021): 7398.

[10] B. Gustavsen and A. Semlyen, "Rational approximation of frequency domain responses by vector fitting", IEEE Trans. Power Delivery, vol. 14, no. 3, pp. 1052-1061, July 1999.

[11] https://www.sintef.no/en/software/vector-fitting/

[12] OFGEM, "9 August 2019 power outage report," 2020. [Online]. Available: https://www.ofgem.gov.uk/publications/investigation-9-august-2019-power-outage

[13] S. Shah, P. Koralewicz, V. Gevorgian and R. Wallen, "Sequence Impedance Measurement of Utility-Scale Wind Turbines and Inverters – Reference Frame, Frequency Coupling, and MIMO/SISO Forms," in IEEE Transactions on Energy Conversion, vol. 37, no. 1, pp. 75-86, March 2022, doi: 10.1109/TEC.2021.3093516.

[14] SINTEF, "Vector Fitting," available at: https://www.sintef.no/en/software/vector-fitting/. Accessed: May 20, 2024.